



TESIS - SK142502

# **Ti<sub>4</sub>O<sub>7</sub> dengan Luas Permukaan yang Tinggi sebagai Pendukung Katalis Platinum untuk Reaksi Reduksi Oksigen**

IDRIS IBNU MALIK  
NRP 1413 201 004

DOSEN PEMBIMBING  
Prof. Bing-Joe Hwang  
Hamzah Fansuri, Ph.D.

PROGRAM MAGISTER  
BIDANG KEAHLIAN KIMIA ANORGANIK  
JURUSAN KIMIA  
FAKULTAS MATEMATIKA DAN ILMU PENGETAHUAN ALAM  
INSTITUT TEKNOLOGI SEPULUH NOPEMBER  
SURABAYA  
2015



THESIS - SK142502

# High Surface Area $\text{Ti}_4\text{O}_7$ Supported Platinum Catalyst for Oxygen Reduction Reaction

IDRIS IBNU MALIK  
NRP 1413 201 004

ADVISOR  
Prof. Bing-Joe Hwang  
Hamzah Fansuri, Ph.D.

MASTER PROGRAM  
EXPERTISE OF INORGANIC CHEMISTRY  
DEPARTMENT OF CHEMISTRY  
FACULTY OF MATHEMATICS AND NATURAL SCIENCES  
INSTITUT TEKNOLOGI SEPULUH NOPEMBER  
SURABAYA  
2015

## MASTER THESIS RECOMMENDATION FORM

was arranged as requirement to complete the degree  
Master of Science  
in

Institut Teknologi Sepuluh Nopember, Indonesia

**IDRIS IBNU MALIK**  
**NRP 1413201004**

Date: July 24<sup>th</sup> 2015

Graduation period: September 2015

Approved by:

1. Prof. Bing-Joe Hwang (NTUST Advisor/ Examination Committee)



2. Hamzah Fansuri, Ph. D. (ITS Advisor)  
NIP. 19691017 199412 1 001



3. Prof. Wei-Nien Su (Examination Committee)



4. Prof. Hung-Lung Chou (Examination Committee)





## ABSTRAK

$\text{Ti}_4\text{O}_7$  merupakan kandidat material pendukung katalis yang menjanjikan karena konduktivitas serta stabilitasnya yang tinggi terhadap korosi. Namun, untuk mendapatkan  $\text{Ti}_4\text{O}_7$  dengan luas permukaan yang tinggi merupakan tantangan tersendiri. Dalam penelitian ini, material pendukung  $\text{Ti}_4\text{O}_7$  dengan luas permukaan yang tinggi berhasil disintesis dari Ti(IV) etoksida sebagai prekursor titanium dan PEG 400 sebagai agen pereduksi. Hasil karakterisasi XRD menunjukkan bahwa rasio terbaik Ti(IV) etoksida dan PEG 400 untuk menghasilkan  $\text{Ti}_4\text{O}_7$  adalah 10:4 rasio berat. Penggunaan PEG 400 sebagai agen pereduksi menyisakan residu karbon amorf sekitar 7,57-9,44%. Hasil analisa fisisorpsi menunjukkan adanya mesopori pada  $\text{Ti}_4\text{O}_7$  dengan distribusi ukuran pori rata-rata 4-8 nm dan luas permukaan 154,9 hingga 187,6  $\text{m}^2 \text{g}^{-1}$ . Hasil ini juga didukung dengan gambar SEM yang secara jelas menunjukkan adanya struktur pori.  $\text{Ti}_4\text{O}_7$  hasil sintesis memiliki konduktivitas elektronik sebesar 95,47 hingga 172,96  $\text{S cm}^{-1}$ , nilai ini lebih tinggi dari material berbasis titanium lainnya. Tidak adanya puncak pada hasil analisa CV menunjukkan kestabilan  $\text{Ti}_4\text{O}_7$  di lingkungan asam. Selain itu, nanopartikel platinum berhasil didepositkan pada material pendukung  $\text{Ti}_4\text{O}_7$  menggunakan metode sintesis polyol dengan bantuan microwave. Akan tetapi, aktivitas katalitik dari katalis 20% Pt/ $\text{Ti}_4\text{O}_7$  lebih rendah daripada katalis komersial 20% Pt/C dalam hal potensial onset, kerapatan arus kinetik pada 0,9 V vs RHE dan aktivitas massa. Selain itu, residu karbon amorf juga belum berhasil dihilangkan dari material pendukung  $\text{Ti}_4\text{O}_7$ .



## ABSTRACT

$\text{Ti}_4\text{O}_7$  is a promising catalyst support material candidate due to its high conductivity and stability against corrosion, but obtaining high surface area  $\text{Ti}_4\text{O}_7$  is very challenging. High surface area  $\text{Ti}_4\text{O}_7$  support material was successfully synthesized by utilizing Ti(IV) ethoxide as titanium precursor and PEG 400 as reducing agent. The XRD result revealed that the best Ti(IV) ethoxide and PEG 400 ratio in  $\text{Ti}_4\text{O}_7$  synthesis was 10:4 weight ratio. Since the synthesis utilized PEG 400 as reducing agent, 7.57 to 9.44 wt% amorphous carbon residue remained in the obtained  $\text{Ti}_4\text{O}_7$ . Physisorption analysis result revealed that it consisted of mesopores with average pore size distribution around 4-8 nm and the surface area was 154.9 to 187.6  $\text{m}^2 \text{g}^{-1}$ . The result was supported by SEM images which clearly showed the existence of pore structure. The electronic conductivity range from 95.47 to 172.96  $\text{S cm}^{-1}$ , the value is much higher than the other titanium based materials. CV analysis results revealed that it was stable in acidic environment since no peaks were observed. Furthermore, platinum nanoparticles were successfully deposited on  $\text{Ti}_4\text{O}_7$  support material by utilizing microwave-assisted polyol synthesis. Unfortunately, the ORR activity of 20 wt% Pt/ $\text{Ti}_4\text{O}_7$  catalysts was lower than the commercial 20 wt% Pt/C in terms of the onset potential, kinetic current density at 0.9 V vs. RHE and mass activity. In addition, the amorphous carbon residue was not completely removed from the  $\text{Ti}_4\text{O}_7$  support material.

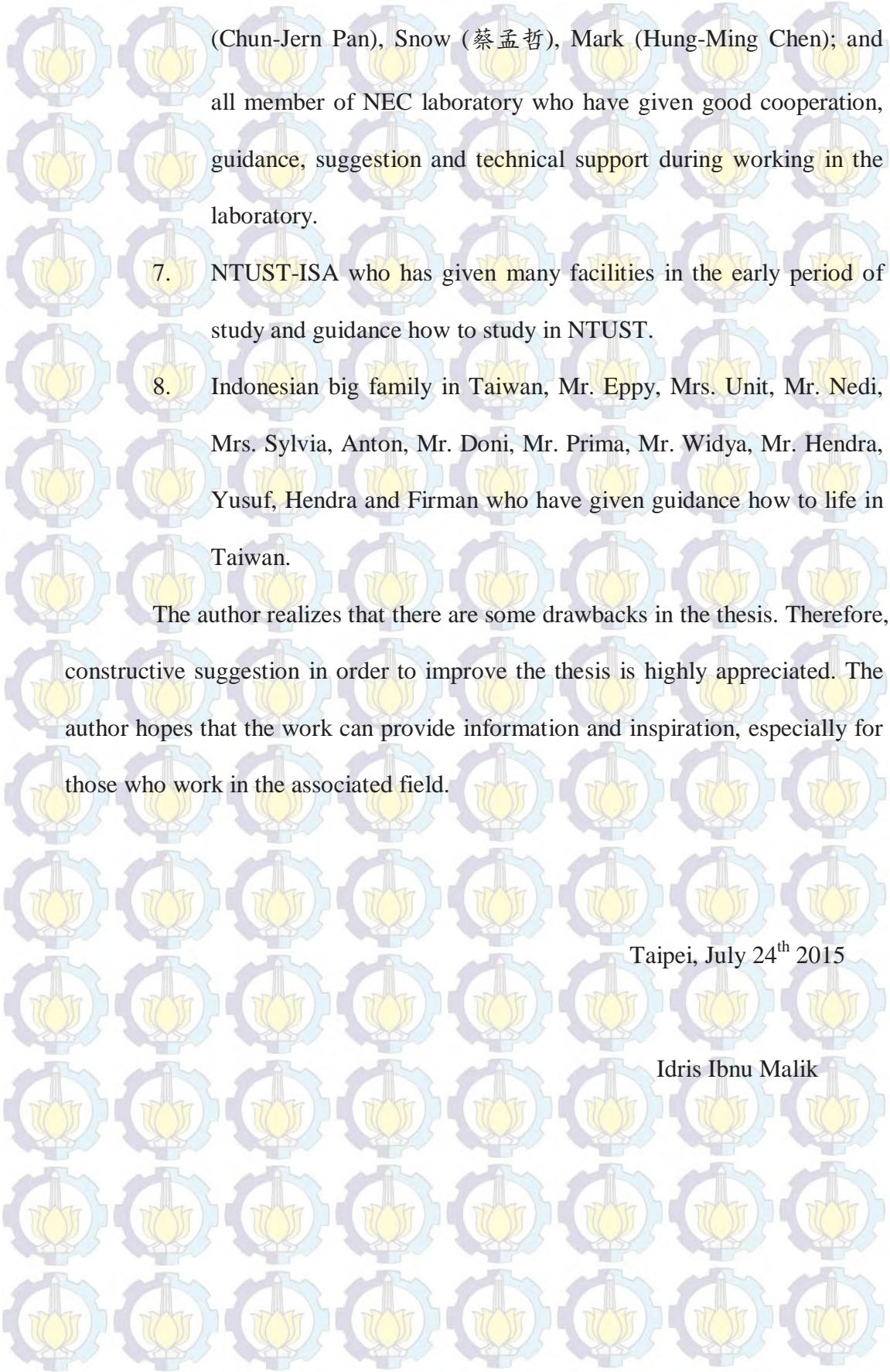


## ACKNOWLEDGEMENT

In the name of Allah, the Beneficent and the Merciful. Praise and Gratitude be to Allah who has given the author strength and guidance in finishing the thesis. Peace and Blessing be to Prophet Muhammad SAW, his families and all his followers. The author gratefully acknowledge to those who have helped in the thesis completion, especially to:

1. Prof. Bing-Joe Hwang as supervisor who has given research facility, support and guidance in finishing the thesis.
2. Hamzah Fansuri, Ph.D. as supervisor who has given motivation, support and guidance during the study.
3. Direktorat Jenderal Pendidikan Tinggi, Ministry of Education and Culture, Indonesia, who has given continuous financial support.
4. National Taiwan University of Science and Technology, Taiwan and Institut Teknologi Sepuluh Nopember, Indonesia who have given the opportunity in double degree program.
5. The beloved parents, Ibnu Shobir and Siti Muyassaroh; the beloved wife, Prestika Yustisi; the beloved parents in law, Sujarwoko and Sunarti; who always give motivation, support, guidance and courage in every single step of the life.
6. The lab mates, Hogiarttha Sutiono, Mawan Nugraha, Alemayehu Dubale, Ryker (董旺熾), Vic (蔡承佑), Momo (毛鈺翔), Jane (黃筱君), Minh Kha Nguyen, Huynh Tan Thanh; the postdoc, Peter





(Chun-Jern Pan), Snow (蔡孟哲), Mark (Hung-Ming Chen); and all member of NEC laboratory who have given good cooperation, guidance, suggestion and technical support during working in the laboratory.

7. NTUST-ISA who has given many facilities in the early period of study and guidance how to study in NTUST.

8. Indonesian big family in Taiwan, Mr. Eppy, Mrs. Unit, Mr. Nedi, Mrs. Sylvia, Anton, Mr. Doni, Mr. Prima, Mr. Widya, Mr. Hendra, Yusuf, Hendra and Firman who have given guidance how to life in Taiwan.

The author realizes that there are some drawbacks in the thesis. Therefore, constructive suggestion in order to improve the thesis is highly appreciated. The author hopes that the work can provide information and inspiration, especially for those who work in the associated field.

Taipei, July 24<sup>th</sup> 2015

Idris Ibnu Malik



## TABLE OF CONTENT

ABSTRAK.....	iv
ABSTRACT.....	v
ACKNOWLEDGEMENT.....	vi
TABLE OF CONTENT.....	viii
LIST OF FIGURE.....	xi
LIST OF TABLE.....	xvi
LIST OF APPENDIX.....	xvii
CHAPTER 1 - OVERVIEW.....	1
1.1 Background.....	1
1.2 Motivation.....	6
CHAPTER 2 - LITERATURE REVIEW.....	7
2.1 Fuel Cell Catalyst.....	7
2.1.1 Carbon Corrosion.....	10
2.1.2 Oxygen Reduction Reaction.....	11
2.1.3 Electrocatalyst Characterization.....	13
2.2 Ti <sub>4</sub> O <sub>7</sub> Synthesis.....	17
2.2.1 Recent Developments.....	17
2.2.2 Summary.....	23
CHAPTER 3 - EXPERIMENTAL SECTION.....	25
3.1 Chemicals and Equipments.....	25



3.1.1 Chemicals .....	25
3.1.2 Equipments .....	25
3.2 Synthesis Methodology .....	26
3.2.1 Synthesis of $\text{Ti}_4\text{O}_7$ Support Material .....	26
3.2.2 Synthesis of 20 wt% Pt/ $\text{Ti}_4\text{O}_7$ Catalyst .....	26
3.3 Carbon removal of $\text{Ti}_4\text{O}_7$ Support Material .....	27
3.3.1 Extraction treatment .....	27
3.3.2 Solvent treatment .....	28
3.3.3 Acid-base treatment .....	28
3.4 Material Characterization .....	29
3.5 Electrochemical Measurement .....	29
CHAPTER 4 - RESULT AND DISCUSSION .....	33
4.1 Characterization of $\text{Ti}_4\text{O}_7$ Support Material .....	33
4.1.1 XRD Results .....	34
4.1.2 Thermogravimetric Results .....	35
4.1.3 Physisorption Results .....	37
4.1.4 SEM Results .....	39
4.1.5 Electronic Conductivity Results .....	40
4.1.6 CV Analysis Results .....	41
4.1.7 Summary .....	42
4.2 Carbon Removal of $\text{Ti}_4\text{O}_7$ Support Material .....	43
4.2.1 Extraction Treatment Result .....	43



4.2.2 Solvent Treatment Result .....	45
4.2.3 Acid-Base Treatment Result .....	46
4.2.4 Summary .....	46
4.3 Characterization of 20 wt% Pt/Ti <sub>4</sub> O <sub>7</sub> Catalyst .....	47
4.3.1 XRD Results .....	48
4.3.2 Electrochemical Performance of 20 wt% Pt/Ti <sub>4</sub> O <sub>7</sub> Catalyst ..	49
4.3.3 Summary .....	60
CHAPTER 5 - CONCLUSION AND OUTLOOK .....	63
5.1 Conclusion .....	63
5.2 Outlook .....	63
BIBLIOGRAPHY .....	65
APPENDIX.....	71
BIOGRAPHY .....	81



## LIST OF FIGURE

Figure 1.1 Supply and demand of energy consumption. <sup>1</sup> .....	1
Figure 1.2 Challenges in realizing hydrogen fuel cell. <sup>4</sup> .....	2
Figure 1.3 Comparison of energy transformations in fuel cells, batteries and heat engines. <sup>5</sup> .....	3
Figure 1.4 Degradation of carbon support in fuel cell catalyst. <sup>13</sup> .....	4
Figure 2.1 Schematic of polymer electrolyte membrane fuel cell. <sup>26</sup> .....	7
Figure 2.2 Schematic of a membrane electrode assembly which consist of diffusion layer, catalytic layer and polymer electrolyte membrane. <sup>15</sup> ...	8
Figure 2.3 Schematic of catalyst layer components. <sup>15</sup> .....	9
Figure 2.4 Simplified representation of suggested degradation mechanisms for platinum particles on a carbon support in fuel cells. <sup>30</sup> .....	10
Figure 2.5 Volcano plot for ORR activity. <sup>32</sup> .....	11
Figure 2.6 Cyclic voltammogram of platinum electrocatalyst. <sup>34</sup> .....	14
Figure 2.7 Evaluation of electrocatalyst activity towards ORR for carbon supported Pt and Pt-Co. (a) LSV result in 0.5 M H <sub>2</sub> SO <sub>4</sub> at 25 °C with rotation speed 2,500 rpm and sweep rate 1 mV s <sup>-1</sup> , (b) Tafel plots and (c) mass activity measured at 0.95 V vs. RHE. <sup>36</sup> .....	16
Figure 2.8 SEM images of (a) prepared Ti <sub>4</sub> O <sub>7</sub> support and (b) 5% Pt/Ti <sub>4</sub> O <sub>7</sub> . Polarization curves of a single cell with (c) 5% Pt/Ti <sub>4</sub> O <sub>7</sub> and (d) 30% Pt/XC72-HTT cathodes at the initial state and after potential holding in O <sub>2</sub> at 1.2–1.5 V for 1 hour. <sup>20</sup> .....	18



Figure 2.9 Scanning and transmission electron microscopic images of (a) as-spun  $\text{TiO}_2/\text{PVP}$  composite, (b)  $\text{Ti}_4\text{O}_7$  nanofibers and (c) 20-wt%  $\text{Pt}/\text{Ti}_4\text{O}_7$ . 19

Figure 2.10 Cyclic voltammograms of (a) 20-wt%  $\text{Pt}/\text{Ti}_4\text{O}_7$  catalyst before and after durability test, (b) plot of the ECSA and its percentage loss as a function of potential cycles number, ORR curves of 20-wt%  $\text{Pt}/\text{Ti}_4\text{O}_7$  nanofiber catalysts (c) before and (d) after durability test.<sup>23</sup> ..... 20

Figure 2.11 Multistep reaction pathway in synthesizing NS- $\text{Ti}_4\text{O}_7$ . ..... 20

Figure 2.12 CV plots of (a)  $\text{Pt}/\text{NS-Ti}_4\text{O}_7$ , (b)  $\text{Pt}/\text{XC-72}$  obtained at room temperature and (c) normalized ECSA as a function of cycle number for  $\text{Pt}/\text{NS-Ti}_4\text{O}_7$  and  $\text{Pt}/\text{XC-72}$ . ..... 21

Figure 2.13 TEM images of  $\text{Pt}/\text{NS-Ti}_4\text{O}_7$  (a) before and (c) after durability test. TEM images of  $\text{Pt}/\text{XC-72}$  (e) before and (g) after durability test.<sup>24</sup> .... 21

Figure 2.14 X-ray diffraction pattern of  $\text{Ti}_4\text{O}_7$ .<sup>25</sup> ..... 22

Figure 2.15 (a) Rietveld refinement of the as synthesized  $\text{Ti}_4\text{O}_7$  powder XRD pattern. (b) Pore size distribution of  $\text{Ti}_4\text{O}_7$  with the inset image showing the type-IV nitrogen adsorption-desorption isotherm.<sup>45</sup> ..... 23

Figure 3.1 A three-electrode cell which was used to measure electrochemical activity of the catalyst.<sup>46</sup> ..... 30

Figure 4.1 XRD patterns of (a)  $\text{Ti10PEG03}$ , (b)  $\text{Ti10PEG04}$ , (c)  $\text{Ti10PEG05}$ , (d)  $\text{Ti}_4\text{O}_7$  (PDF 50-0787), (e) anatase- $\text{TiO}_2$  (PDF 84-1286) and (f) rutile- $\text{TiO}_2$  (PDF 84-1284)..... 33

Figure 4.2 Thermogravimetric analysis results of  $\text{Ti}_4\text{O}_7$  support materials, heating rate =  $10\text{ }^\circ\text{C min}^{-1}$  ..... 35

Figure 4.3 Adsorption and desorption isotherms of  $\text{Ti}_4\text{O}_7$  support materials. .... 37



Figure 4.4 Pore size distributions of $\text{Ti}_4\text{O}_7$ support materials.....	38
Figure 4.5 SEM images of $\text{Ti}_4\text{O}_7$ support materials (a) Ti10PEG03, (b) Ti10PEG04 and (c) Ti10PEG05 sample.....	39
Figure 4.6 Cyclic voltammograms of $\text{Ti}_4\text{O}_7$ support materials and carbon black for comparison in Ar-saturated 0.5 M $\text{H}_2\text{SO}_4$ solution at room temperature and scan rate $25 \text{ mV s}^{-1}$ .....	41
Figure 4.7 Thermogravimetric analysis results of carbon removal by extraction treatment, heating rate = $10 \text{ }^\circ\text{C min}^{-1}$ .....	43
Figure 4.8 Thermogravimetric analysis results of carbon removal by solvent treatment, heating rate = $10 \text{ }^\circ\text{C min}^{-1}$ .....	44
Figure 4.9 Thermogravimetric analysis results of carbon removal by acid-base treatment, heating rate = $10 \text{ }^\circ\text{C min}^{-1}$ .....	46
Figure 4.10 XRD patterns of (a) 20 wt% Pt/Ti10PEG03, (b) 20 wt% Pt/Ti10PEG04, (c) 20 wt% Pt/Ti10PEG05, (d) $\text{Ti}_4\text{O}_7$ (PDF 50-0787) and (e) platinum (PDF 04-0802).....	48
Figure 4.11 Cyclic voltammograms of 20 wt% Pt/Ti10PEG03, 20 wt% Pt/Ti10PEG04, 20 wt% Pt/Ti10PEG05 and commercial 20 wt% Pt/C catalyst which were previously dispersed in 500 $\mu\text{L}$ 0.5% Nafion 117 ( $0.2 \text{ mg}_{\text{Pt}} \text{ cm}^{-2}$ ) recorded at room temperature in Ar-saturated 0.5 M $\text{H}_2\text{SO}_4$ solution at scan rate $25 \text{ mV s}^{-1}$ .....	50
Figure 4.12 Cyclic voltammograms of 20 wt% Pt/Ti10PEG03, 20 wt% Pt/Ti10PEG04, 20 wt% Pt/Ti10PEG05 and commercial 20 wt% Pt/C catalyst which were previously dispersed in 500 $\mu\text{L}$ 0.1% Nafion 117	



(0.2 mg <sub>Pt</sub> cm <sup>-2</sup> ) recorded at room temperature in Ar-saturated 0.5 M H <sub>2</sub> SO <sub>4</sub> solution at scan rate 25 mV s <sup>-1</sup> . .....	51
Figure 4.13 Cyclic voltammograms of 20 wt% Pt/Ti10PEG03, 20 wt% Pt/Ti10PEG04, 20 wt% Pt/Ti10PEG05 and commercial 20 wt% Pt/C catalyst which were previously dispersed in 500 μL mixture of isopropanol and DI water (95:5 volume ratio) and followed by dropping 7 μL 0.01% Nafion 117 (0.2 mg <sub>Pt</sub> cm <sup>-2</sup> ) recorded at room temperature in Ar-saturated 0.5 M H <sub>2</sub> SO <sub>4</sub> solution at scan rate 25 mV s <sup>-1</sup> .....	52
Figure 4.14 The ECSA summary of (A) 20 wt% Pt/Ti10PEG03, (B) 20 wt% Pt/Ti10PEG04, (C) 20 wt% Pt/Ti10PEG05 and (D) commercial 20 wt% Pt/C catalyst in different catalyst ink preparation.....	54
Figure 4.15 Polarization curves of 20 wt% Pt/Ti10PEG03, 20 wt% Pt/Ti10PEG04, 20 wt% Pt/Ti10PEG05 and commercial 20 wt% Pt/C catalyst which were previously dispersed in 500 μL 0.5% Nafion 117 (0.2 mg <sub>Pt</sub> cm <sup>-2</sup> ) recorded at room temperature in oxygen-saturated 0.5 M H <sub>2</sub> SO <sub>4</sub> solution at scan rate 1 mV s <sup>-1</sup> . The current was normalized to the geometric area of the glassy carbon electrode (0.1964 cm <sup>2</sup> ).....	55
Figure 4.16 Polarization curves of 20 wt% Pt/Ti10PEG03, 20 wt% Pt/Ti10PEG04, 20 wt% Pt/Ti10PEG05 and commercial 20 wt% Pt/C catalyst which were previously dispersed in 500 μL 0.1% Nafion 117 (0.2 mg <sub>Pt</sub> cm <sup>-2</sup> ) recorded at room temperature in oxygen-saturated 0.5 M H <sub>2</sub> SO <sub>4</sub> solution at scan rate 1 mV s <sup>-1</sup> . The current was normalized to the geometric area of the glassy carbon electrode (0.1964 cm <sup>2</sup> ).....	56



Figure 4.17 Polarization curves of 20 wt% Pt/Ti10PEG03, 20 wt% Pt/Ti10PEG04, 20 wt% Pt/Ti10PEG05 and commercial 20 wt% Pt/C catalyst which were previously dispersed in 500  $\mu\text{L}$  mixture of isopropanol and DI water (95:5 volume ratio) and followed by dropping 7  $\mu\text{L}$  0.01% Nafion 117 ( $0.2 \text{ mg}_{\text{Pt}} \text{ cm}^{-2}$ ) recorded at room temperature in oxygen-saturated 0.5 M  $\text{H}_2\text{SO}_4$  solution at scan rate  $1 \text{ mV s}^{-1}$ . The current was normalized to the geometric area of the glassy carbon electrode ( $0.1964 \text{ cm}^2$ ). ..... 58

Figure 4.18 The kinetic current density at 0.9 V vs. RHE of (A) 20 wt% Pt/Ti10PEG03, (B) 20 wt% Pt/Ti10PEG04, (C) 20 wt% Pt/Ti10PEG05 and (D) commercial 20 wt% Pt/C catalyst in different catalyst ink preparation..... 59





## LIST OF TABLE

Table 2.1 Phase composition in the temperature range of 800-1,025 °C.<sup>22</sup> ..... 19

Table 2.2 Summary of Ti<sub>4</sub>O<sub>7</sub> synthesis strategy, sorted by the surface area..... 24

Table 4.1 Amount of amorphous carbon residue of Ti<sub>4</sub>O<sub>7</sub> support materials. .... 36

Table 4.2 BET surface area of Ti<sub>4</sub>O<sub>7</sub> support materials..... 38

Table 4.3 Electronic conductivity of Ti<sub>4</sub>O<sub>7</sub> support materials. .... 40

Table 4.4 Summary of carbon removal result. .... 46



# CHAPTER 1

## OVERVIEW

### 1.1 Background

Fossil fuels currently supply most of the world's energy needs, however unacceptable their long-term consequences, the supplies are likely to remain adequate for the next few generations.<sup>1</sup> The energy consumer commonly divided by three parts, they are residential and commercial, industrial and transportation sector such as explained in Figure 1.1.

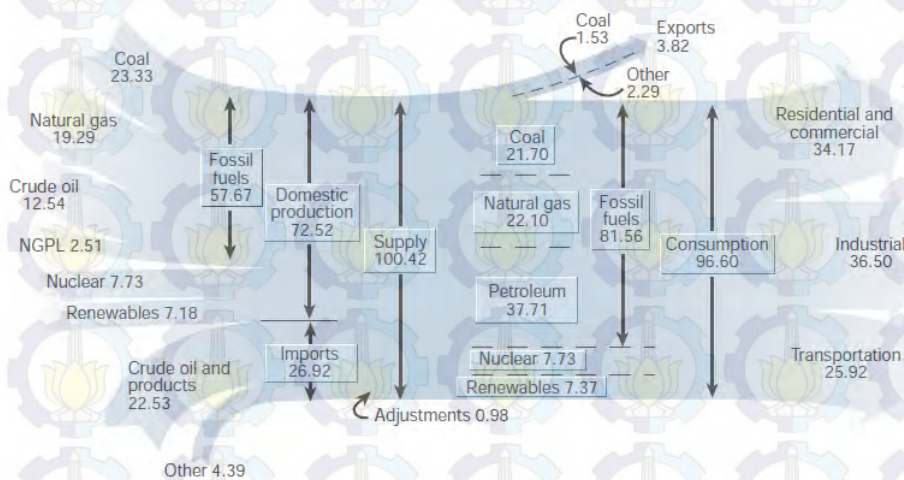


Figure 1.1 Supply and demand of energy consumption.<sup>1</sup>

Therefore, clean energy is an emerging issue that should be addressed since the utilization of the fossil fuel also causes environmental damage such as degradation of ozone layer and global warming. That's why peoples now attempt to find another energy sources such as hydropower, nuclear fission, biomass, wind,



geothermal, solar and ocean energy since they are able to generate electricity without releasing CO<sub>2</sub> that is usually resulted from heat engine.<sup>2</sup>

Another way to avoid fossil fuel consumption and also carbon emission is to utilize hydrogen fuel cells. But, it will take some time due to some problem that should be overcome before its wide commercialization.<sup>3</sup> The challenges in realizing hydrogen fuel cell can be divided into four main parts such as explained in Figure 1.2, they are source of hydrogen, infrastructure in hydrogen distribution, hydrogen storage and fuel cell itself.<sup>4</sup>

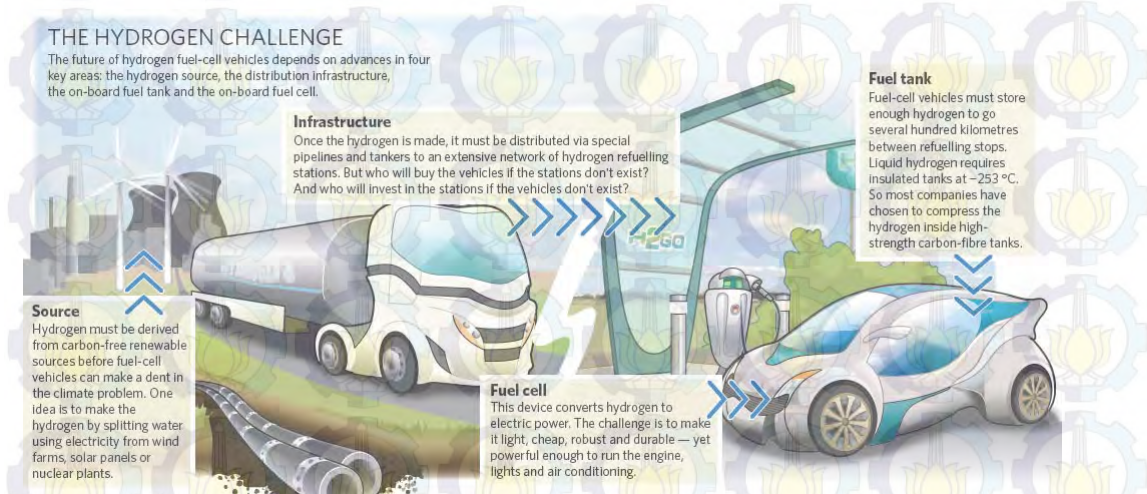


Figure 1.2 Challenges in realizing hydrogen fuel cell.<sup>4</sup>

Fuel cell was discovered by William Grove on early 1800s, but it is still very interesting for many researches in recent years since its promising application which can generate electricity directly from chemicals, especially hydrogen gas. Compared to the heat engine, fuel cell is more efficient in generating electric or mechanical energy since it has short process chain<sup>5</sup> such as explained in Figure 1.3.



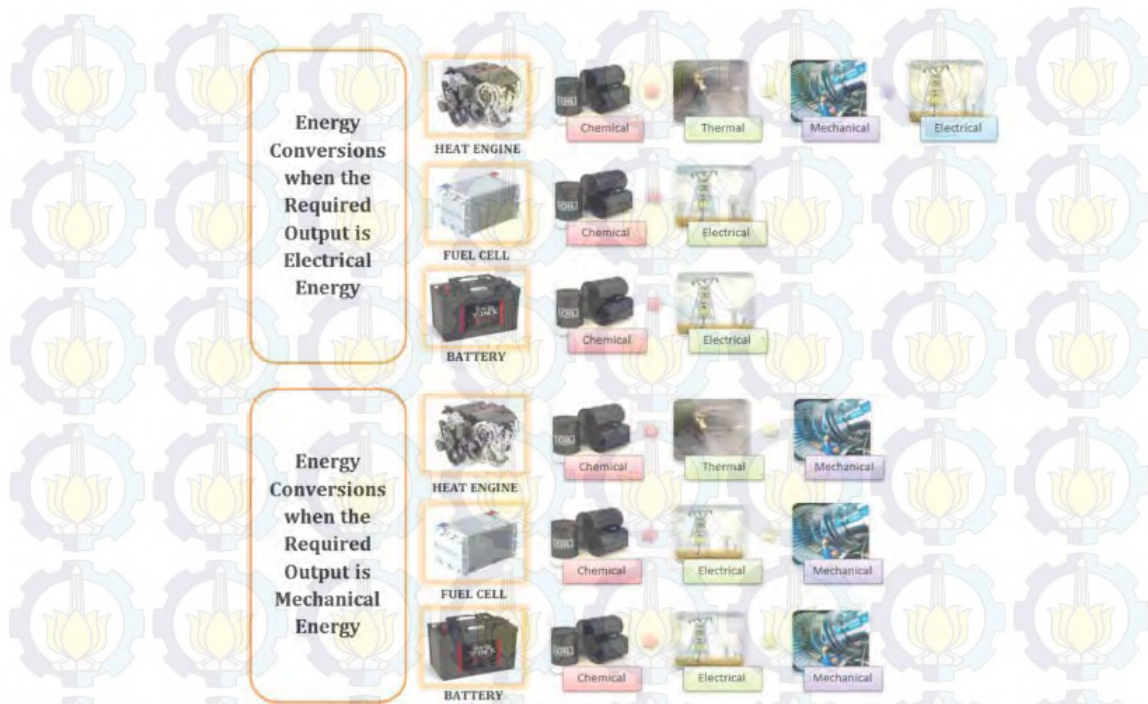


Figure 1.3 Comparison of energy transformations in fuel cells, batteries and heat engines.<sup>5</sup>

Two main issues that should be faced against wide utilization of fuel cell are the cost and performance. Fuel cell cost may be very expensive since it utilizes platinum catalyst in both anode and cathode. Platinum is noble metal that is very limited in earth crust.<sup>6</sup> Therefore, several attempts have been made by researches in recent years such as reducing platinum particle size,<sup>7</sup> alloying platinum with other metals<sup>8-11</sup> and utilizing non noble metal as catalyst.<sup>12</sup> In the other hand, long term fuel cell performance is still insufficient to meet the requirement due to catalyst degradation.<sup>6</sup>

Fuel cell catalyst which is commercially available consists of metal catalyst and support material. Most of them utilize carbon as support material, such as Pt/C or PtRu/C. Utilizing carbon as support material remains disadvantage in long term fuel cell performance since carbon may be oxidized into CO<sub>2</sub>. It



causes detachment and coalescence of platinum particles such as explained in Figure 1.4. Therefore, catalyst durability issue due to carbon corrosion is a problem that should be addressed in order to get better long term fuel cell performance.<sup>13</sup>

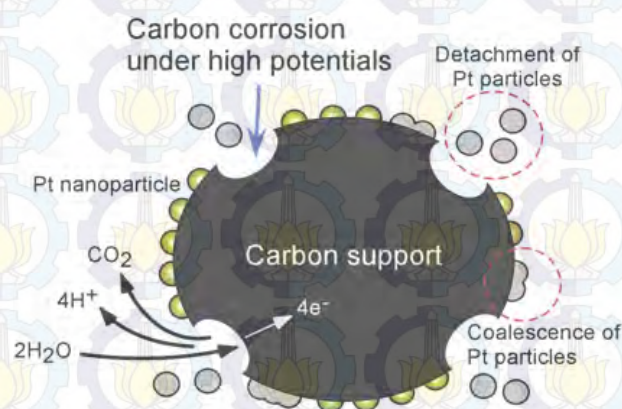


Figure 1.4 Degradation of carbon support in fuel cell catalyst.<sup>13</sup>

There are some requirements that have to be fulfilled in order to obtain good fuel cell catalyst support material. It should have strong metal-support interaction,<sup>14</sup> high surface area, good electronic conductivity and stability against corrosion.<sup>15</sup> In recent years, researchers have attempted to replace carbon support material by utilizing metal oxide, metal carbide and metal nitride as fuel cell catalyst support material.<sup>16</sup>

$\text{Ti}_4\text{O}_7$ , substoichiometric titanium oxide which is known as Magnéli phase and has general formula  $\text{Ti}_n\text{O}_{2n-1}$  ( $4 < n < 10$ ),<sup>17</sup> is a promising catalyst support material candidate due to its high conductivity and stability against corrosion. Electronic conductivity of  $\text{Ti}_4\text{O}_7$  at room temperature is  $10^3 \text{ S cm}^{-1}$ , which is the highest compared to other series of Magnéli phase titanium oxide.<sup>18</sup>



In addition, Magnéli-phase titanium oxides are known to be highly resistant against oxidation since no peaks or waves are observed between 0.0 and 2.0 V vs RHE in 1 M sulfuric acid at 298 K.<sup>19</sup>

The synthesis of  $\text{Ti}_4\text{O}_7$  is very challenging since its formation temperature is about 1,000 °C.<sup>20</sup> High temperature annealing produces uncontrollable particle growth that may reduce the surface area. Therefore, several strategies have been made by researches in order to obtain high surface area  $\text{Ti}_4\text{O}_7$ .

Ioroi et al synthesized  $\text{Ti}_4\text{O}_7$  by reducing  $\text{TiO}_2$  at 1,050 °C for 6 hours in  $\text{H}_2$  atmosphere, it resulted very low surface area  $\text{Ti}_4\text{O}_7$ ,  $0.95 \text{ m}^2 \text{ g}^{-1}$ .<sup>21</sup> Zhu et al synthesized  $\text{Ti}_4\text{O}_7$  by different approach, they used carbon black to reduce  $\text{TiO}_2$  at 1,025 °C for 2 hours in vacuum atmosphere, it resulted low surface area  $\text{Ti}_4\text{O}_7$ , about  $4 \text{ m}^2 \text{ g}^{-1}$ .<sup>22</sup> Senevirathne et al synthesized  $\text{Ti}_4\text{O}_7$  by utilizing electrospinning in order to obtain high surface area  $\text{TiO}_2$ . Furthermore, they reduced it at 1,050 °C for 6 hours in  $\text{H}_2:\text{N}_2$  atmosphere,  $\text{Ti}_4\text{O}_7$  that was produced by this method with low surface area, about  $6 \text{ m}^2 \text{ g}^{-1}$ .<sup>23</sup> Yao et al utilized silica to cover nanotube  $\text{TiO}_2$ , it aimed to prevent particle agglomeration during reduction process at 1,050 °C for 4 hours in  $\text{H}_2$  atmosphere.  $\text{Ti}_4\text{O}_7$  which was prepared by this approach with higher surface area than the previous one. The surface area was  $26 \text{ m}^2 \text{ g}^{-1}$ .<sup>24</sup>

Nazar's group successfully synthesized high surface area  $\text{Ti}_4\text{O}_7$  for Li batteries purpose by utilizing Ti(IV) ethoxide and poly(ethylene glycol), average  $\text{Mw} = 400$  (PEG 400). In this method, PEG 400 served as reducing agent since it mainly consists of carbon, while its polymeric structure has ability to prevent particle agglomeration during the reduction process at 950 °C in Ar atmosphere.

$\text{Ti}_4\text{O}_7$  that was synthesized with high surface area, about  $290 \text{ m}^2 \text{ g}^{-1}$ , and amorphous carbon residue about 15.4 wt%.<sup>25</sup>

## 1.2 Motivation

In this work, high surface area  $\text{Ti}_4\text{O}_7$  was synthesized by following Nazar's group approach and would be used to support platinum catalyst for fuel cell application. By employing high surface area  $\text{Ti}_4\text{O}_7$ , three requirements of good fuel cell catalyst support including high surface area, good electronic conductivity and stability can be achieved.



## CHAPTER 2

### LITERATURE REVIEW

#### 2.1 Fuel Cell Catalyst

Fuel cell is an electrochemical device which converts chemical reaction into electrical energy. It consists of an electrolyte that separates an anode and a cathode. The fuel is fed to the anode and can be either a liquid or a gas. In case of hydrogen fuel cell, hydrogen is oxidized in the anode side to release electrons and protons. Then, these electrons flow through an electronic conductor and protons flow through polymer electrolyte membrane (PEM) to the cathode side. In the cathode side, oxygen is reduced into water in the presence of electrons and protons.<sup>15</sup> This overall process is also explained in Figure 2.1.

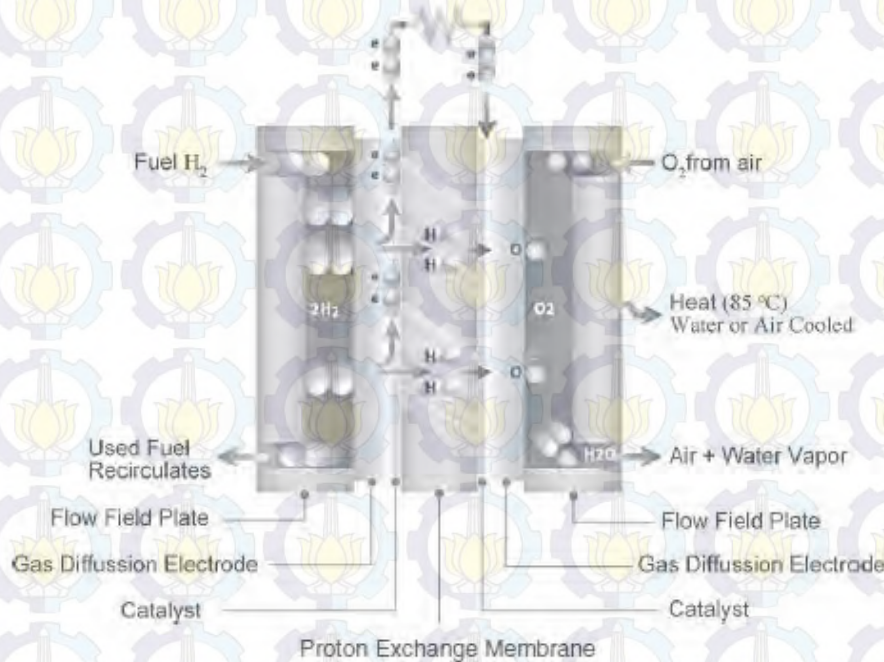


Figure 2.1 Schematic of polymer electrolyte membrane fuel cell.<sup>26</sup>

Fuel cell catalyst is laid in catalyst layers. The catalyst is deposited on the opposite sides both of anode and cathode and separated by the polymer electrolyte membrane (PEM) such as explained in Figure 2.2.

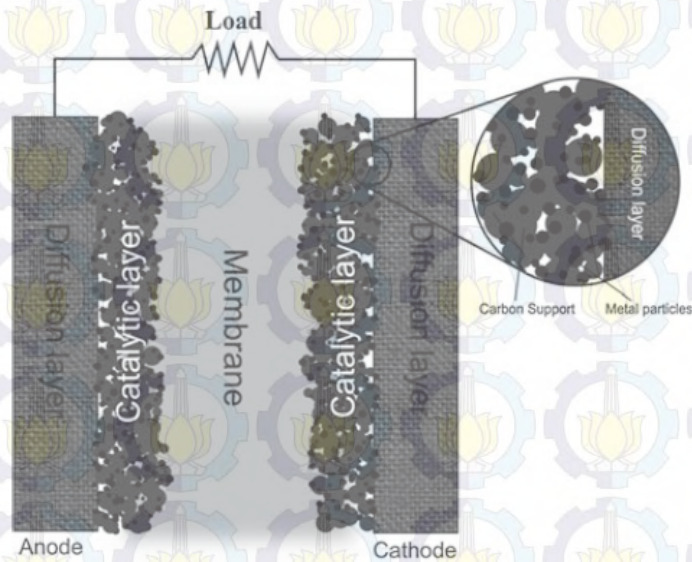


Figure 2.2 Schematic of a membrane electrode assembly which consist of diffusion layer, catalytic layer and polymer electrolyte membrane.<sup>15</sup>

The catalyst layer is built by several components such as explained in Figure 2.3, they are:

1. *Support material*, good support material should has the following requirements:
  - a. *High surface area*, it is very important since it allows dispersion of the electroactive material and fast mass transport of reactants and products due to its porosity.
  - b. *Good electronic conductivity*, the support has to be an electronic conductor since it is required to drive the electrons to the current collectors.



c. *Good stability*, the support has to be stable against corrosion in order to prevent catalyst degradation.

d. *Strong interaction with metal catalyst*, it is very important in order to prevent catalyst detachment from the support and to adjust the d-orbital density of the metal catalyst.<sup>27</sup>

2. *Electroactive phase*, it is the active catalyst such as platinum nanoparticles. The function is to make the kinetics of the spontaneous electrochemical reactions as fast as possible.

3. *The ionomer*, its function is to provide additional ionic conductivity to the catalyst layer.

4. *A binder*, it has role to hold all catalyst layer components to stay together.

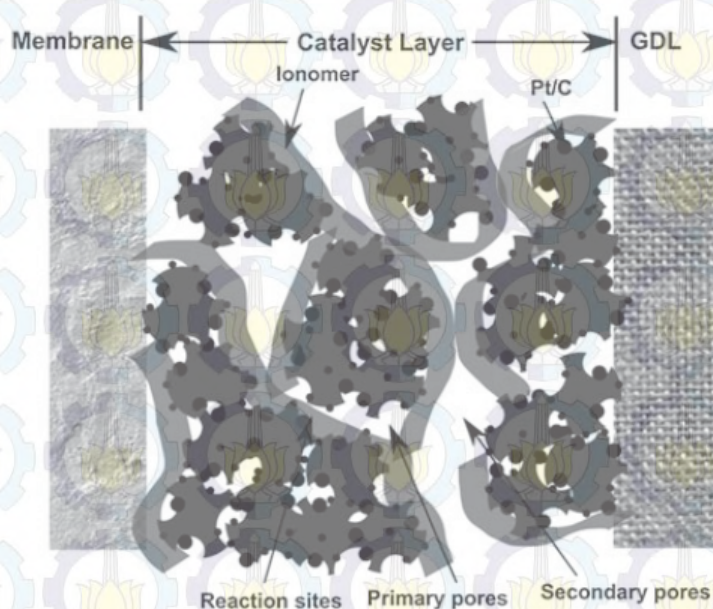


Figure 2.3 Schematic of catalyst layer components.<sup>15</sup>

### 2.1.1 Carbon Corrosion

Carbon based materials are chosen to be support material since its high specific surface area and electronic conductivity. However, carbon corrosion may take place as shown by Equation 2.1.<sup>28</sup> In recent years, carbon corrosion issue gets huge attention from the researches since it decreases fuel cell performance in long term operation.



Corrosion of the carbon support material causes dissolution, detachment and agglomeration of platinum nanoparticles such as explained in Figure 2.4.

Therefore, some support materials that is stable against corrosion have been developed such as conducting metal oxides, titanium diboride, etc.<sup>29</sup>

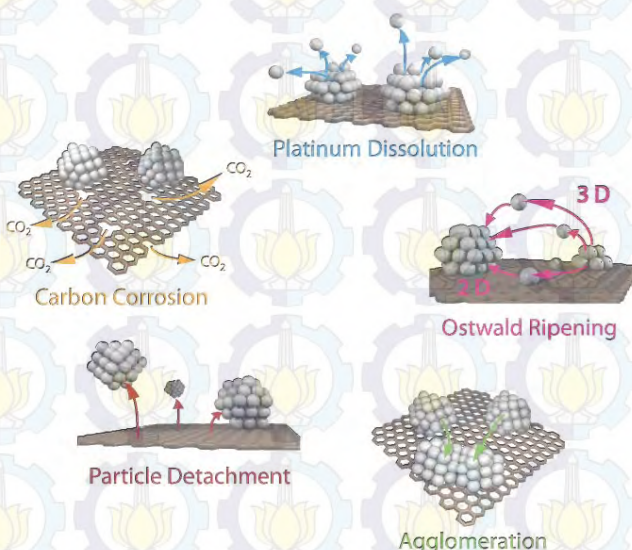


Figure 2.4 Simplified representation of suggested degradation mechanisms for platinum particles on a carbon support in fuel cells.<sup>30</sup>



### 2.1.2 Oxygen Reduction Reaction

The oxygen reduction reaction (ORR) is important reaction in proton exchange membrane (PEM) fuel cell. Various fuels such as hydrogen, methanol, ethanol, formic acid, 2-propanol, hydrazine, dimethyl ether, ethylene glycol and dimethoxy methane, depend on the fuel type, are oxidized to form protons and electrons on the anode side. While on cathode side, oxygen is reduced to form water in presence of protons and electrons.<sup>31</sup> Normally, the ORR kinetic is very slow, therefore appropriate ORR catalyst is needed in order to increase the reaction rate. The best oxygen reduction reaction activity is achieved by platinum such as explained in Figure 2.5.

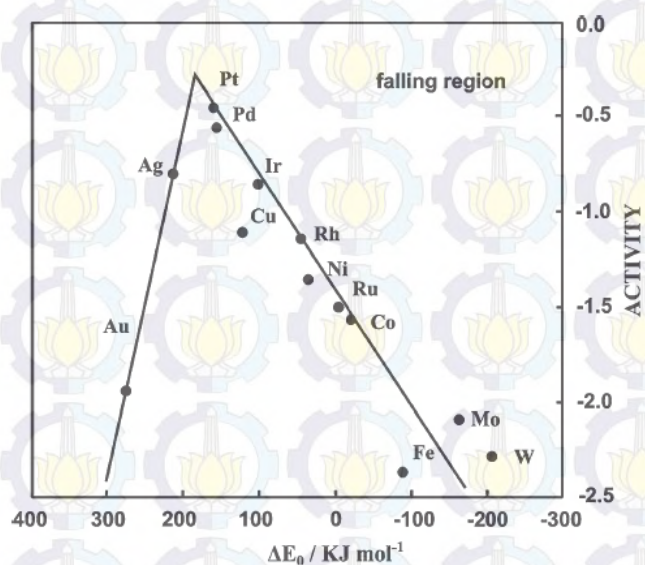


Figure 2.5 Volcano plot for ORR activity.<sup>32</sup>

ORR in aqueous solutions mainly occurs by two pathways. The first is direct 4-electrons reduction pathway from oxygen to water and the second is 2-electrons reduction pathway from oxygen to hydrogen peroxide. In the fuel cell

process, direct 4-electron pathway is highly preferred. Several ORR processes with their corresponding thermodynamic electrode potentials at standard conditions are listed below.<sup>33</sup>

*In acidic medium*



or



*In alkaline medium*



or



ORR on platinum metal is the most extensively studied mechanism. ORR catalysis is multi-electron process with a number of elementary steps, involving different reaction intermediates. It has been investigated by theoretical calculation based on the electronic structure, using density functional theory. The dissociative and associative mechanism has also been proposed.<sup>34</sup> But nowadays, the most accepted ORR catalysis process on the molecular level is the associative mechanism.<sup>35</sup> The detailed mechanism of both dissociative and associative mechanism is listed below.<sup>33</sup>



#### *Dissociative mechanism*



#### *Associative mechanism*



### **2.1.3 Electrocatalyst Characterization**

In order to evaluate catalyst performance, electrochemical method is very important since they are required in characterization of electrocatalyst. Some electrochemical methods, such as cyclic voltammetry (CV), linear sweep voltammetry (LSV) and rotating disk electrode (RDE), are commonly used to characterize the electrocatalyst.<sup>34</sup>

#### **2.1.3.1 ECSA Evaluation**

Electrochemically active surface area (ECSA) can be evaluated by performing cyclic voltammetry (CV) of electrocatalyst in oxygen free electrolyte.<sup>35</sup> In CV measurement, cyclic voltammogram is obtained by plotting the current at working electrode versus applied potential. In case of platinum

electrocatalyst, cyclic voltammogram which has some regions such as explained in Figure 2.6 will be obtained.

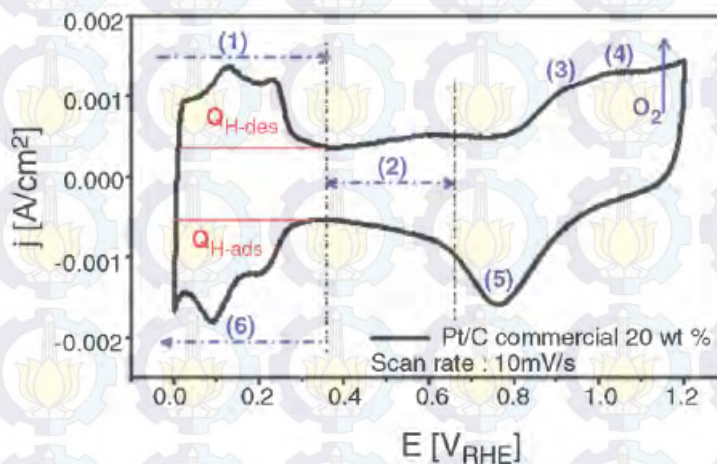


Figure 2.6 Cyclic voltammogram of platinum electrocatalyst.<sup>34</sup>

The different regions describe different processes which occur on the surface of platinum electrocatalyst. Region 1, extending from 0.00 to 0.35 V vs. RHE, represents the desorption process of adsorbed hydrogen from the surface of platinum electrocatalyst. The integrated anodic charge under hydrogen desorption area, in Coulombs, is denoted as  $Q_{\text{H-des}}$ . Appearance of some well-defined peaks indicates the presence of different platinum crystalline facets. The double layer charging and discharging are shown in Region 2, ranging from 0.35 to 0.65 V vs. RHE. The existence of two peaks in Region 3 and 4, higher than 0.65 V vs. RHE, are resulted by the formation of OH and O on the surface of platinum electrocatalyst respectively since platinum catalyzes water dissociation. Beyond Region 4, oxygen gas evolution starts to dominate.

Reversing the scan direction causes reduction of oxide layer which is observed in Region 5. Compared to the oxide formation peak, the oxide reduction



peak is shifted to the lower potentials. During the cathodic scan from 0.35 V vs. RHE, the under-potential deposition of hydrogen atoms occurs since protons are reduced. The integrated cathodic charge of hydrogen adsorption area, in Coulombs, is denoted as  $Q_{H-ads}$ . The hydrogen adsorption exhibits some well-defined peaks due to different platinum crystalline facets which is similar in hydrogen desorption process.

The ECSA ( $\text{m}^2 \text{g}^{-1}$ ) can be calculated by using formula in Equation 2.16, where  $Q_{H-des}$  is integrated anodic charge under hydrogen desorption area (C) and  $w_{Pt}$  is mass of platinum catalyst (g). While  $qH$  is the adsorption charge of hydrogen monolayer on platinum surface which has been estimated to be  $210 \mu\text{C cm}^{-2}$ . Normally, smaller platinum particle size gives large ECSA.<sup>34</sup>

$$ECSA = \frac{Q_{H-des} (C)}{qH \times w_{Pt} (g)} \quad (2.16)$$

#### 2.1.3.2 ORR Activity Evaluation

The combination of linear sweep voltammetry (LSV) and rotating disk electrode (RDE) can be utilized to obtain several intrinsic parameters of the electrocatalyst. In LSV, the potential of the working electrode is scanned from potential which is no reaction occurs to potential which is reaction occurs. Furthermore, if the overpotential is high enough, the reaction rate will be determined by diffusion mass transport of the reactant on rotating electrode.

Mass transport can be increased by introducing a forced convection which allows the electrolyte to flow and reaches working electrode. RDE is a



popular method in creating the relative movement by rotating a working electrode. Therefore, RDE is also known as hydrodynamic working electrode since steady-state current is determined by solution flow rather than diffusion.

The activity of the electrocatalyst includes kinetic parameter of Tafel slope, mass activity and specific activity. Figure 2.7 shows a representative sequence steps in evaluating the activity of carbon supported Pt and Pt-Co catalyst towards ORR.

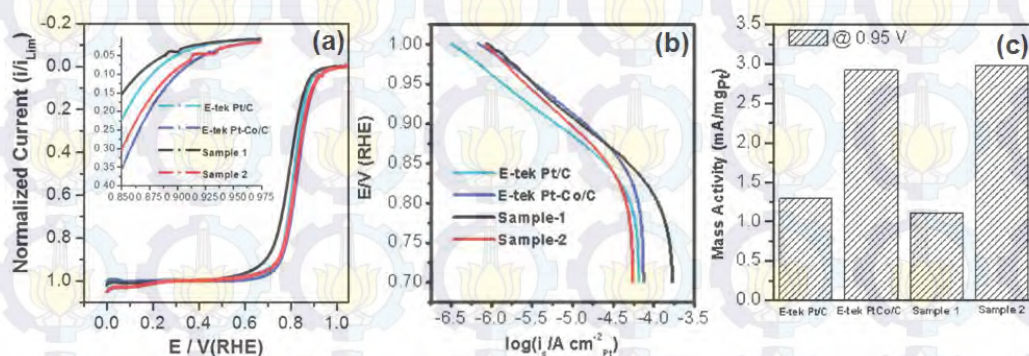


Figure 2.7 Evaluation of electrocatalyst activity towards ORR for carbon supported Pt and Pt-Co. (a) LSV result in 0.5 M  $H_2SO_4$  at 25 °C with rotation speed 2,500 rpm and sweep rate 1  $mV\ s^{-1}$ , (b) Tafel plots and (c) mass activity measured at 0.95 V vs. RHE.<sup>36</sup>

The ORR on all those electrocatalysts is diffusion-controlled region since the potential is less than 0.7 V vs. RHE, and is under a mixed control region of diffusion-kinetics when the potential is ranging from 0.7 to 0.85 V vs. RHE such as shown in the Figure 2.7 (a). The value of diffusion limited can also be obtained by linearizing the observed current in 0.00 to 0.7 V vs. RHE since the values are almost constant. The result of the linearization is known as the diffusion limited current, denoted as  $i_d$ , which can be used to compare ORR activity of the



electrocatalysts. In the mixed potential and Tafel region, higher than 0.85 V vs. RHE, the ORR activities show a significant difference in their magnitudes. It can be clearly visualized from the inset of Figure 2.7 (a) that E-Tek Pt-Co/C and Sample 2 show drastically enhanced activity compared to E-Tek Pt/C. On the other hand, the Sample 1 shows poor activity toward ORR.<sup>34</sup>

## 2.2 Ti<sub>4</sub>O<sub>7</sub> Synthesis

Titanium oxides generally feature low environmental burden, biocompatibility, low cost, and chemical stability.<sup>37</sup> Recently, conductive Magnéli phase materials such as Ti<sub>n</sub>O<sub>2n-1</sub> (4 < n < 10) have been explored as electrode material or conductive support in electrochemical systems. These materials are very interesting since its high conductivity and stability against corrosion in acidic and alkaline electrolytes. Among the series of distinct mixed-valence oxides, Ti<sub>4</sub>O<sub>7</sub> exhibits the highest electronic conductivity, about 10<sup>3</sup> S cm<sup>-1</sup> at room temperature.<sup>38</sup> Due to its superior conductivity and stability against corrosion, Ti<sub>4</sub>O<sub>7</sub> has been utilized as support material in fuel cell catalyst.<sup>13,20,21,23,24,28,39-43</sup>

Synthesis of Ti<sub>4</sub>O<sub>7</sub> is very challenging since it requires high temperature. Generally, Ti<sub>4</sub>O<sub>7</sub> is synthesized by reducing TiO<sub>2</sub> high temperature, about 1,000 °C, in H<sub>2</sub> atmosphere.<sup>44</sup> This condition results uncontrollable particle growth of Ti<sub>4</sub>O<sub>7</sub> that may reduce its surface area.

### 2.2.1 Recent Developments

Ioroi et al synthesized Ti<sub>4</sub>O<sub>7</sub> by reducing commercial TiO<sub>2</sub> at 1,050 °C for 6 hours in H<sub>2</sub> atmosphere, it resulted very low surface area Ti<sub>4</sub>O<sub>7</sub>, 2 m<sup>2</sup> g<sup>-1</sup>.



Furthermore, they deposited platinum on  $\text{Ti}_4\text{O}_7$  by impregnation-reduction method using  $\text{Pt}(\text{NO}_2)_2(\text{NH}_3)_2$  solution as platinum precursor. The catalyst and cell performance which they obtained was shown in Figure 2.8.

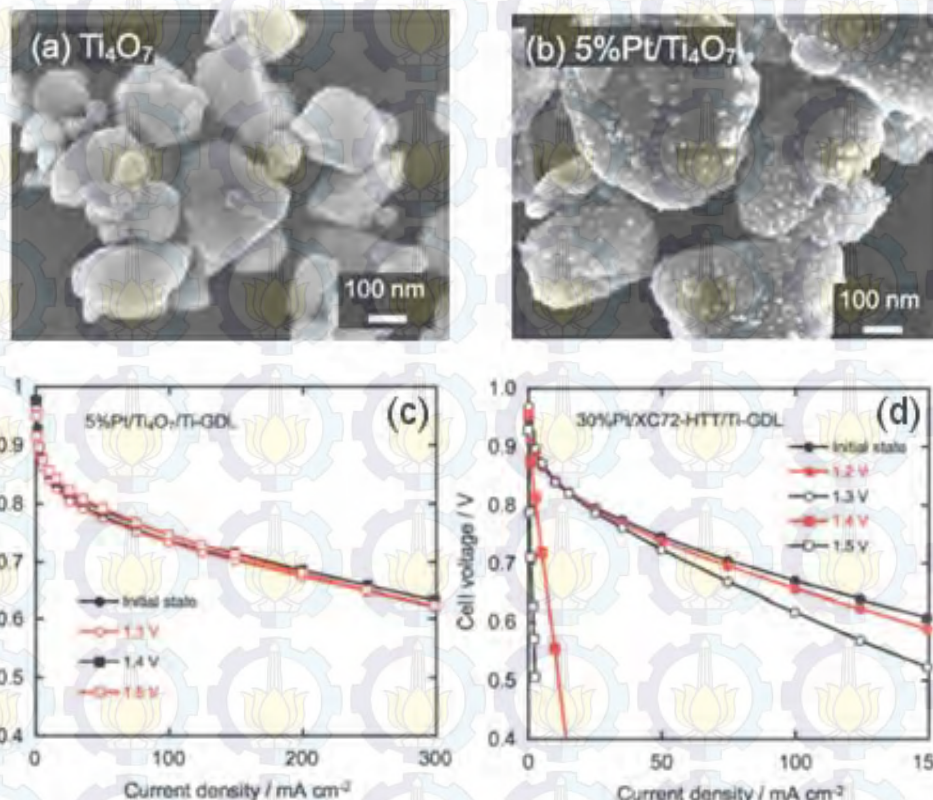


Figure 2.8 SEM images of (a) prepared  $\text{Ti}_4\text{O}_7$  support and (b) 5% Pt/ $\text{Ti}_4\text{O}_7$ . Polarization curves of a single cell with (c) 5% Pt/ $\text{Ti}_4\text{O}_7$  and (d) 30% Pt/XC72-HTT cathodes at the initial state and after potential holding in  $\text{O}_2$  at 1.2–1.5 V for 1 hour.<sup>20</sup>

Zhu et al synthesized  $\text{Ti}_4\text{O}_7$  by using different approach, they utilized carbon black to reduce  $\text{TiO}_2$  at 1,100 °C for 2 hours in vacuum atmosphere.  $\text{Ti}_4\text{O}_7$  which was resulted has low surface area, about  $4 \text{ m}^2 \text{ g}^{-1}$ . They also optimized the optimum temperature in synthesizing  $\text{Ti}_4\text{O}_7$  by this method, they found that optimum temperature was 1,025 °C such as explained in Table 2.1.



Table 2.1 Phase composition in the temperature range of 800-1,025 °C.<sup>22</sup>

Sample temperature (°C)	Phase composition (according to X-ray data)
800	TiO <sub>2</sub> (r) + TiO <sub>2</sub> (a)
900	TiO <sub>2</sub> (r) + Ti <sub>9</sub> O <sub>17</sub>
1,000	Ti <sub>9</sub> O <sub>17</sub> + Ti <sub>6</sub> O <sub>11</sub> + Ti <sub>7</sub> O <sub>13</sub>
1,025	Ti <sub>4</sub> O <sub>7</sub> + Ti <sub>5</sub> O <sub>9</sub>

Senevirathne et al synthesized Ti<sub>4</sub>O<sub>7</sub> by utilizing electrospinning in order to obtain high surface area TiO<sub>2</sub>. Then, they reduced it at 1,050 °C for 6 hours in H<sub>2</sub>:N<sub>2</sub> atmosphere. Surface area of TiO<sub>2</sub> that was resulted by electrospinning was 13 m<sup>2</sup> g<sup>-1</sup>. While the surface of Ti<sub>4</sub>O<sub>7</sub> that was resulted after reduction process decreased to 6 m<sup>2</sup> g<sup>-1</sup>. Furthermore, they deposited platinum on Ti<sub>4</sub>O<sub>7</sub> by NaBH<sub>4</sub> reduction method using H<sub>2</sub>PtCl<sub>6</sub> as a platinum precursor in order to obtain 20 wt% Pt/Ti<sub>4</sub>O<sub>7</sub>. The morphology of their materials in each step was shown in Figure 2.9. Finally, they also performed durability test for 20 wt% Pt/Ti<sub>4</sub>O<sub>7</sub> and found that it was stable support material since amount of loss ECSA was very low. In addition, the ORR mass activity of 20 wt% Pt/Ti<sub>4</sub>O<sub>7</sub> was not decrease significantly before and after durability test such as shown in Figure 2.10.

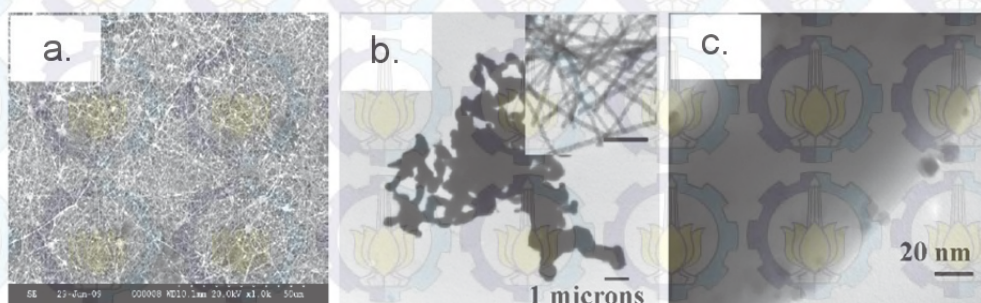


Figure 2.9 Scanning and transmission electron microscopic images of (a) as-spun TiO<sub>2</sub>/PVP composite, (b) Ti<sub>4</sub>O<sub>7</sub> nanofibers and (c) 20-wt% Pt/Ti<sub>4</sub>O<sub>7</sub>.



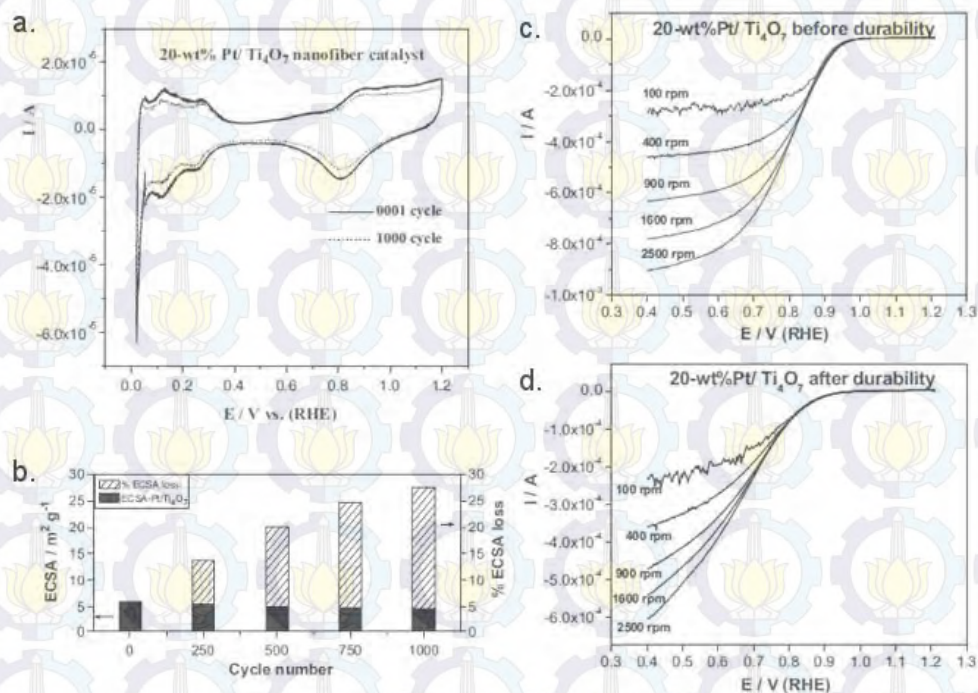


Figure 2.10 Cyclic voltammograms of (a) 20-wt% Pt/Ti<sub>4</sub>O<sub>7</sub> catalyst before and after durability test, (b) plot of the ECSA and its percentage loss as a function of potential cycles number, ORR curves of 20-wt% Pt/Ti<sub>4</sub>O<sub>7</sub> nanofiber catalysts (c) before and (d) after durability test.<sup>23</sup>

Yao et al utilized silica to cover nanotube TiO<sub>2</sub>, it aimed to protect particle agglomeration during heat treatment at 1,050 °C for 4 hours in H<sub>2</sub> atmosphere. The scheme of this method was shown in Figure 2.11.

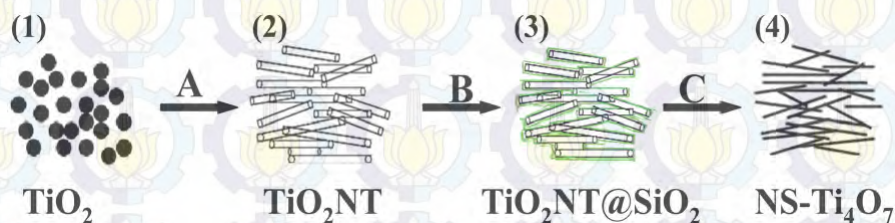


Figure 2.11 Multistep reaction pathway in synthesizing NS-Ti<sub>4</sub>O<sub>7</sub>.

Ti<sub>4</sub>O<sub>7</sub> which was resulted by this approach had higher surface area than the previous methods, it was  $26 m^2 g^{-1}$ . Furthermore, they deposited platinum on



Ti<sub>4</sub>O<sub>7</sub> by a modified ethylene glycol reduction method using Pt(acac)<sub>2</sub> as platinum precursor in order to obtain 13% Pt/NS-Ti<sub>4</sub>O<sub>7</sub>. Then, they performed durability test by potential cycling until 3,000 cycles. They found that it was stable support material since amount of loss ECSA was lower than carbon support such as explained in Figure 2.12. TEM images also had good agreement with those result which clearly showed in Figure 2.13 that particles size of Pt/XC-72 and Pt/NS-Ti<sub>4</sub>O<sub>7</sub> grow from 3.0 to 10.2 and 4.8 to 6.1 nm respectively.

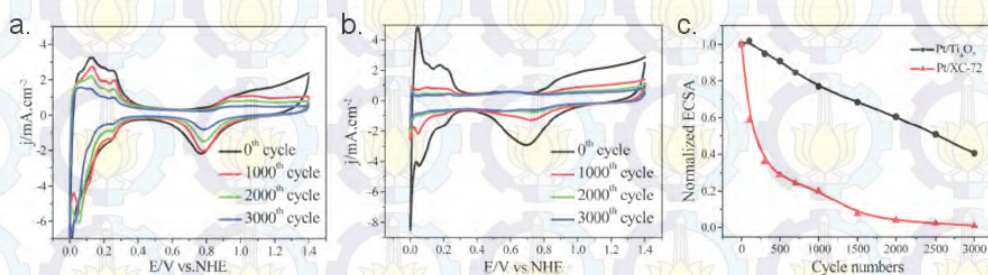


Figure 2.12 CV plots of (a) Pt/NS-Ti<sub>4</sub>O<sub>7</sub>, (b) Pt/XC-72 obtained at room temperature and (c) normalized ECSA as a function of cycle number for Pt/NS-Ti<sub>4</sub>O<sub>7</sub> and Pt/XC-72.

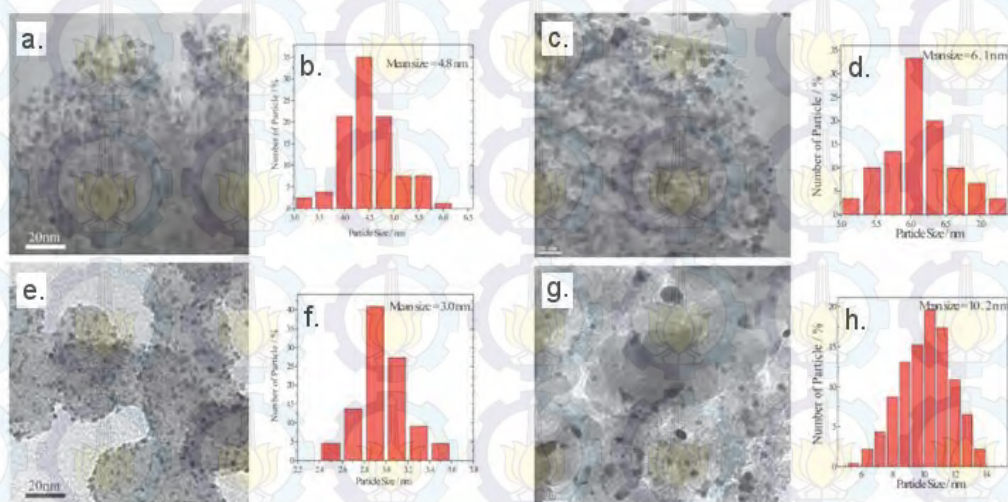


Figure 2.13 TEM images of Pt/NS-Ti<sub>4</sub>O<sub>7</sub> (a) before and (c) after durability test. TEM images of Pt/XC-72 (e) before and (g) after durability test.



The highest surface area  $\text{Ti}_4\text{O}_7$  was achieved by Nazar's group that successfully synthesized  $\text{Ti}_4\text{O}_7$  for Li batteries purpose by utilizing Ti(IV) ethoxide and poly(ethylene glycol), average  $M_w = 400$  (PEG 400). PEG 400 had two functions in this method, first it served as reducing agent since it contained carbon. Second, it prevented particle agglomeration during heat treatment at  $950^\circ\text{C}$  in Ar atmosphere due to its polymeric structure. The surface area of  $\text{Ti}_4\text{O}_7$  that was  $290\text{ m}^2\text{ g}^{-1}$ , but it contained amorphous carbon residue about 15.4 wt%. Figure 2.14 showed XRD pattern of  $\text{Ti}_4\text{O}_7$  which was obtained by this new method.

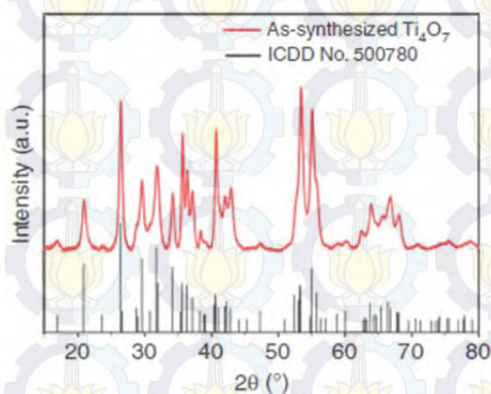


Figure 2.14 X-ray diffraction pattern of  $\text{Ti}_4\text{O}_7$ .<sup>25</sup>

Since 15.4 wt% amorphous carbon residues remained in  $\text{Ti}_4\text{O}_7$ , they attempted to modify the previous method by decreasing reduction temperature to  $870^\circ\text{C}$  and replacing PEG with ethylenimine (oligomer mixture,  $M_n \sim 400$ ). XRD pattern of the  $\text{Ti}_4\text{O}_7$  was shown in Figure 2.15. Since carbon content of ethylenimine was lower than PEG, the amount of amorphous carbon residue could



be successfully reduced to less than 2 wt%. Unfortunately the surface area of  $\text{Ti}_4\text{O}_7$  was also decrease to  $180 \text{ m}^2 \text{ g}^{-1}$ .

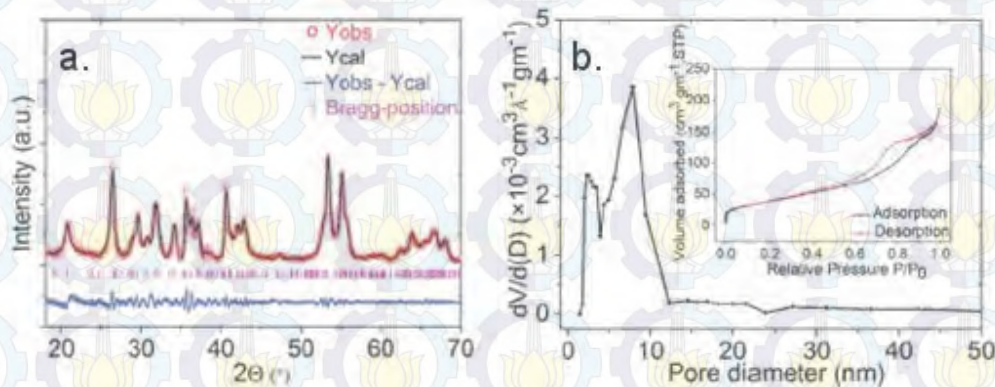


Figure 2.15 (a) Rietveld refinement of the as synthesized  $\text{Ti}_4\text{O}_7$  powder XRD pattern. (b) Pore size distribution of  $\text{Ti}_4\text{O}_7$  with the inset image showing the type-IV nitrogen adsorption-desorption isotherm.<sup>45</sup>

### 2.2.2 Summary

In order to obtain high surface area  $\text{Ti}_4\text{O}_7$ , researchers have made various synthesis condition of  $\text{Ti}_4\text{O}_7$  which is summarized in Table 2.2. It shows that the best synthesis condition to obtain high surface area  $\text{Ti}_4\text{O}_7$  is achieved by Nazar's group, but the drawback of their method is the presence of amorphous carbon residue. Therefore, utilizing the method in synthesizing  $\text{Ti}_4\text{O}_7$  for fuel cell catalyst support should be reconsidered. At least, some modification or follow up should be made in order to avoid or reduce the presence of amorphous carbon residue in the final product of  $\text{Ti}_4\text{O}_7$ .

Table 2.2 Summary of Ti<sub>4</sub>O<sub>7</sub> synthesis strategy, sorted by the surface area.

Ti(IV) source	Reduction condition			Reducing agent	Surface area (m <sup>2</sup> g <sup>-1</sup> )	Carbon content (wt%)	Conductivity (S cm <sup>-1</sup> )	Ref.
	Temp. (°C)	Time (h)	Atm.					
TiO <sub>2</sub>	1,050	6	H <sub>2</sub>	H <sub>2</sub>	2	n.a.	n.a.	20
TiO <sub>2</sub>	1,025	2	vacuum	carbon black	~4	n.a.	n.a.	22
titanium(IV) isopropoxide	1,050	6	H <sub>2</sub> :N <sub>2</sub>	H <sub>2</sub>	6	n.a.	3.4×10 <sup>-5</sup>	23
TiO <sub>2</sub>	1,050	4	H <sub>2</sub>	H <sub>2</sub>	26	n.a.	n.a.	24
titanium(IV) ethoxide	860	3-4	Ar	PEI	180	<2	5	45
titanium(IV) ethoxide	950	n.a.	Ar	PEG	290	15.4	3.2±0.1	25



## CHAPTER 3

### EXPERIMENTAL SECTION

#### 3.1 Chemicals and Equipments

##### 3.1.1 Chemicals

The chemicals which were used in the work were ethanol (Acros Organics), titanium(IV) ethoxide (33-35% TiO<sub>2</sub>, Acros Organics), poly(ethylene glycol) (Mw = 400, Acros Organics), ethylene glycol (99+%, extra pure, Acros Organics), hexachloroplatinic acid hexahydrate (Acros Organics), NaOH pellets (Fisher Scientific), n-heptane (Acros Organics), 1,2-dichlorobenzene (Acros Organics), H<sub>2</sub>SO<sub>4</sub> (95-98%, Scharlau), 5% Nafion 117 (Sigma-Aldrich), ethanol (99.5%, Shimakyu's Pure Chemicals), isopropanol (99+%, Acros Organics), carbon black (Alfa Aesar) and 20 wt% Pt/C (Alfa Aesar).

##### 3.1.2 Equipments

The equipments which were used in the work were hotplate and stirrer (Corning), micropipette (10 µL; 500 µL; 1000 µL), tubular furnace (SJ High Technology Company), ultrasonic cleaner (Delta), pH meter (Mettler Toledo SevenGo), microwave reactor (CEM Discover), centrifuge machine (Beckman Coulter Allegra 64R), X-ray diffractometer (Bruker D2 Phaser), thermogravimetric analyzer (TA Instruments Q500), physisorption analyzer (Micromeritics ASAP 2020), scanning electron microscope (JEOL JSM 6500F), standard four-probe equipment (KeithLink Technology Taiwan),

potentiostat/galvanostat (Autolab PGSTAT302N), glassy carbon electrode ( $0.1964 \text{ cm}^2$  geometric surface area, Pine Instruments), rotating disk electrode (Pine Instrument), Pt wire and Ag/AgCl reference electrode (Metrohm).

## **3.2 Synthesis Methodology**

### **3.2.1 Synthesis of $\text{Ti}_4\text{O}_7$ Support Material**

$\text{Ti}_4\text{O}_7$  was synthesized by following Nazar's group method<sup>25</sup> with several modifications. The synthesis was started by adding 3 mL ethanol (Acros Organics) and then followed by adding 1 g titanium(IV) ethoxide (33-35%  $\text{TiO}_2$ , Acros Organics) and 0.3, 0.4 and 0.5 g poly(ethylene glycol) ( $M_w = 400$ , Acros Organics) respectively. The mixture was stirred at 60-80 °C for 24 hours on the hotplate (Corning) in order to homogenize it and followed by heating at 100 °C for 4-6 hours in order to obtain white flakes. Then, it was grinded using mortar and pestle and followed by calcinations at 950 °C for 4 hours (heating rate = 5 °C  $\text{min}^{-1}$ ) in Ar atmosphere. The calcinations were done in the tubular furnace (SJ High Technology Company).

### **3.2.2 Synthesis of 20 wt% Pt/ $\text{Ti}_4\text{O}_7$ Catalyst**

Platinum nanopartilces were deposited on the  $\text{Ti}_4\text{O}_7$  support by following Ho's work<sup>27</sup> which utilized microwave-assisted polyol synthesis. The synthesis of 20 wt% Pt/ $\text{Ti}_4\text{O}_7$  catalyst was started by adding 1 g  $\text{Ti}_4\text{O}_7$  support material into 20 mL ethylene glycol (99+%, extra pure, Acros Organics) and followed by ultrasonication for one hour. Yellowish solution which was prepared by adding 0.0664 g hexachloroplatinic acid hexahydrate (Acros Organics) into 5 mL



ethylene glycol (99+%, extra pure, Acros Organics) was added into the mixture and followed by ultrasonication for one hour. 0.8 M NaOH which was prepared by adding 0.8 g NaOH pellets (Fisher Scientific) into 25 mL ethylene glycol (99+%, extra pure, Acros Organics) was added into the mixture until pH = 11. The pH value was measured by pH meter (Mettler Toledo SevenGo). Then, the mixture was heated at 160 °C (200 W) for one hour (heating rate = 10 °C min<sup>-1</sup>) by utilizing microwave reactor (CEM Discover). When the reaction finished, the sample was cooled, collected by repeated centrifugation and washed with acetone. The centrifugation was done by utilizing centrifuge machine (Beckman Coulter Allegra 64R) in F0850 rotor and rotation speed 16,500 rpm. Finally, the sample was dried at 80 °C for 12 hours in the oven.

### **3.3 Carbon removal of Ti<sub>4</sub>O<sub>7</sub> Support Material**

#### **3.3.1 Extraction treatment**

The carbon removal of Ti<sub>4</sub>O<sub>7</sub> support material by extraction treatment was begun by adding 0.2 g sample into the bottle and followed by adding 6 mL DI water, 4 mL n-heptane (Acros Organics) and 2 mL 1,2-dichlorobenzene (Acros Organics). The mixture was shaken and followed by removal of organic phase, the extraction process was repeated three times. Then, the sample was collected by repeated centrifugation and washed with ethanol. The centrifugation was done by utilizing centrifuge machine (Beckman Coulter Allegra 64R) in F0850 rotor and rotation speed 10,000 rpm. Finally, the sample was dried at 80 °C for 24 hours in the oven.

### 3.3.2 Solvent treatment

The carbon removal of  $\text{Ti}_4\text{O}_7$  support material by solvent treatment was begun by adding 0.2 g sample into the bottle and followed by adding 5 mL 1,2-dichlorobenzene (Acros Organics) and stirring at 80 °C for one hour. Then, the sample was collected by repeated centrifugation and washed with acetone. The centrifugation was done by utilizing centrifuge machine (Beckman Coulter Allegra 64R) in F0850 rotor and rotation speed 10,000 rpm. Finally, the sample was dried at 80 °C for 24 hours in the oven.

### 3.3.3 Acid-base treatment

The carbon removal of  $\text{Ti}_4\text{O}_7$  support material by acid-base treatment was begun by adding 0.2 g sample into the bottle and followed by adding 5 mL 2 M  $\text{H}_2\text{SO}_4$  and 5 mL 2 M NaOH respectively and stirring at 80 °C for one hour. Then, the sample was collected by repeated centrifugation and washed with DI water. The centrifugation was done by utilizing centrifuge machine (Beckman Coulter Allegra 64R) in F0850 rotor and rotation speed 10,000 rpm. Finally, the sample was dried at 80 °C for 24 hours in the oven.

Prior to the treatment, 2 M  $\text{H}_2\text{SO}_4$  was prepared by adding small amount of DI water into 100 mL volumetric flask and followed by adding 11.1 mL  $\text{H}_2\text{SO}_4$  (95-98%, Scharlau) and DI water until the line. While 2 M NaOH was prepared by adding 8 g NaOH pellets (Fisher Scientific) into 100 mL volumetric flask and followed by adding DI water until the line.



### 3.4 Material Characterization

Powder X-ray diffraction (XRD) patterns of  $\text{Ti}_4\text{O}_7$  support material and 20 wt% Pt/ $\text{Ti}_4\text{O}_7$  catalyst were obtained by utilizing X-ray diffractometer (Bruker D2 Phaser). The data were collected from  $20^\circ$  to  $80^\circ$  in  $2\theta$  scale by using Cu K $\alpha$  radiation. Amorphous carbon residue amount of  $\text{Ti}_4\text{O}_7$  support material was obtained by utilizing thermogravimetric analyzer (TA Instruments Q500). The measurement was done in air atmosphere and the data were collected from 40 to 800  $^\circ\text{C}$ . Surface area and pore size of  $\text{Ti}_4\text{O}_7$  support material were obtained by utilizing physisorption analyzer (Micromeritics ASAP 2020). The measurement was begun by sample degassing at 200  $^\circ\text{C}$  for 6 hours in order to completely vaporize water molecules and other impurities in the oxide pores. Morphology of the  $\text{Ti}_4\text{O}_7$  support material was obtained by utilizing scanning electron microscope (JEOL JSM 6500F) with an accelerating voltage 15 kV. Electronic conductivity of the  $\text{Ti}_4\text{O}_7$  support material was measured by utilizing standard four-probe equipment (KeithLink Technology Taiwan). Before the measurement,  $\text{Ti}_4\text{O}_7$  powder was made into pellet by utilizing hydraulic press, ~13 mm diameter and ~1 mm thickness.

### 3.5 Electrochemical Measurement

A three-electrode cell including working electrode, counter electrode and reference electrode which was connected to a potentiostat/galvanostat (Autolab PGSTAT302N) was used to measure electrochemical activity of  $\text{Ti}_4\text{O}_7$  support material and 20 wt% Pt/ $\text{Ti}_4\text{O}_7$  catalyst. For comparison, electrochemical activity of carbon black (Alfa Aesar) and 20 wt% Pt/C (Alfa Aesar) were also measured.

The working electrode was the sample which was coated on glassy carbon electrode ( $0.1964\text{ cm}^2$  geometric surface area, Pine Instruments), while the counter electrode was platinum wire and the reference electrode was Ag/AgCl (Metrohm). The entire electrodes were assembled such as explained in Figure 3.1.

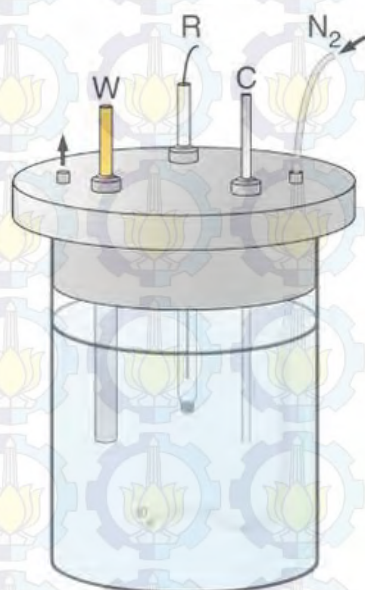


Figure 3.1 A three-electrode cell which was used to measure electrochemical activity of the catalyst.<sup>46</sup>

A known amount of  $\text{Ti}_4\text{O}_7$  support material and 20 wt% Pt/ $\text{Ti}_4\text{O}_7$  catalyst was dispersed in 500  $\mu\text{L}$  0.5% Nafion 117 solution by ultrasonication for 30 minutes respectively. Prior to sample dispersion, 0.5% Nafion 117 solution was previously prepared by dissolving 100  $\mu\text{L}$  5% Nafion 117 (Sigma-Aldrich) into 900  $\mu\text{L}$  ethanol (99.5%, Shimakyu's Pure Chemicals). For comparison, a known amount of 20 wt% Pt/ $\text{Ti}_4\text{O}_7$  catalyst was dispersed in 500  $\mu\text{L}$  0.1% Nafion 117 solution by ultrasonication for 30 minutes. Prior to sample dispersion, 0.1% Nafion 117 solution was previously prepared by dissolving 20  $\mu\text{L}$  5% Nafion 117

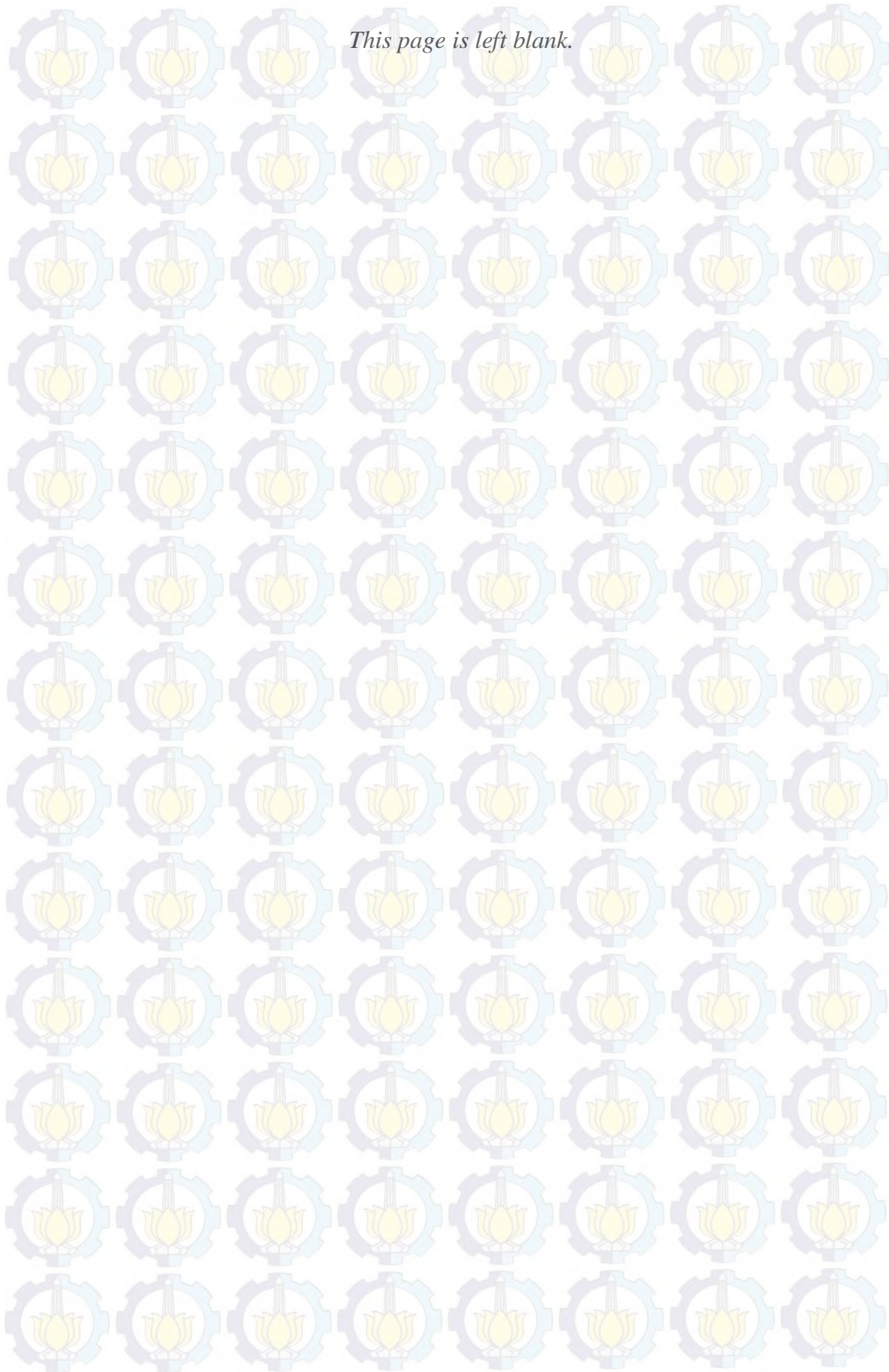


(Sigma-Aldrich) into 980  $\mu\text{L}$  ethanol (99.5%, Shimakyu's Pure Chemicals). Then, 7  $\mu\text{L}$  of the suspension was placed on the glassy carbon electrode and dried in order to obtain uniform thin film.

Another catalyst coating technique on the glassy carbon electrode was prepared by dispersing known amount of 20 wt%  $\text{Pt}/\text{Ti}_4\text{O}_7$  catalyst in the mixture of isopropanol (99+%, Acros Organics) and DI water (95:5 volume ratio) and followed by ultrasonication for 30 minutes. Then, 7  $\mu\text{L}$  of the suspension was placed on the glassy carbon electrode and dried in order to obtain uniform thin film. Finally, 7  $\mu\text{L}$  of 0.01% Nafion 117 solution which was previously prepared by dissolving 1  $\mu\text{L}$  5% Nafion 117 (Sigma-Aldrich) into 499  $\mu\text{L}$  ethanol (99.5%, Shimakyu's Pure Chemicals) was dropped on it and dried.

0.5 M  $\text{H}_2\text{SO}_4$  which was previously prepared by adding small amount of DI water into 2,000 mL volumetric flask and followed by adding 55.48 mL  $\text{H}_2\text{SO}_4$  (95-98%, Scharlau) and DI water until the line was utilized as the electrolyte in all electrochemical measurements. CV measurement of entire samples was done under Ar purging and potential was swept from 0.05 to 1.10 V vs. RHE at the scan rate 25  $\text{mV s}^{-1}$ . Prior to the CV measurement, the solution was purged by Ar for 30 minutes and the electrode was activated by 10 times potential cycling at the scan rate 50  $\text{mV s}^{-1}$ . Steady-state polarization measurement of ORR was done under oxygen purging and the potential was swept from 1.0 to 0.05 V vs. RHE (backward scan) at the scan rate 1  $\text{mV s}^{-1}$ . Prior to the measurement, the solution was purged by oxygen for 30 minutes and the electrode was rotated at 1,600 rpm until the measurement finished.

*This page is left blank.*





## CHAPTER 4

### RESULT AND DISCUSSION

#### 4.1 Characterization of $\text{Ti}_4\text{O}_7$ Support Material

High surface area  $\text{Ti}_4\text{O}_7$  was synthesized by following Nazar's group approach which utilized Ti(IV) ethoxide as Ti(IV) precursor and PEG 400 as reducing agent.<sup>25</sup> The method was chosen since it had some advantages compared to other methods. First, it had ability to fabricate high surface area  $\text{Ti}_4\text{O}_7$  since the polymeric structure of PEG 400 was capable to prevent particle agglomeration during heat treatment. Second, it was safer than the others since it didn't utilize  $\text{H}_2$  gas to reduce Ti(IV) into  $\text{Ti}_4\text{O}_7$ . So the accidental risk due to  $\text{H}_2$  gas explosion could be avoided. Third, it was cheaper than the others since it was capable to fabricate  $\text{Ti}_4\text{O}_7$  in relatively lower reduction temperature. So the electricity cost can be minimized. But, the presence small amount of amorphous carbon residue was drawback of the method since it utilized PEG 400 which mainly consisted of carbon as reducing agent.

Several variations has been made in order to find the best Ti(IV) ethoxide and PEG 400 ratio due to the amount of reducing agent was very important in the synthesis. Amount of PEG 400 which exceeded the requirement would cause formation of amorphous carbon residue in large number. But, if amount of PEG 400 was less than the requirement,  $\text{Ti}_4\text{O}_7$  wouldn't be formed since reducing agent was insufficient.

Therefore, amount of Ti(IV) ethoxide was made to be constant, 1 g, while amount of PEG 400 was varied to 0.3, 0.4 and 0.5 g. Furthermore, the entire samples were named as Ti10PEG03, Ti10PEG04 and Ti10PEG05 respectively.

#### 4.1.1 XRD Results

Since the crystal phase of the obtained  $\text{Ti}_4\text{O}_7$  support materials was very important, XRD measurement was employed in the material characterization.

XRD patterns of entire  $\text{Ti}_4\text{O}_7$  support materials are shown in Figure 4.1.

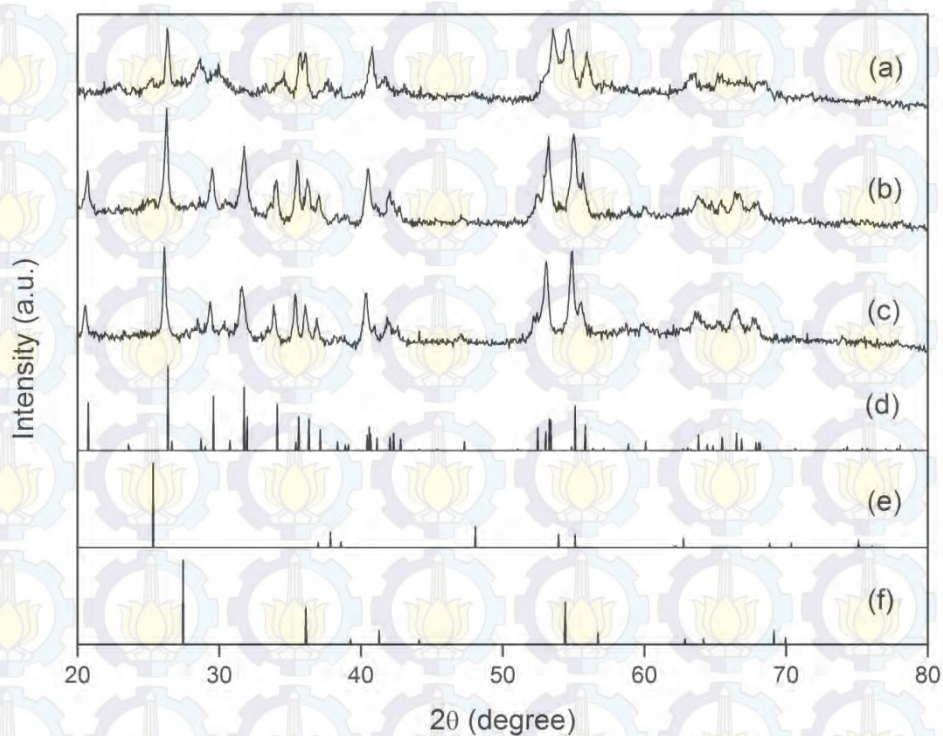


Figure 4.1 XRD patterns of (a) Ti10PEG03, (b) Ti10PEG04, (c) Ti10PEG05, (d)  $\text{Ti}_4\text{O}_7$  (PDF 50-0787), (e) anatase- $\text{TiO}_2$  (PDF 84-1286) and (f) rutile- $\text{TiO}_2$  (PDF 84-1284).

Compared to the standard XRD patterns, it can be clearly seen that the Ti10PEG03 sample doesn't completely match with  $\text{Ti}_4\text{O}_7$  standard XRD patterns.



The disappearance of some peaks at  $20.8^\circ$ ,  $31.8^\circ$ ,  $32^\circ$  and  $34.1^\circ$  indicates that Ti10PEG03 sample doesn't mainly consist of  $\text{Ti}_4\text{O}_7$ . The existence of  $\text{TiO}_2$  in both anatase and rutile phase can be observed from some peaks which belong to anatase- $\text{TiO}_2$  and rutile- $\text{TiO}_2$  at  $36.1^\circ$ ,  $54^\circ$ ,  $54.4^\circ$  and  $55.1^\circ$ .

Based on the XRD result, both of Ti10PEG04 and Ti10PEG05 sample mainly consist of  $\text{Ti}_4\text{O}_7$  since they match with most of  $\text{Ti}_4\text{O}_7$  standard XRD patterns. However, the XRD result of Ti10PEG05 sample little bit shift to the lower  $2\theta$  angle which can be seen from the peak at  $26.4^\circ$ . The result indicates increasing d-spacing value since the  $\theta$  and  $d$  value are on the same side in Bragg's Law. While the XRD result of Ti10PEG04 sample are located in the almost same  $2\theta$  angle with  $\text{Ti}_4\text{O}_7$  standard XRD patterns which indicates the d-spacing value of the sample are almost similar.

The entire XRD results reveal that amount of PEG 400 as reducing agent highly influences the obtained  $\text{Ti}_4\text{O}_7$  support materials. In order to obtain  $\text{Ti}_4\text{O}_7$ , the best amount of PEG 400 which should be added into 1 g Ti(IV) ethoxide is 0.4 g such as observed in Ti10PEG04 sample. Decreasing amount of PEG 400 to 0.3 g causes  $\text{Ti}_4\text{O}_7$  can't be formed since amount of PEG 400 is insufficient such as observed in Ti10PEG03 sample. While increasing amount of PEG 400 to 0.5 g still able to produce  $\text{Ti}_4\text{O}_7$  such as observed in Ti10PEG05 sample.

#### 4.1.2 Thermogravimetric Results

Utilization of PEG 400 which contains a lot of carbon in the synthesis might contribute to the formation of amorphous carbon residue inside the obtained  $\text{Ti}_4\text{O}_7$  support materials. Therefore, amount of amorphous carbon residue should

be determined quantitatively by employing thermogravimetric analysis since their existence may influence the catalyst performance. The thermogravimetric analysis result of entire  $\text{Ti}_4\text{O}_7$  support materials including Ti10PEG03, Ti10PEG04 and Ti10PEG05 sample are shown in Figure 4.2.

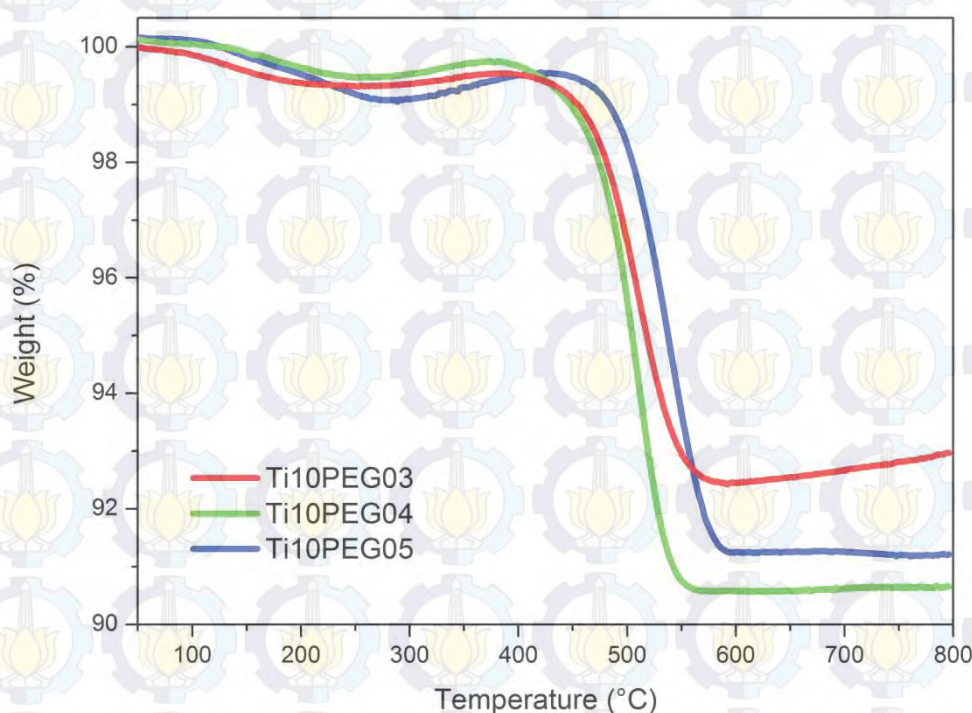


Figure 4.2 Thermogravimetric analysis results of  $\text{Ti}_4\text{O}_7$  support materials, heating rate =  $10\text{ }^{\circ}\text{C min}^{-1}$ .

The slight weight loss in the temperature range 100-350  $^{\circ}\text{C}$  is observed on the entire samples which are probably resulted by evaporation of water molecules and decomposition of some impurities. While in the temperature range 350-450  $^{\circ}\text{C}$ , the weight gain is observed on the entire samples. This phenomenon is probably caused by the oxidation of  $\text{Ti}_4\text{O}_7$  support materials into the stable  $\text{TiO}_2$  which was also found in Senevirathne's work.<sup>23</sup> Later, huge weight loss is observed in the temperature range 450-575  $^{\circ}\text{C}$  which is probably caused by



massive decomposition of remained carbon on the entire samples. Finally, no significant weight loss is observed in the temperature range 575-800 °C which probably indicates the carbon has been completely decomposed.

The carbon decomposition can be occurred since it is oxidized into CO<sub>2</sub> gas in the presence of oxygen. Furthermore, it is used as an indicator to determine amount of amorphous carbon residue which is summarized in Table 4.1. The entire samples contain amorphous carbon residue from 7.57 to 9.44 wt%, this results are lower than reported by Nazar's group since their amorphous carbon residue was 15.4 wt%.<sup>25</sup> The results reveal that the amount of amorphous carbon residue highly influenced the surface area of entire Ti<sub>4</sub>O<sub>7</sub> support materials. In addition, formation of amorphous carbon residue is the consequence which is almost impossible to be avoided in utilizing PEG 400 as reducing agent.

Table 4.1 Amount of amorphous carbon residue of Ti<sub>4</sub>O<sub>7</sub> support materials.

Sample	Amorphous carbon residue amount (wt%)
Ti10PEG03	7.57
Ti10PEG04	9.44
Ti10PEG05	8.82

#### 4.1.3 Physisorption Results

In order to get the information about surface area and pore size of the obtained Ti<sub>4</sub>O<sub>7</sub> support materials, physisorption analysis was employed in the material characterization. The information are very important since high surface area support material is required to allow dispersion of the electroactive material while its porosity contributes to fast mass transport of reactants and products. The

nitrogen sorption (adsorption and desorption) isotherms and their corresponding Barrett-Joyner-Halenda (BJH) pore size distributions of the entire samples are shown in Figure 4.3 and Figure 4.4 respectively, including Ti10PEG03, Ti10PEG04 and Ti10PEG05 sample.

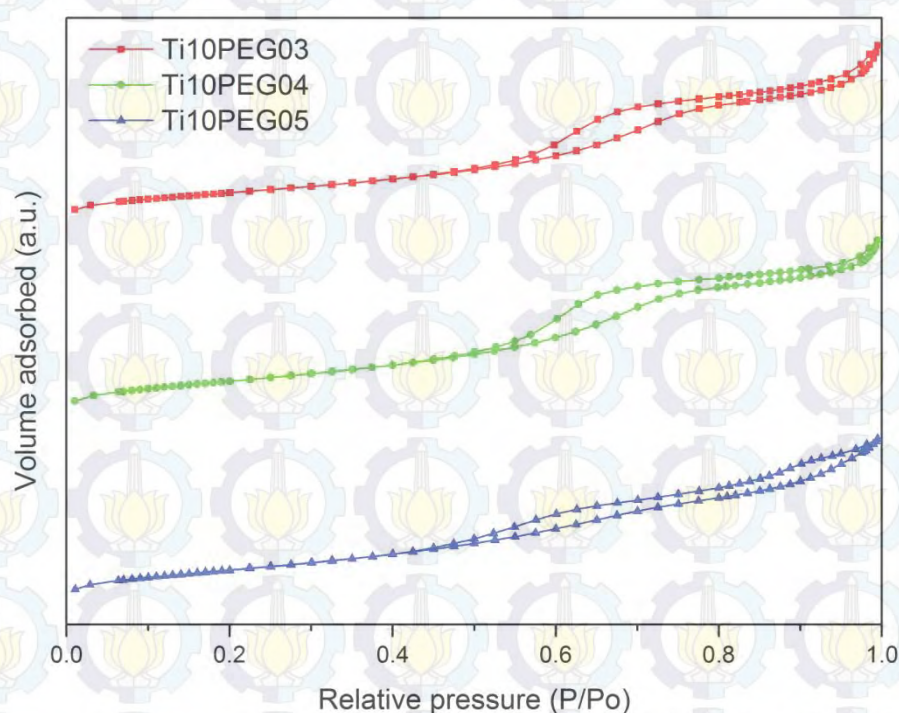


Figure 4.3 Adsorption and desorption isotherms of  $\text{Ti}_4\text{O}_7$  support materials.

The entire  $\text{Ti}_4\text{O}_7$  support materials exhibit type IV isotherm with a hysteric loop. It indicates the presence of mesopores (2-50 nm)<sup>47</sup> in the entire samples. The results are also supported by the pore size distribution results which clearly show that the average pore size distribution of the entire samples is 4-8 nm.

Furthermore, surface area of the entire  $\text{Ti}_4\text{O}_7$  support materials are shown in Table 4.2. The results are lower than commercial carbon support materials, Vulcan XC-72, which has surface area  $232 \text{ m}^2 \text{ g}^{-1}$ .<sup>48</sup> In addition, the results are



also lower than Nazar's group result which is probably caused by the decreasing amount of amorphous carbon residue.<sup>25</sup>

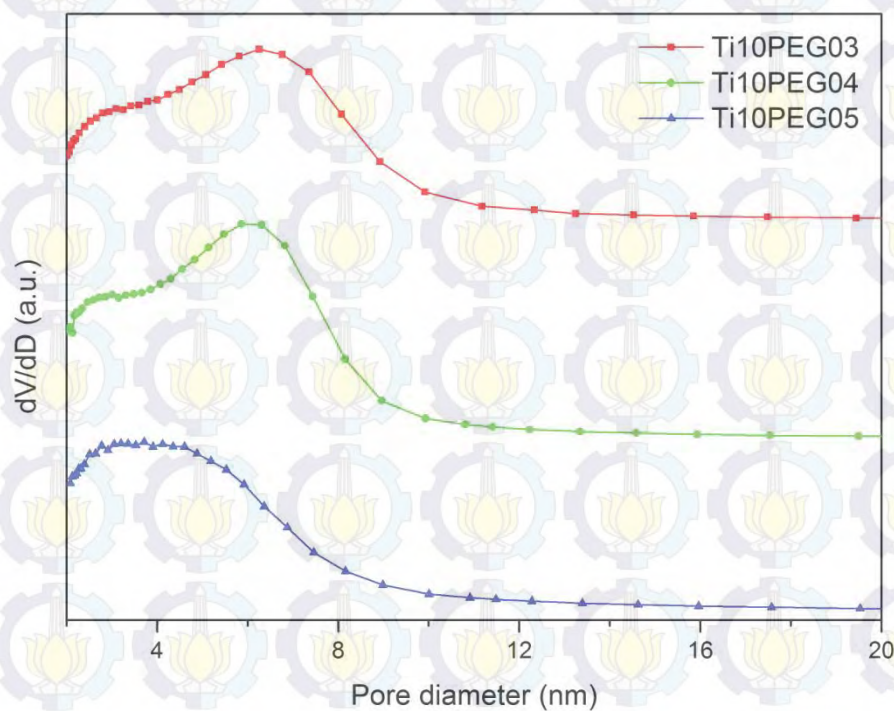


Figure 4.4 Pore size distributions of  $\text{Ti}_4\text{O}_7$  support materials.

Table 4.2 BET surface area of  $\text{Ti}_4\text{O}_7$  support materials.

Sample	BET Surface Area ( $\text{m}^2 \text{g}^{-1}$ )
Ti10PEG03	154.9
Ti10PEG04	187.6
Ti10PEG05	178.3

#### 4.1.4 SEM Results

Information of the sample morphology is required to support the obtained physisorption results of the entire samples. The SEM images of the obtained  $\text{Ti}_4\text{O}_7$  support materials are shown in Figure 4.5.

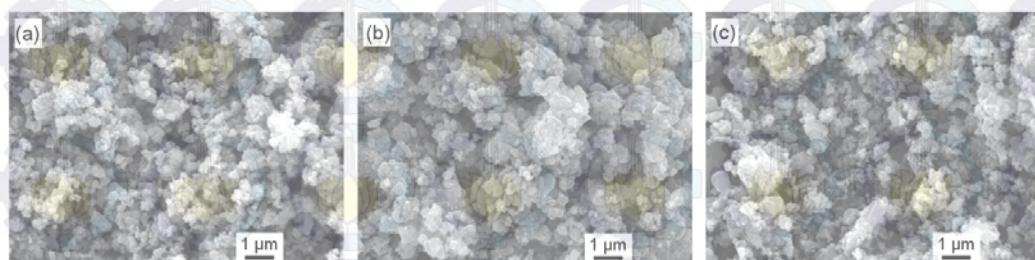


Figure 4.5 SEM images of Ti<sub>4</sub>O<sub>7</sub> support materials (a) Ti10PEG03, (b) Ti10PEG04 and (c) Ti10PEG05 sample.

SEM images of the entire samples clearly show that the morphology of Ti<sub>4</sub>O<sub>7</sub> support materials is built from many small granules. In the calcinations process, the assembly of small granules result large granules and interstitial area. The mesopores which is observed in physisorption analysis result is probably due to the presence of interstitial area between the granules. The results reveal that PEG 400 successfully prevents the uncontrollable particle growth in the calcinations process.

#### 4.1.5 Electronic Conductivity Results

The electronic conductivity of the support material is very important since it is required to drive the electrons to the current collectors. Therefore, electronic conductivity information of the obtained Ti<sub>4</sub>O<sub>7</sub> support materials is required to support their catalytic performance data since they relate each other. The electronic conductivity of the entire samples is shown in Table 4.3, including Ti10PEG03, Ti10PEG04 and Ti10PEG05 sample.

The electronic conductivity of the entire samples varies from 95.47 to 172.96 S cm<sup>-1</sup>. The results are significantly higher than the other titanium based materials, such as molybdenum doped TiO<sub>2</sub> (Ti<sub>0.7</sub>Mo<sub>0.3</sub>O<sub>2</sub>) and un-doped TiO<sub>2</sub>.



which has electronic conductivity  $2.8 \times 10^{-4}$  and  $1.37 \times 10^{-7} \text{ S cm}^{-1}$  respectively.<sup>27</sup> However, the results is lower than electronic conductivity value ( $10^3 \text{ S cm}^{-1}$ ) in the beginning of  $\text{Ti}_4\text{O}_7$  invention<sup>18</sup> which is probably caused by the existence of amorphous carbon residue inside.

Table 4.3 Electronic conductivity of  $\text{Ti}_4\text{O}_7$  support materials.

Sample	Conductivity ( $\text{S cm}^{-1}$ )
Ti10PEG03	95.47
Ti10PEG04	172.96
Ti10PEG05	113.43

#### 4.1.6 CV Analysis Results

Stability of the support material is very important since it is required to avoid catalyst degradation. The stability can be evaluated by performing CV analysis, the peak in the resulted cyclic voltammogram can be used to determine whether the support material is stable or not.<sup>19</sup> The cyclic voltammograms of the obtained  $\text{Ti}_4\text{O}_7$  support materials are shown in Figure 4.6, including Ti10PEG03, Ti10PEG04, Ti10PEG05 sample and carbon black for comparison.

The cyclic voltammograms of obtained  $\text{Ti}_4\text{O}_7$  support materials clearly show that no oxidation-reduction peak is observed. The absence of oxidation peaks indicate the stability of obtained  $\text{Ti}_4\text{O}_7$  support materials in acidic environment. In addition, the thickness of the cyclic voltammogram is associated with the conductivity. Figure 4.6 clearly shows the thickest cyclic voltammogram is achieved by Ti10PEG04 sample, while the thinnest is achieved by Ti10PEG03 sample.

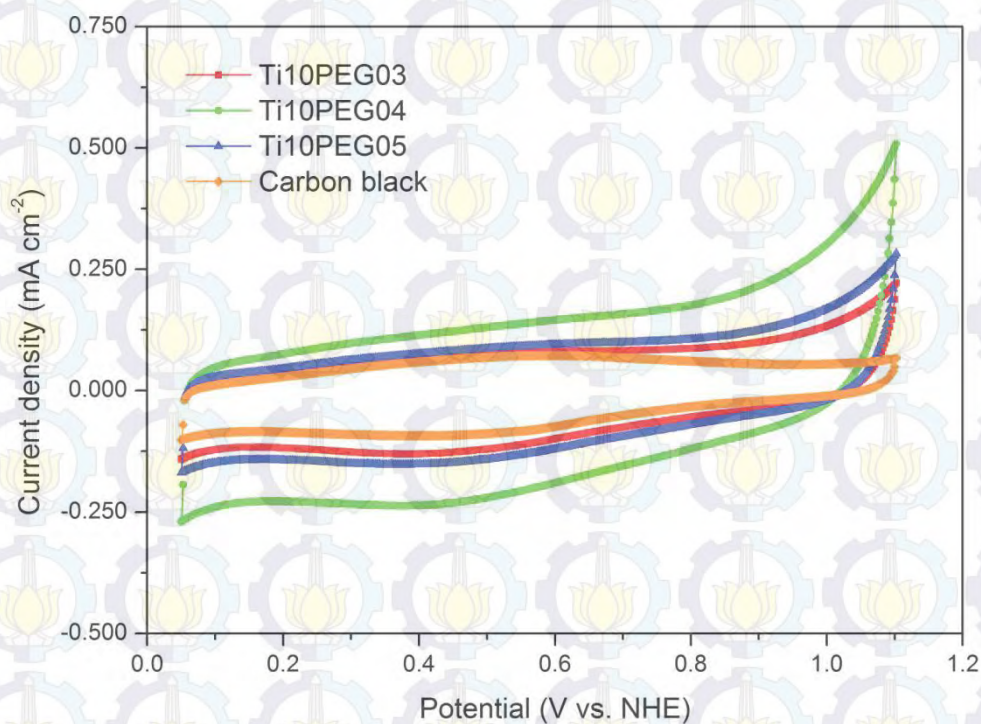


Figure 4.6 Cyclic voltammograms of  $\text{Ti}_4\text{O}_7$  support materials and carbon black for comparison in Ar-saturated 0.5 M  $\text{H}_2\text{SO}_4$  solution at room temperature and scan rate  $25 \text{ mV s}^{-1}$ .

The results are in accordance with the electronic conductivity results which reveal that the most conductive is Ti10PEG04 sample and the most nonconductive is Ti10PEG03 sample. The cyclic voltammogram of carbon is the thinnest among the samples, it indicated that carbon black has lower electronic conductivity than the obtained  $\text{Ti}_4\text{O}_7$  support materials.

#### 4.1.7 Summary

The obtained  $\text{Ti}_4\text{O}_7$  support materials were characterized in terms of crystal phase, amount of amorphous carbon residue, porosity, surface area, conductivity and stability. The XRD patterns of the entire samples revealed that the best Ti(IV) ethoxide and PEG 400 ratio in  $\text{Ti}_4\text{O}_7$  synthesis was 10:4 weight



ratio. Since the synthesis utilized PEG 400 as reducing agent, 7.57 to 9.44 wt% amorphous carbon residue remained in the obtained  $\text{Ti}_4\text{O}_7$  support materials such as observed in thermogravimetric analysis results. Physisorption analysis results revealed that the obtained  $\text{Ti}_4\text{O}_7$  support materials consisted of mesopores with average pore size distribution 4-8 nm. In addition, the surface area of the entire samples was 154.9 to 187.6  $\text{m}^2 \text{g}^{-1}$ . The results were supported by SEM images which clearly show that the entire samples had pore structure. The electronic conductivity of the entire samples varied from 95.47 to 172.96  $\text{S cm}^{-1}$ . CV analysis results revealed that the entire samples were stable in acidic environment since no peaks were observed.

## **4.2 Carbon Removal of $\text{Ti}_4\text{O}_7$ Support Material**

Since the  $\text{Ti}_4\text{O}_7$  support material synthesis utilized PEG 400 as reducing agent, formation of amorphous carbon residue was the consequence which was almost impossible to be avoided. Therefore, some efforts in removing amorphous carbon residue had been made including extraction, solvent and acid-base treatment and the effectiveness of carbon removal process was evaluated by thermogravimetric analysis.

### **4.2.1 Extraction Treatment Result**

Amorphous carbon residue removal by extraction treatment utilized 1,2-dichlorobenzene as extractor agent due to its ability in dissolving carbon. Compared to the other solvents, the highest carbon solubility was achieved by 1,2-dichlorobenzene.<sup>49</sup> n-heptane was added into 1,2-dichlorobenzene in order to keep

the organic phase above the solution phase since the density of n-heptane and 1,2-dichlorobenzene was 0.68 and 1.30 g cm<sup>-3</sup> respectively. By utilizing the method in removing carbon, the expected result was carbon dissolution in the organic phase while the Ti<sub>4</sub>O<sub>7</sub> support material remained in aqueous phase. Therefore, the amorphous carbon residue could be easily separated from Ti<sub>4</sub>O<sub>7</sub> support material. The thermogravimetric analysis result of extraction treatment is shown in Figure 4.7. Amount of decomposition decreases from 7.33% to 6.72%, the result indicates some carbons have been removed. The observed decomposition between 150-400 °C is probably caused by evaporation of trapped solvent in Ti<sub>4</sub>O<sub>7</sub> support material.

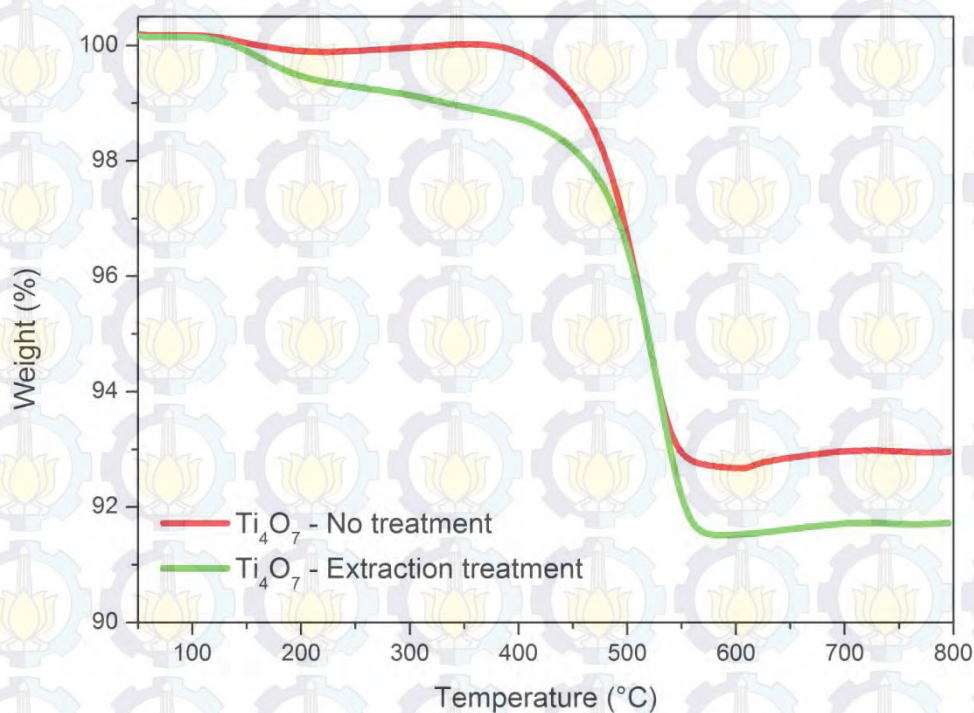


Figure 4.7 Thermogravimetric analysis results of carbon removal by extraction treatment, heating rate = 10 °C min<sup>-1</sup>.



#### 4.2.2 Solvent Treatment Result

1,2-dichlorobenzene was utilized as solvent since it had good solubility in dissolving carbon.<sup>49</sup> Heating and stirring which was employed in the treatment aimed to accelerate the carbon dissolution in the solvent. The expected result in utilizing solvent treatment was carbon dissolution in the solvent while the  $\text{Ti}_4\text{O}_7$  support material remained as precipitation in the bottom. Furthermore, the thermogravimetric analysis of the solvent treatment result is shown in Figure 4.8 which is similar with the previous result. Decomposition amount decreases from 7.33% to 6.43% after treatment, it indicates some carbon have been dissolved in the solvent and removed from  $\text{Ti}_4\text{O}_7$  support material.

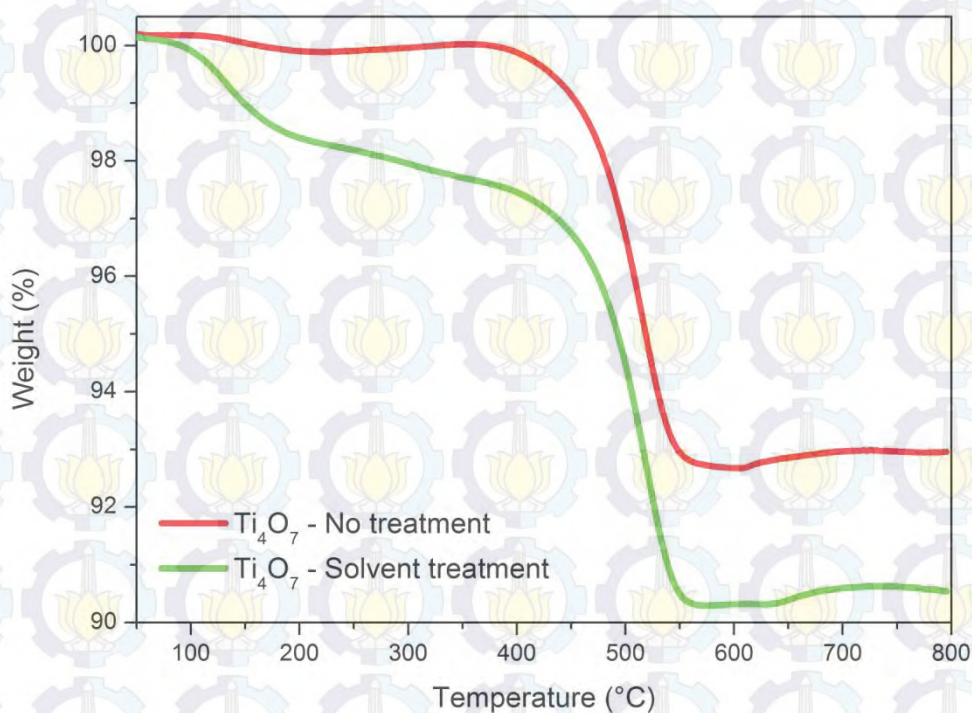


Figure 4.8 Thermogravimetric analysis results of carbon removal by solvent treatment, heating rate =  $10\text{ }^{\circ}\text{C min}^{-1}$ .

### 4.2.3 Acid-Base Treatment Result

2 M  $\text{H}_2\text{SO}_4$  and 2 M  $\text{NaOH}$  were utilized in amorphous carbon residue removal by acid-base treatment. Acid was chosen since it had ability to dissolve carbon. While the base,  $\text{NaOH}$ , was chosen since its ability in dissolving amorphous carbon such as reported in the literature.<sup>50</sup> Utilization of acid-base treatment in removing carbon was expected to reduce amorphous carbon residue since some carbon would be dissolved or decomposed in the presence of acid or base. The result of thermogravimetric analysis is shown in Figure 4.9 which is almost similar with the two previous results. The decomposition amount of acid treatment increases from 7.33% to 7.67%, while the decomposition of base treatment decreases from 7.33% to 6.86%. The increasing weight after acid treatment indicates sulfuric acid area trapped in the  $\text{Ti}_4\text{O}_7$  support material. In contrast, the decreasing weight after base treatment indicates that  $\text{NaOH}$  has successfully dissolved some carbon in the  $\text{Ti}_4\text{O}_7$  support material.

### 4.2.4 Summary

Extraction, solvent and acid-base treatment had been made in order to completely remove amorphous carbon residue from  $\text{Ti}_4\text{O}_7$  support material. Based on the thermogravimetric analysis results, amorphous carbon residue was not completely removed from  $\text{Ti}_4\text{O}_7$  support material. However, extraction, solvent and base treatment successfully removed small amount of carbon, while acid treatment didn't successfully remove amorphous carbon residue. Furthermore, the results is summarized in the Table 4.4, it clearly shows that the solvent treatment was the best compare to the others.



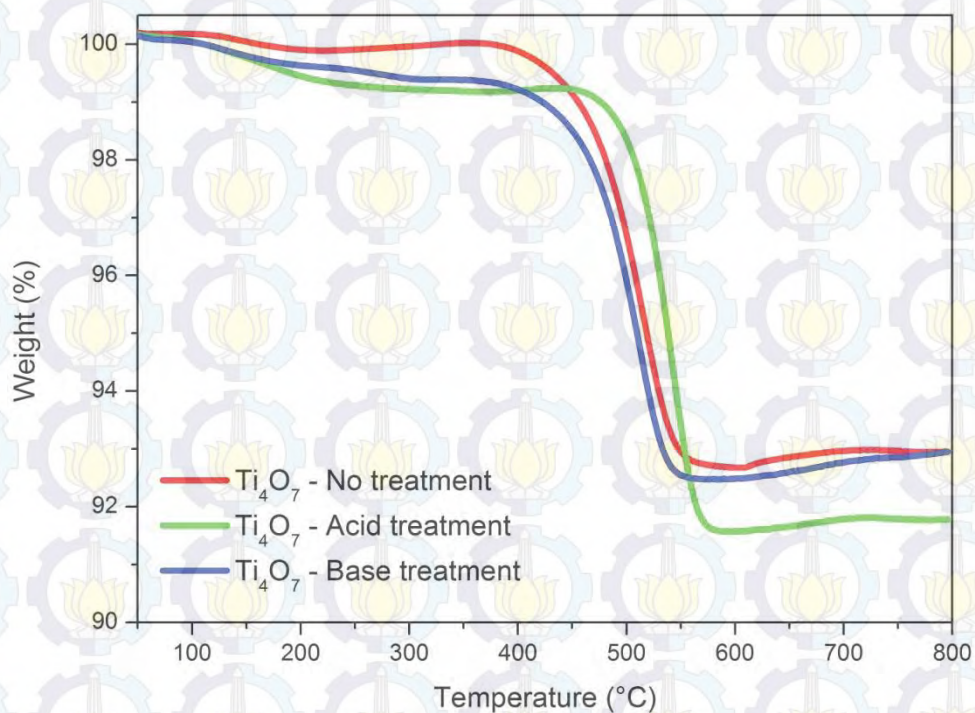


Figure 4.9 Thermogravimetric analysis results of carbon removal by acid-base treatment, heating rate =  $10\text{ }^{\circ}\text{C min}^{-1}$ .

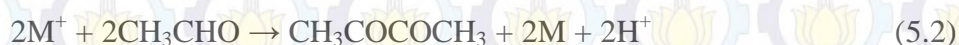
Table 4.4 Summary of carbon removal result.

Treatment	Carbon content (%)		Efficiency (%)
	Initial	Final	
Extraction	7.33	6.72	8.32
Solvent	7.33	6.43	12.28
Acid	7.33	7.67	-4.64
Base	7.33	6.86	6.41

### 4.3 Characterization of 20 wt% Pt/Ti<sub>4</sub>O<sub>7</sub> Catalyst

20 wt% Pt/Ti<sub>4</sub>O<sub>7</sub> was synthesized by following Ho's work<sup>27</sup> which utilized microwave-assisted polyol synthesis. The polyol synthesis was chosen since it provided a simple approach in obtaining noble-metal nanostructures.<sup>51</sup> In the synthesis, ethylene glycol was utilized as both solvent and reducing agent to

deposit platinum on the  $\text{Ti}_4\text{O}_7$  support materials, while microwave served as the heat source. Furthermore,  $\text{Pt}^{4+}$  ion from hexachloroplatinic acid hexahydrate ( $\text{H}_2\text{PtCl}_6 \cdot 6\text{H}_2\text{O}$ ) was reduced by acetaldehyde which was resulted by oxidation of ethylene glycol at 160 °C such as shown in the Equation 5.2 and 5.3.<sup>51</sup>



In order to evaluate the catalytic activity from the three different obtained  $\text{Ti}_4\text{O}_7$  support materials in supporting platinum, the platinum nanoparticles were deposited on them. Furthermore, the entire catalysts were named as 20 wt% Pt/Ti10PEG03, 20 wt% Pt/Ti10PEG04 and 20 wt% Pt/Ti10PEG05 respectively. Since the catalytic activity was highly influenced by the dispersion of catalyst ink,<sup>52–55</sup> three different catalyst ink preparation was performed before evaluating the catalyst activity.

#### 4.3.1 XRD Results

The formation of crystalline platinum nanoparticles on the  $\text{Ti}_4\text{O}_7$  support materials was verified by XRD measurement. XRD patterns of platinum nanoparticles on the  $\text{Ti}_4\text{O}_7$  support materials and the standard XRD patterns of  $\text{Ti}_4\text{O}_7$  and platinum are shown in Figure 4.10.



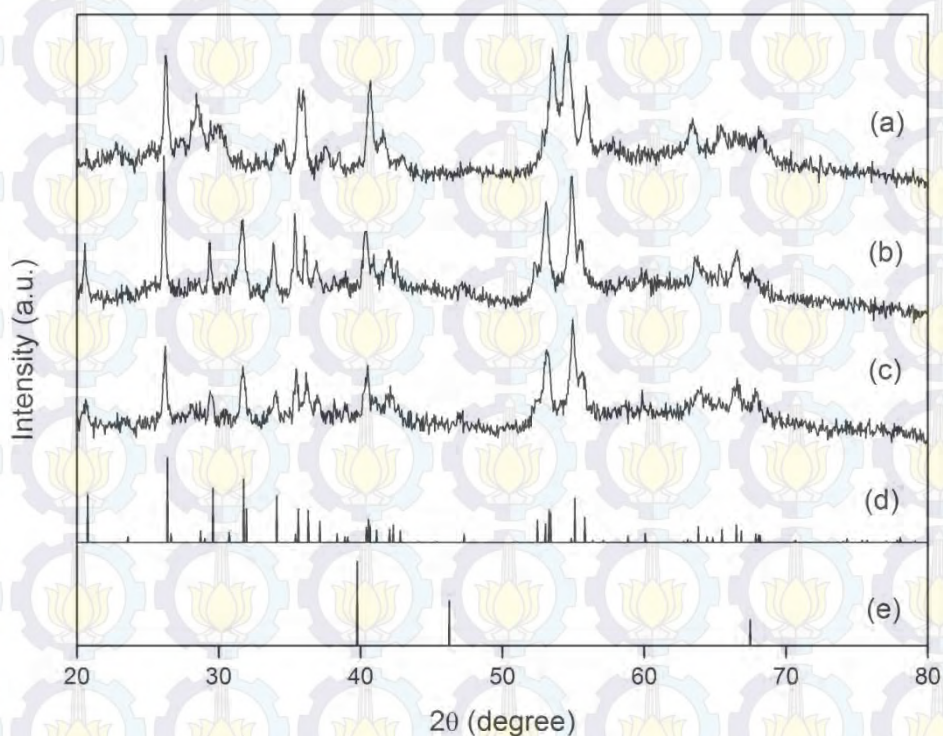


Figure 4.10 XRD patterns of (a) 20 wt% Pt/Ti10PEG03, (b) 20 wt% Pt/Ti10PEG04, (c) 20 wt% Pt/Ti10PEG05, (d)  $\text{Ti}_4\text{O}_7$  (PDF 50-0787) and (e) platinum (PDF 04-0802).

The XRD patterns show that the characteristic peaks of platinum at  $39.8^\circ$ ,  $46.2^\circ$  and  $67.5^\circ$  can't be clearly observed. The results are probably caused by the amount of platinum which is relatively low compared to the support materials. In addition, the characteristic peaks of platinum overlap with the peaks of  $\text{Ti}_4\text{O}_7$ . However, the presence of platinum nanoparticles on the  $\text{Ti}_4\text{O}_7$  support materials can be observed in the cyclic voltammogram.

### 4.3.2 Electrochemical Performance of 20 wt% Pt/ $\text{Ti}_4\text{O}_7$ Catalyst

#### 4.3.2.1 ECSA Evaluation

The electrochemically active surface area (ECSA) of the entire 20 wt% Pt/ $\text{Ti}_4\text{O}_7$  catalysts including 20 wt% Pt/Ti10PEG03, 20 wt% Pt/Ti10PEG04, 20



wt% Pt/Ti10PEG05 catalyst were evaluated by performing cyclic voltammetry (CV) in oxygen free electrolyte. In order to compare their performance, the commercial 20 wt% Pt/C catalyst was also evaluated.

The cyclic voltammograms of the entire catalysts was recorded at room temperature in Ar-saturated 0.5 M H<sub>2</sub>SO<sub>4</sub> solution, the potential was scanned from 0.05 to 1.1 V vs. RHE at scan rate 25 mV s<sup>-1</sup>. The obtained ECSA value (m<sup>2</sup> g<sup>-1</sup>) of the entire catalysts were calculated by integrating anodic charge under hydrogen desorption area after double-layer correction and the adsorption charge of hydrogen monolayer on platinum surface was assumed to be 210  $\mu\text{C cm}^{-2}$ .

Prior to the measurement, the catalyst ink was prepared by dispersing known amount of catalyst in 500  $\mu\text{L}$  0.5% Nafion 117 solution and followed by ultrasonication for 30 minutes. Furthermore, the catalyst ink preparation was named as Catalyst Ink 1. The obtained cyclic voltammograms of 20 wt% Pt/Ti10PEG03, 20 wt% Pt/Ti10PEG04, 20 wt% Pt/Ti10PEG05 and commercial 20 wt% Pt/C catalyst are shown in Figure 4.11. It clearly shows the identical cyclic voltammogram of platinum which consists of some peaks including hydrogen adsorption-desorption peak and platinum oxidation-reduction peak. However, the peaks of 20 wt% Pt/Ti10PEG03 catalysts can't be clearly observed which is probably caused by the low amount of platinum.

By utilizing 500  $\mu\text{L}$  0.5% Nafion 117 solution in catalyst ink preparation, the highest ECSA is achieved by 20 wt% Pt/Ti10PEG05 catalyst. In addition, the ECSA of 20 wt% Pt/Ti10PEG03, 20 wt% Pt/Ti10PEG04, 20 wt% Pt/Ti10PEG05 and commercial 20 wt% Pt/C catalyst are found to be 2.72, 10.38, 15.55 and 11.99 m<sup>2</sup> g<sup>-1</sup> respectively.



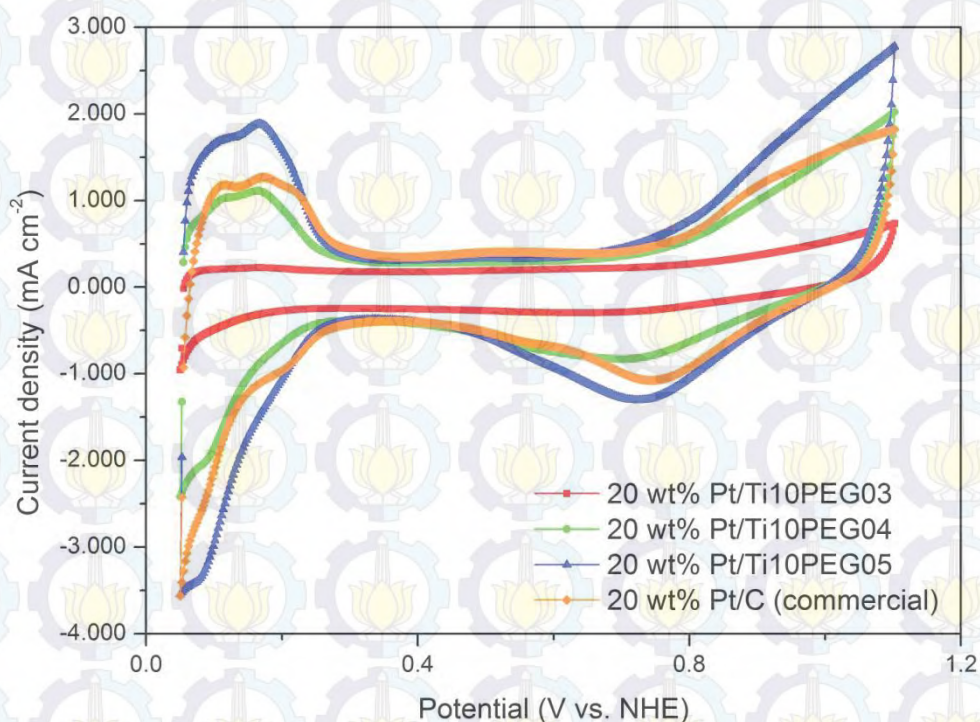


Figure 4.11 Cyclic voltammograms of 20 wt% Pt/Ti10PEG03, 20 wt% Pt/Ti10PEG04, 20 wt% Pt/Ti10PEG05 and commercial 20 wt% Pt/C catalyst which were previously dispersed in 500  $\mu\text{L}$  0.5% Nafion 117 ( $0.2 \text{ mg}_{\text{Pt}} \text{ cm}^{-2}$ ) recorded at room temperature in Ar-saturated 0.5 M  $\text{H}_2\text{SO}_4$  solution at scan rate  $25 \text{ mV s}^{-1}$ .

In order to compare the obtained result, the lower concentration of Nafion 117 solution was utilized in catalyst ink preparation. The catalyst ink was prepared by dispersing known amount of catalyst in 500  $\mu\text{L}$  0.1% Nafion 117 solution and followed by ultrasonication for 30 minutes. Furthermore, the catalyst ink preparation was named as Catalyst Ink 2. The obtained cyclic voltammograms of 20 wt% Pt/Ti10PEG03, 20 wt% Pt/Ti10PEG04, 20 wt% Pt/Ti10PEG05 and commercial 20 wt% Pt/C catalyst are shown in Figure 4.12. It clearly shows some peaks including hydrogen adsorption-desorption peak and platinum oxidation-reduction peak which are commonly observed in cyclic voltammogram of platinum.



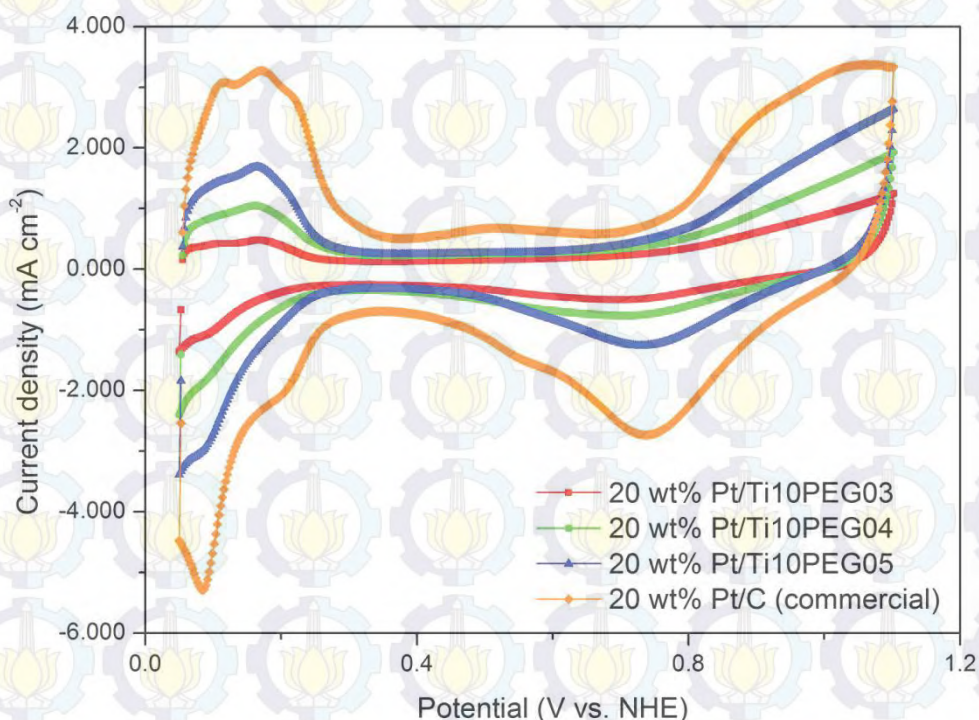


Figure 4.12 Cyclic voltammograms of 20 wt% Pt/Ti10PEG03, 20 wt% Pt/Ti10PEG04, 20 wt% Pt/Ti10PEG05 and commercial 20 wt% Pt/C catalyst which were previously dispersed in 500  $\mu\text{L}$  0.1% Nafion 117 ( $0.2 \text{ mg}_{\text{Pt}} \text{ cm}^{-2}$ ) recorded at room temperature in Ar-saturated 0.5 M  $\text{H}_2\text{SO}_4$  solution at scan rate  $25 \text{ mV s}^{-1}$ .

Utilization of 500  $\mu\text{L}$  0.1% Nafion 117 in catalyst ink preparation results different ECSA. The ECSA of 20 wt% Pt/Ti10PEG03, 20 wt% Pt/Ti10PEG04, 20 wt% Pt/Ti10PEG05 and commercial 20 wt% Pt/C catalyst are found to be 3.65, 8.44, 13.45 and  $30.55 \text{ m}^2 \text{ g}^{-1}$  respectively. In addition, the highest ECSA is achieved by 20 wt% Pt/C catalyst, it indicates that 20 wt% Pt/C catalyst is highly dispersed in the solution and forms highly uniform thin film on the glassy carbon electrode.

Finally, the catalyst ink was prepared by dispersing known amount catalyst in 500  $\mu\text{L}$  mixture of isopropanol and DI water (95:5 volume ratio) and



followed by ultrasonication for 30 minutes. Then, catalyst ink was dropped on the glassy carbon electrode and followed by dropping 7  $\mu\text{L}$  0.01% Nafion 117 solution on it. Furthermore, the catalyst ink preparation was named as Catalyst Ink 3. The obtained cyclic voltammograms of the entire catalyst, including 20 wt% Pt/Ti10PEG03, 20 wt% Pt/Ti10PEG04, 20 wt% Pt/Ti10PEG05 and commercial 20 wt% Pt/C catalyst, are shown in Figure 4.13. It shows similar cyclic voltammogram with previous results which consists of some peaks including hydrogen adsorption-desorption peak and platinum oxidation-reduction peak.

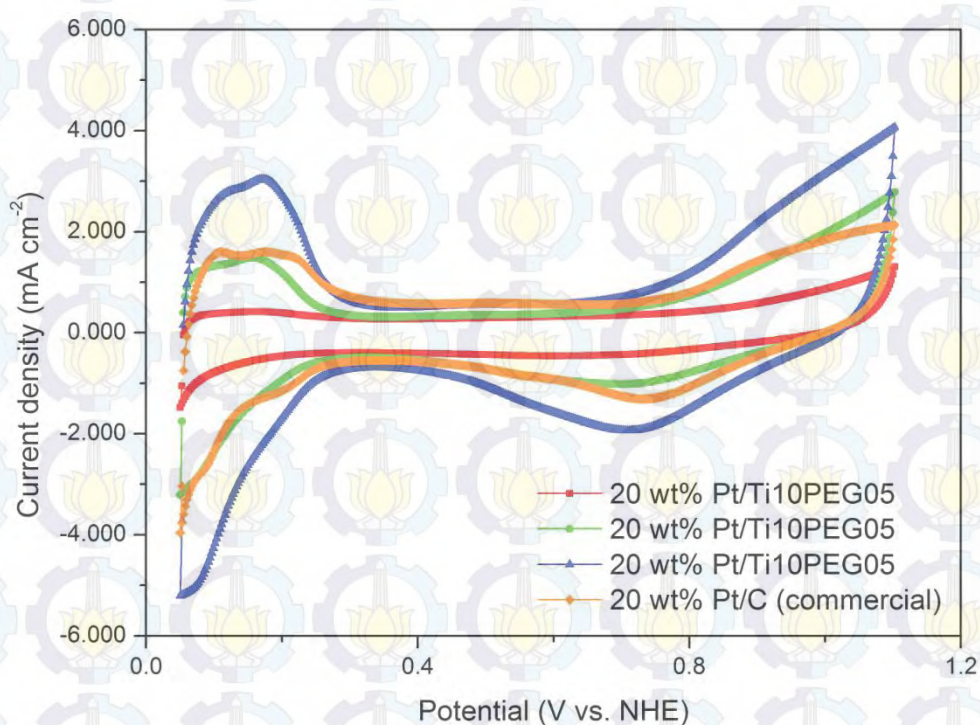


Figure 4.13 Cyclic voltammograms of 20 wt% Pt/Ti10PEG03, 20 wt% Pt/Ti10PEG04, 20 wt% Pt/Ti10PEG05 and commercial 20 wt% Pt/C catalyst which were previously dispersed in 500  $\mu\text{L}$  mixture of isopropanol and DI water (95:5 volume ratio) and followed by dropping 7  $\mu\text{L}$  0.01% Nafion 117 ( $0.2 \text{ mg}_{\text{Pt}} \text{ cm}^{-2}$ ) recorded at room temperature in Ar-saturated 0.5 M  $\text{H}_2\text{SO}_4$  solution at scan rate  $25 \text{ mV s}^{-1}$ .



The obtained ECSA of 20 wt% Pt/Ti10PEG03, 20 wt% Pt/Ti10PEG04, 20 wt% Pt/Ti10PEG05 and commercial 20 wt% Pt/C catalyst which is previously prepared by this catalyst ink preparation technique are found to be 4.69, 12.61, 26.22 and 17.35 m<sup>2</sup> g<sup>-1</sup> respectively. In addition, the highest ECSA is achieved by Pt/Ti10PEG05 catalyst, it indicates that Pt/Ti10PEG05 catalyst is suitable with the catalyst ink preparation technique.

The summary of ECSA results including (A) 20 wt% Pt/Ti10PEG03, (B) 20 wt% Pt/Ti10PEG04, (C) 20 wt% Pt/Ti10PEG05 and (D) commercial 20 wt% Pt/C catalyst is shown in Figure 4.14. It clearly shows that the measurement results are highly influenced by the catalyst ink preparation technique. Moreover, the highest ECSA is achieved by the commercial 20 wt% Pt/C catalyst which is previously prepared by utilizing Catalyst Ink 2. The result indicates that the catalyst is well dispersed in the solution and forms highly uniform thin film on the glassy carbon electrode.

#### 4.3.2.2 ORR Activity Evaluation

ORR activity of the entire 20 wt% Pt/Ti<sub>4</sub>O<sub>7</sub> catalysts including 20 wt% Pt/Ti10PEG03, 20 wt% Pt/Ti10PEG04, 20 wt% Pt/Ti10PEG05 catalyst were evaluated by performing the combination of linear sweep voltammetry (LSV) and rotating disk electrode (RDE) in oxygen-saturated electrolyte. The commercial 20 wt% Pt/C catalyst was also evaluated in order to compare the entire catalyst performance.



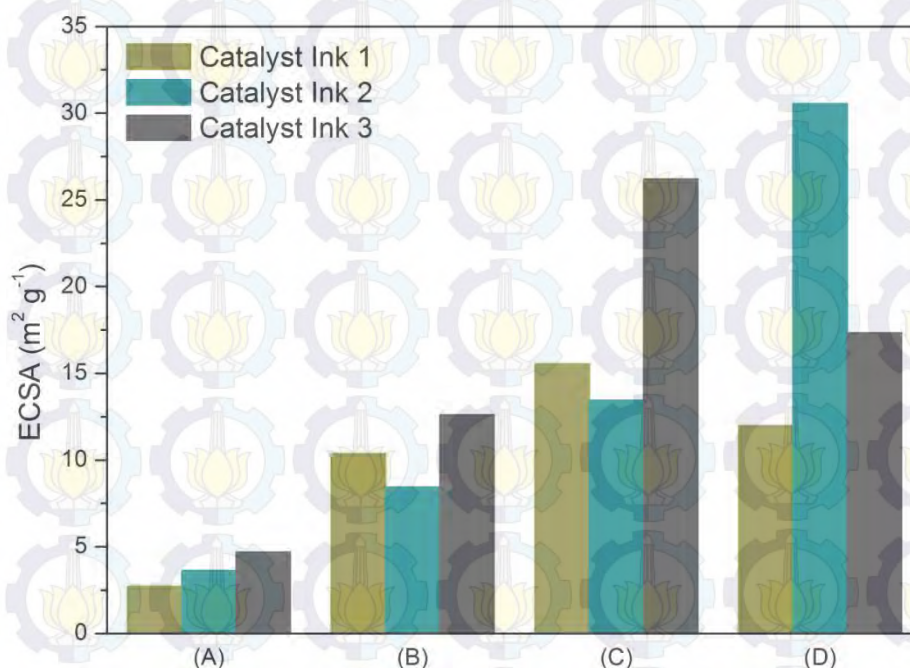


Figure 4.14 The ECSA summary of (A) 20 wt% Pt/Ti10PEG03, (B) 20 wt% Pt/Ti10PEG04, (C) 20 wt% Pt/Ti10PEG05 and (D) commercial 20 wt% Pt/C catalyst in different catalyst ink preparation.

The ORR activity was evaluated at room temperature in oxygen-saturated 0.5 M  $\text{H}_2\text{SO}_4$  solution, the potential was swept from 1.0 to 0.05 V vs. RHE (backward scan) at the scan rate  $1 \text{ mV s}^{-1}$ . Prior to the measurement, the solution was purged by oxygen for 30 minutes and the electrode was rotated at 1,600 rpm until the measurement finished. The catalyst ink was also prepared by the same dispersion technique in ECSA evaluation including 0.5% Nafion 117 solution (Catalyst Ink 1), 0.1% Nafion 117 solution (Catalyst Ink 2) and mixture of isopropanol and DI water (95:5 volume ratio) which was followed by dropping 0.01% Nafion 117 solution (Catalyst Ink 3).

The polarization curves of 20 wt% Pt/Ti10PEG03, 20 wt% Pt/Ti10PEG04, 20 wt% Pt/Ti10PEG05 and commercial 20 wt% Pt/C catalyst which is previously prepared by Catalyst Ink 1 are shown in Figure 4.15. It clearly



shows that the activity of entire catalysts toward ORR is lower than the commercial catalyst.

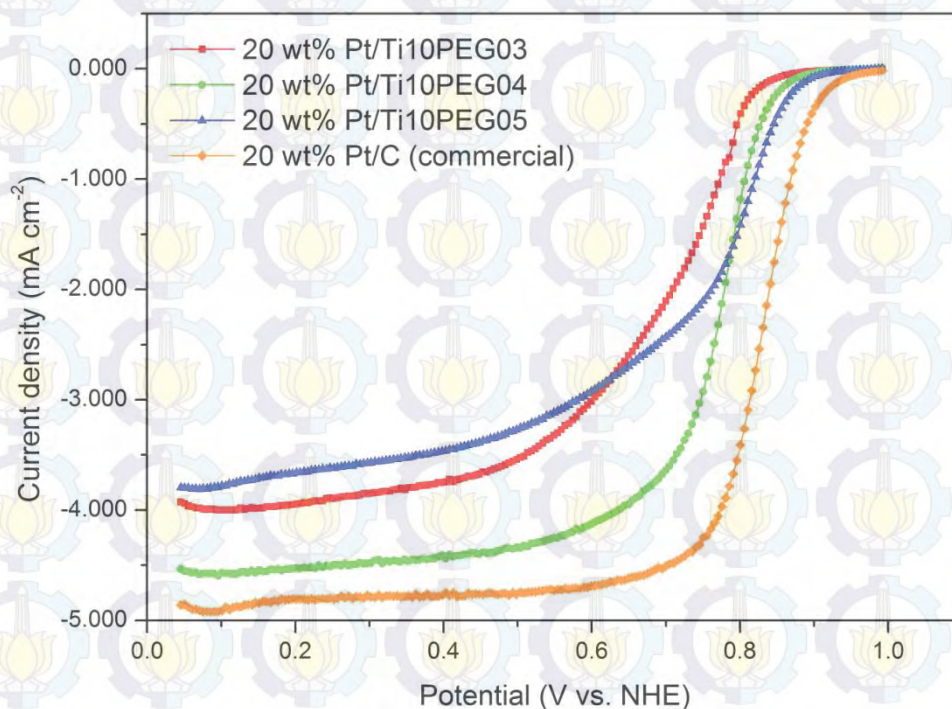


Figure 4.15 Polarization curves of 20 wt% Pt/Ti10PEG03, 20 wt% Pt/Ti10PEG04, 20 wt% Pt/Ti10PEG05 and commercial 20 wt% Pt/C catalyst which were previously dispersed in 500  $\mu\text{L}$  0.5% Nafion 117 ( $0.2 \text{ mg}_{\text{Pt}} \text{ cm}^{-2}$ ) recorded at room temperature in oxygen-saturated 0.5 M  $\text{H}_2\text{SO}_4$  solution at scan rate  $1 \text{ mV s}^{-1}$ . The current was normalized to the geometric area of the glassy carbon electrode ( $0.1964 \text{ cm}^2$ ).

The low activity of entire catalysts can be observed in the onset potential, kinetic current density at 0.9 V vs. RHE and mass activity. The onset potential of 20 wt% Pt/Ti10PEG03, 20 wt% Pt/Ti10PEG04, 20 wt% Pt/Ti10PEG05 and commercial 20 wt% Pt/C catalyst are found to be 0.82, 0.84, 0.87 and 0.89 V vs. RHE respectively. While the kinetic current density at 0.9 V vs. RHE of 20 wt% Pt/Ti10PEG03, 20 wt% Pt/Ti10PEG04, 20 wt% Pt/Ti10PEG05 and commercial 20 wt% Pt/C catalyst are found to be 0.01884, 0.03534, 0.06851 and 0.34395 mA



$\text{cm}^{-2}$ . In addition, the mass activity of the commercial 20 wt% Pt/C catalyst is also the highest compared to the others.

For comparison, the polarization curves of 20 wt% Pt/Ti10PEG03, 20 wt% Pt/Ti10PEG04, 20 wt% Pt/Ti10PEG05 and commercial 20 wt% Pt/C catalyst which is previously prepared by Catalyst Ink 2 are shown in Figure 4.16. It clearly shows that the activity of entire catalysts toward ORR is similar with the previous result which is lower than the commercial catalyst in terms of the onset potential, kinetic current density at 0.9 V vs. RHE and mass activity.

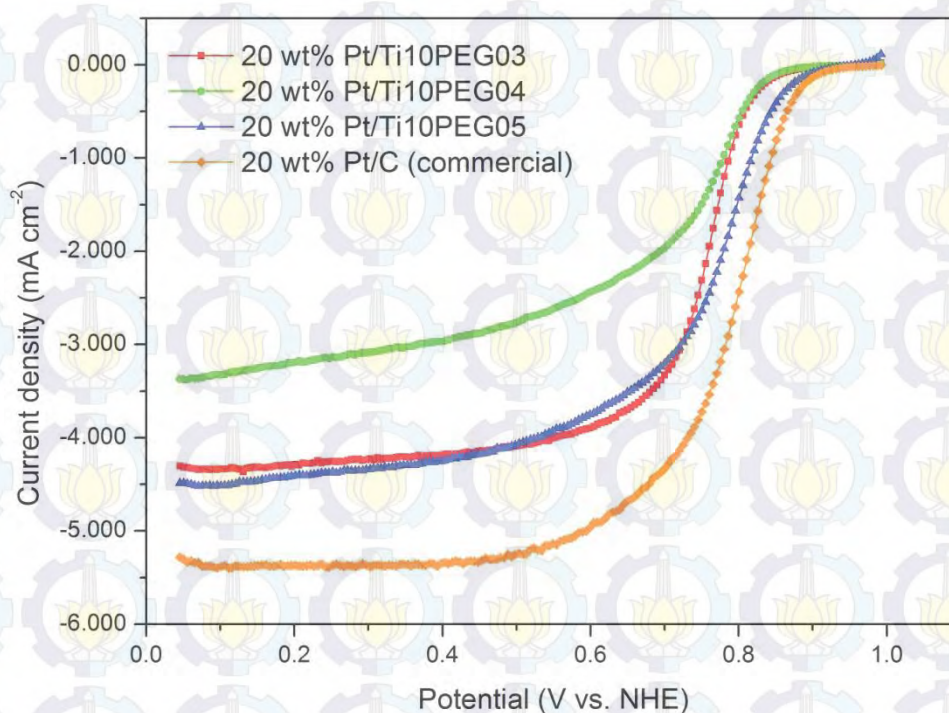


Figure 4.16 Polarization curves of 20 wt% Pt/Ti10PEG03, 20 wt% Pt/Ti10PEG04, 20 wt% Pt/Ti10PEG05 and commercial 20 wt% Pt/C catalyst which were previously dispersed in 500  $\mu\text{L}$  0.1% Nafion 117 ( $0.2 \text{ mg}_{\text{Pt}} \text{ cm}^{-2}$ ) recorded at room temperature in oxygen-saturated 0.5 M  $\text{H}_2\text{SO}_4$  solution at scan rate  $1 \text{ mV s}^{-1}$ . The current was normalized to the geometric area of the glassy carbon electrode ( $0.1964 \text{ cm}^2$ ).



The onset potential of 20 wt% Pt/Ti10PEG03, 20 wt% Pt/Ti10PEG04, 20 wt% Pt/Ti10PEG05 and commercial 20 wt% Pt/C catalyst are found to be 0.83, 0.82, 0.86 and 0.89 V vs. RHE respectively. While the kinetic current density at 0.9 V vs. RHE of 20 wt% Pt/Ti10PEG03, 20 wt% Pt/Ti10PEG04, 20 wt% Pt/Ti10PEG05 and commercial 20 wt% Pt/C catalyst are found to be 0.02569, 0.01962, 0.07988 and 0.12643 mA cm<sup>-2</sup>. Moreover, the mass activity of the commercial 20 wt% Pt/C catalyst is also the highest compared to the others.

Finally, in order to confirm the two previous results, the entire catalysts and commercial 20 wt% Pt/C catalyst is prepared by utilizing Catalyst Ink 3 and the results are shown in Figure 4.17.

The result doesn't significantly change and even is getting worse since the activity of entire catalysts toward ORR has large deviation in terms of mass activity compared to the commercial 20 wt% Pt/C catalyst. The onset potential of 20 wt% Pt/Ti10PEG03, 20 wt% Pt/Ti10PEG04, 20 wt% Pt/Ti10PEG05 and commercial 20 wt% Pt/C catalyst are found to be 0.82, 0.87, 0.88 and 0.89 V vs. RHE respectively. While the kinetic current density at 0.9 V vs. RHE of 20 wt% Pt/Ti10PEG03, 20 wt% Pt/Ti10PEG04, 20 wt% Pt/Ti10PEG05 and commercial 20 wt% Pt/C catalyst are found to be 0.03285, 0.07552, 0.06695 and 0.41588 mA cm<sup>-2</sup>. Furthermore, the mass activity exhibits very large deviation between the entire catalysts and commercial 20 wt% Pt/C catalyst.



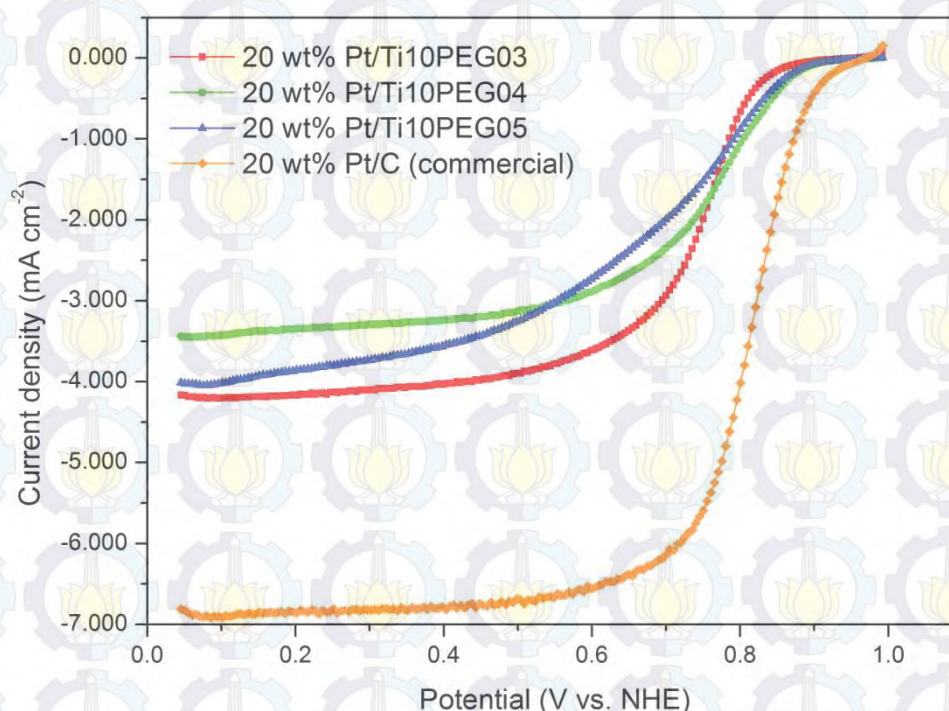


Figure 4.17 Polarization curves of 20 wt% Pt/Ti10PEG03, 20 wt% Pt/Ti10PEG04, 20 wt% Pt/Ti10PEG05 and commercial 20 wt% Pt/C catalyst which were previously dispersed in 500  $\mu\text{L}$  mixture of isopropanol and DI water (95:5 volume ratio) and followed by dropping 7  $\mu\text{L}$  0.01% Nafion 117 ( $0.2 \text{ mg}_{\text{Pt}} \text{ cm}^{-2}$ ) recorded at room temperature in oxygen-saturated 0.5 M  $\text{H}_2\text{SO}_4$  solution at scan rate  $1 \text{ mV s}^{-1}$ . The current was normalized to the geometric area of the glassy carbon electrode ( $0.1964 \text{ cm}^2$ ).

ORR activity results of (A) 20 wt% Pt/Ti10PEG03, (B) 20 wt% Pt/Ti10PEG04, (C) 20 wt% Pt/Ti10PEG05 and (D) commercial 20 wt% Pt/C catalyst in terms of kinetic current density at 0.9 V vs. RHE is summarized in Figure 4.18. It clearly shows that the commercial 20 wt% Pt/C catalyst exhibits the best performance in all catalyst ink preparation technique. The result indicates that the catalyst ink preparation technique doesn't highly contribute to the measurement result since the results are almost in the same trends. In addition, the performance of the commercial 20 wt% Pt/C catalyst in terms of onset potential and kinetic current density at 0.9 V vs. RHE is the highest compared to the others.

The low performance results of the entire 20 wt% Pt/Ti<sub>4</sub>O<sub>7</sub> catalysts are probably caused by incomplete platinum deposition on the Ti<sub>4</sub>O<sub>7</sub> support materials.

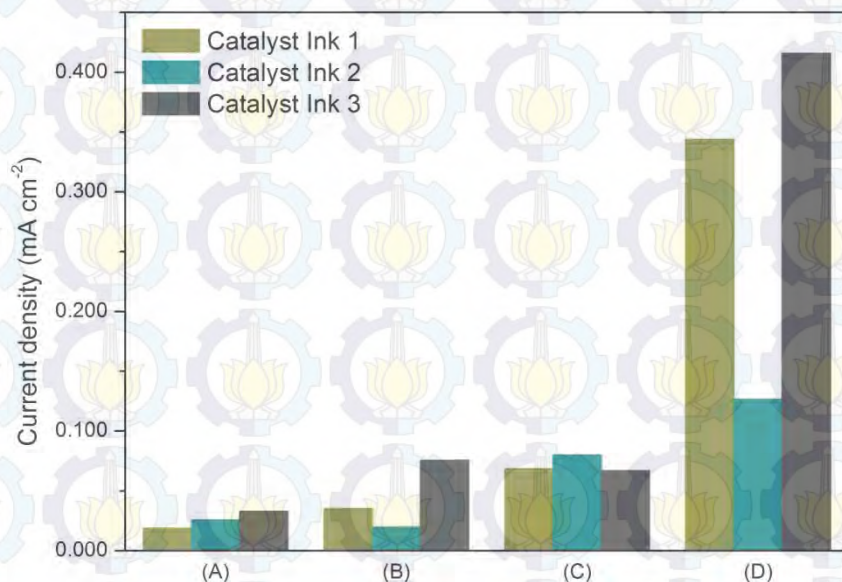


Figure 4.18 The kinetic current density at 0.9 V vs. RHE of (A) 20 wt% Pt/Ti<sub>10</sub>PEG03, (B) 20 wt% Pt/Ti<sub>10</sub>PEG04, (C) 20 wt% Pt/Ti<sub>10</sub>PEG05 and (D) commercial 20 wt% Pt/C catalyst in different catalyst ink preparation.

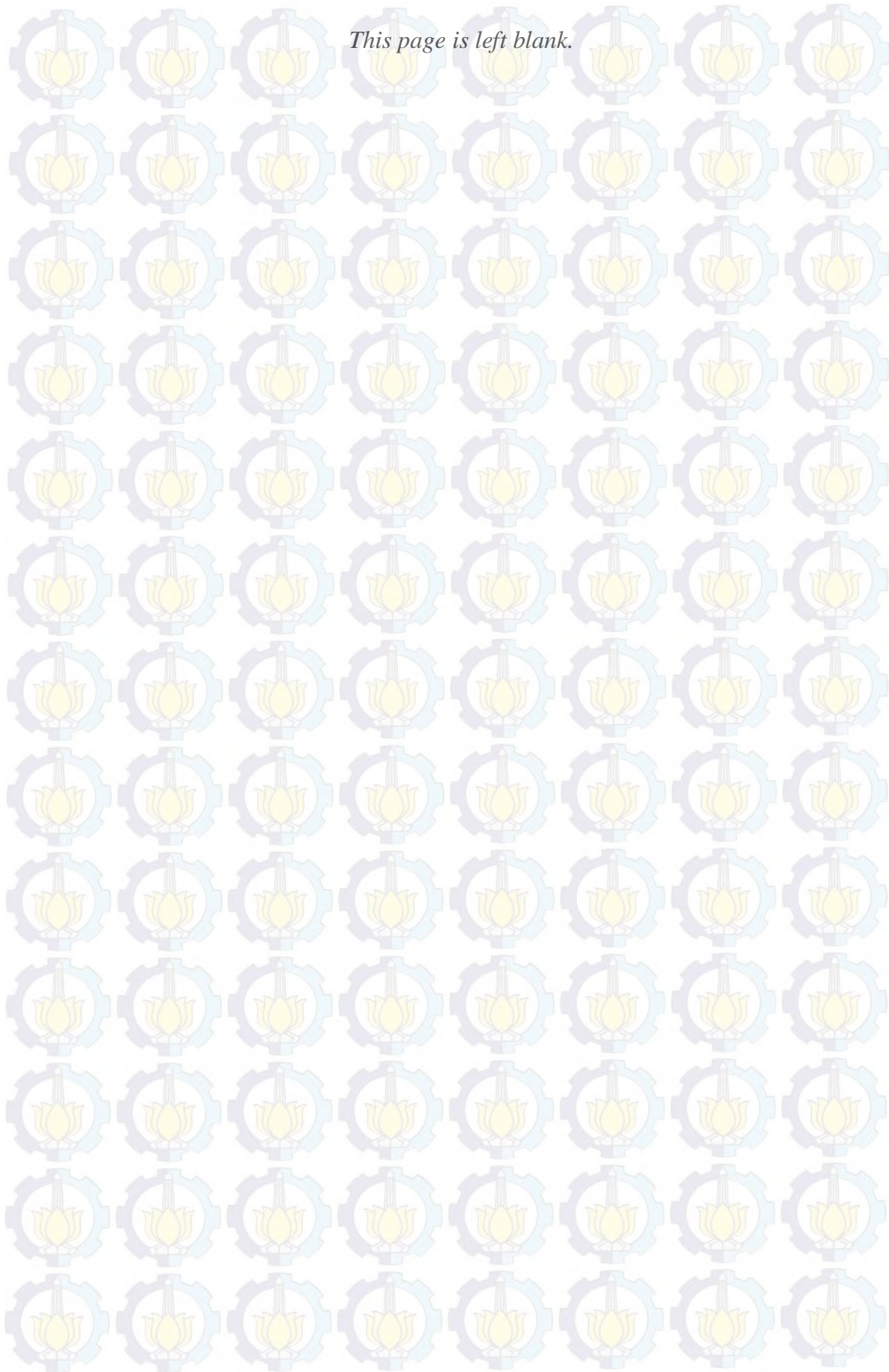
#### 4.3.3 Summary

The entire 20 wt% Pt/Ti<sub>4</sub>O<sub>7</sub> catalysts were characterized in terms of crystal phase of platinum and electrochemical. The characteristic peaks of platinum couldn't be clearly observed in XRD patterns. However, the existence of platinum on the Ti<sub>4</sub>O<sub>7</sub> support materials was observed in the cyclic voltammogram. The different ECSA results of the entire 20 wt% Pt/Ti<sub>4</sub>O<sub>7</sub> catalysts was highly influenced by the catalyst ink preparation technique. While the ORR activity of the entire 20 wt% Pt/Ti<sub>4</sub>O<sub>7</sub> catalysts was lower than the



commercial 20 wt% Pt/C catalyst in terms of the onset potential, kinetic current density at 0.9 V vs. RHE and mass activity.

*This page is left blank.*





## CHAPTER 5

### CONCLUSION AND OUTLOOK

#### 5.1 Conclusion

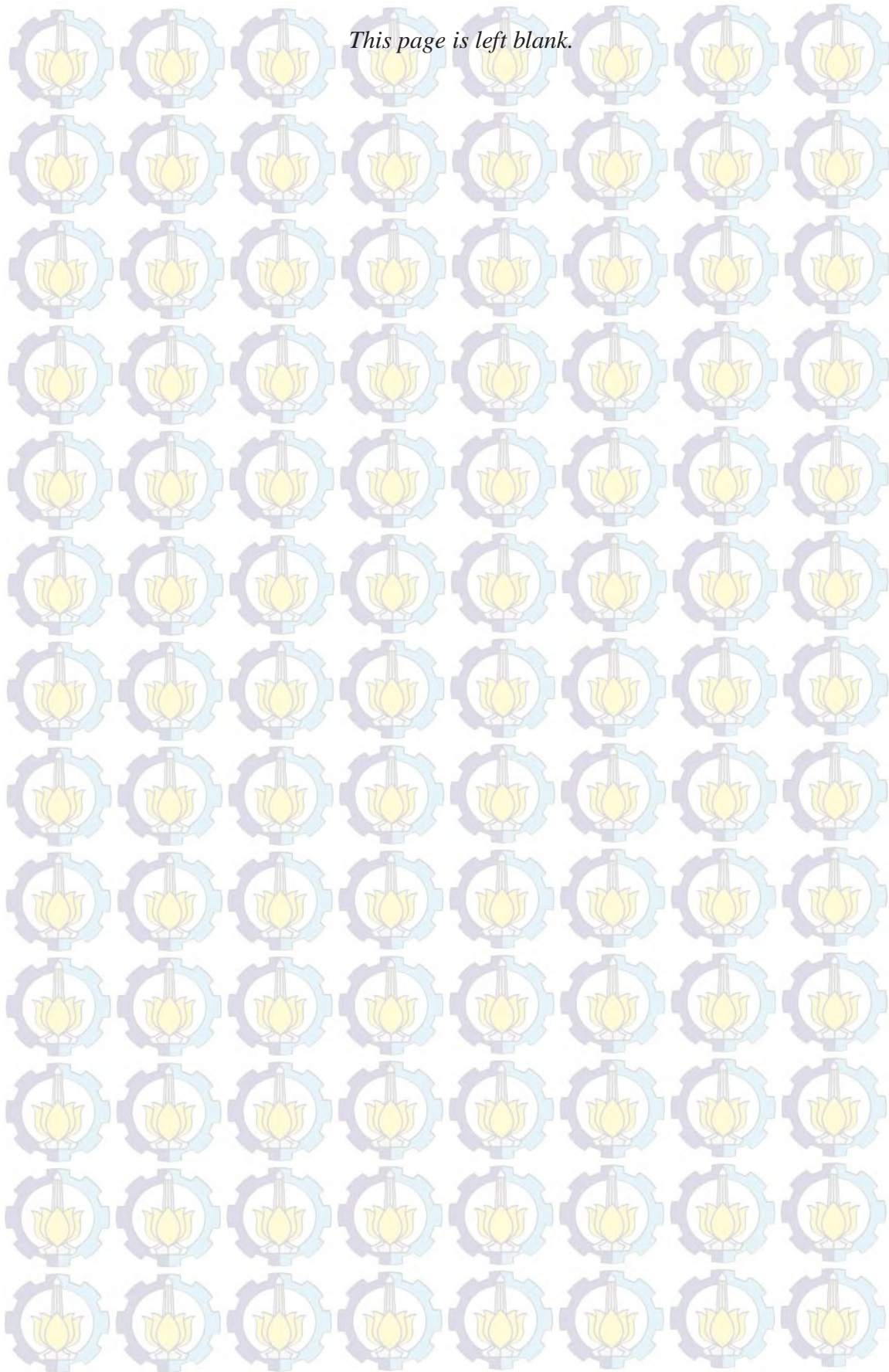
High surface area  $\text{Ti}_4\text{O}_7$  was successfully synthesized by utilizing titanium(IV) ethoxide as titanium precursor and PEG 400 as reducing agent. The platinum nanoparticles were successfully deposited on  $\text{Ti}_4\text{O}_7$  support material by utilizing microwave-assisted polyol synthesis and its electrochemical performance including ECSA and ORR activity was also evaluated. The different ECSA results of the entire catalysts were highly influenced by the catalyst ink preparation technique, while the ORR activity of the entire 20 wt% Pt/ $\text{Ti}_4\text{O}_7$  catalysts was lower than the commercial 20 wt% Pt/C. In addition, the amorphous carbon residue was not completely removed from the  $\text{Ti}_4\text{O}_7$  support material.

#### 5.2 Outlook

The amorphous carbon residue should be removed completely before platinum nanoparticles deposition in order to check its influence in catalytic activity of 20% Pt/ $\text{Ti}_4\text{O}_7$  catalyst. Moreover, another effective and efficient way in removing amorphous carbon residue from  $\text{Ti}_4\text{O}_7$  support material should be developed.



*This page is left blank.*



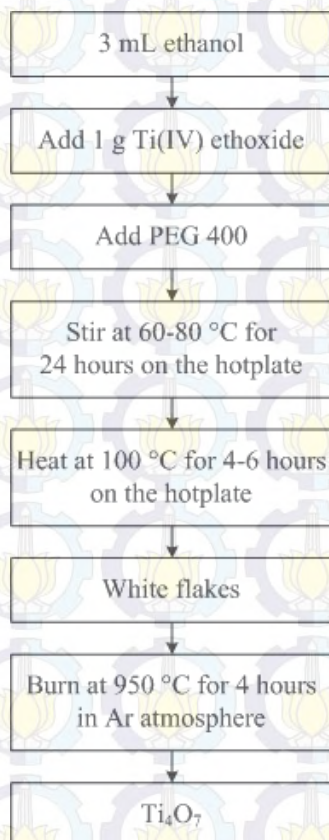


## LIST OF APPENDIX

A.1 Synthesis Flowchart of $\text{Ti}_4\text{O}_7$ .....	71
A.2 Synthesis Flowchart of 20 wt% Pt/ $\text{Ti}_4\text{O}_7$ Catalyst .....	72
A.3 Flowchart of Carbon Removal by Extraction Treatment.....	73
A.4 Flowchart of Carbon Removal by Solvent Treatment .....	74
A.5 Flowchart of Carbon Removal by Acid Treatment .....	75
A.6 Flowchart of Carbon Removal by Base Treatment .....	76
A.7 Flowchart of Catalyst Ink 1 Preparation .....	77
A.8 Flowchart of Catalyst Ink 2 Preparation .....	78
A.9 Flowchart of Catalyst Ink 3 Preparation .....	79

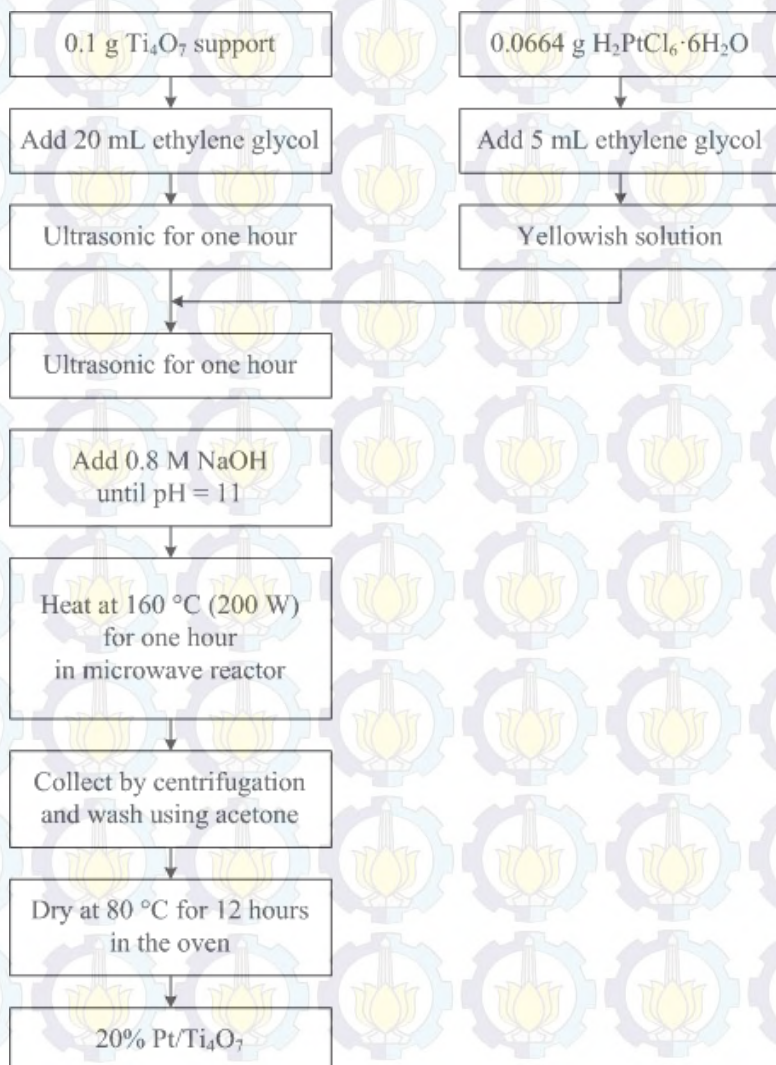
## APPENDIX

### A.1 Synthesis Flowchart of $\text{Ti}_4\text{O}_7$

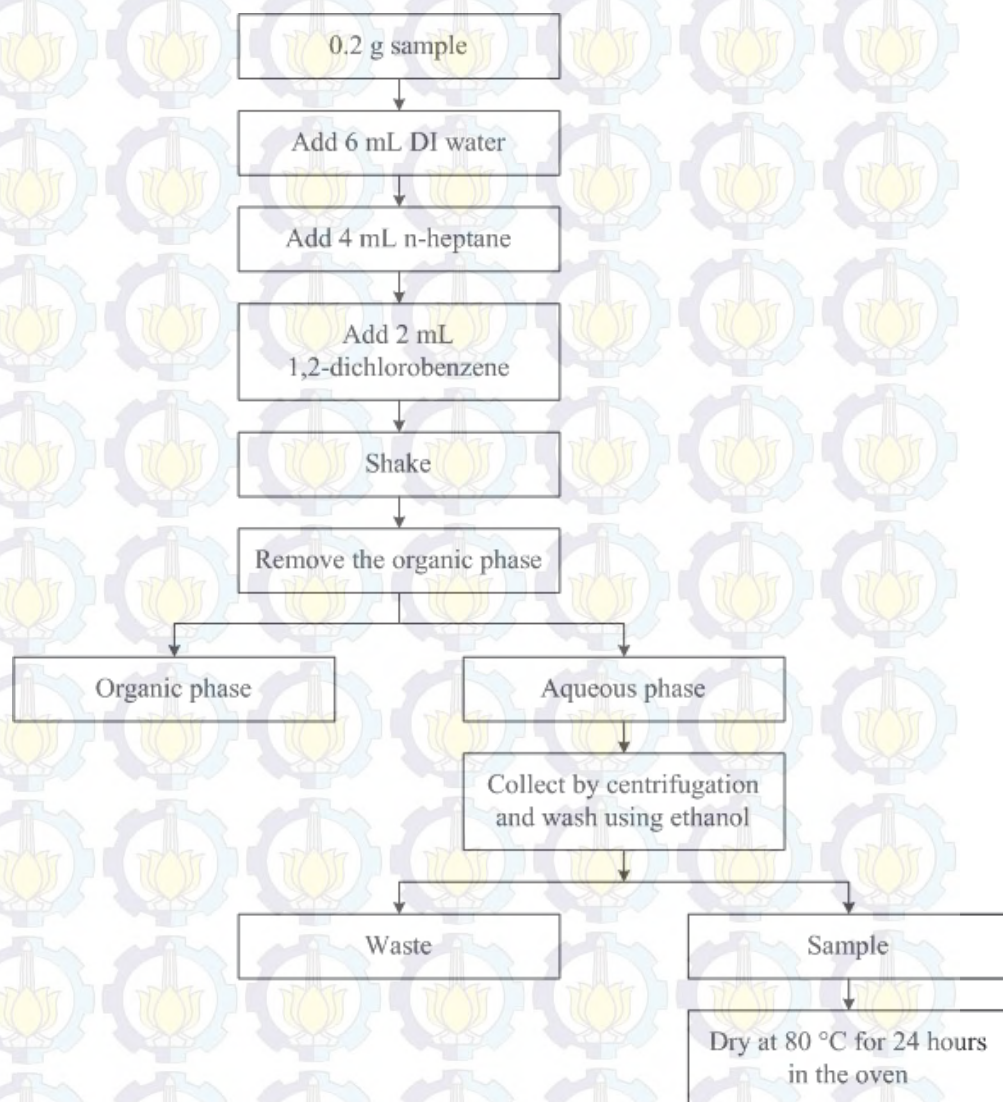




## A.2 Synthesis Flowchart of 20 wt% Pt/Ti<sub>4</sub>O<sub>7</sub> Catalyst

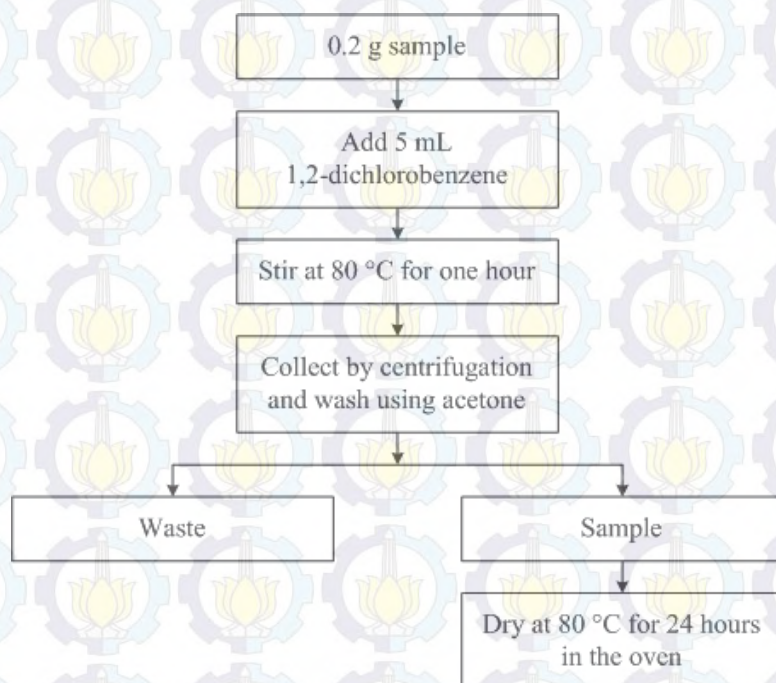


### A.3 Flowchart of Carbon Removal by Extraction Treatment

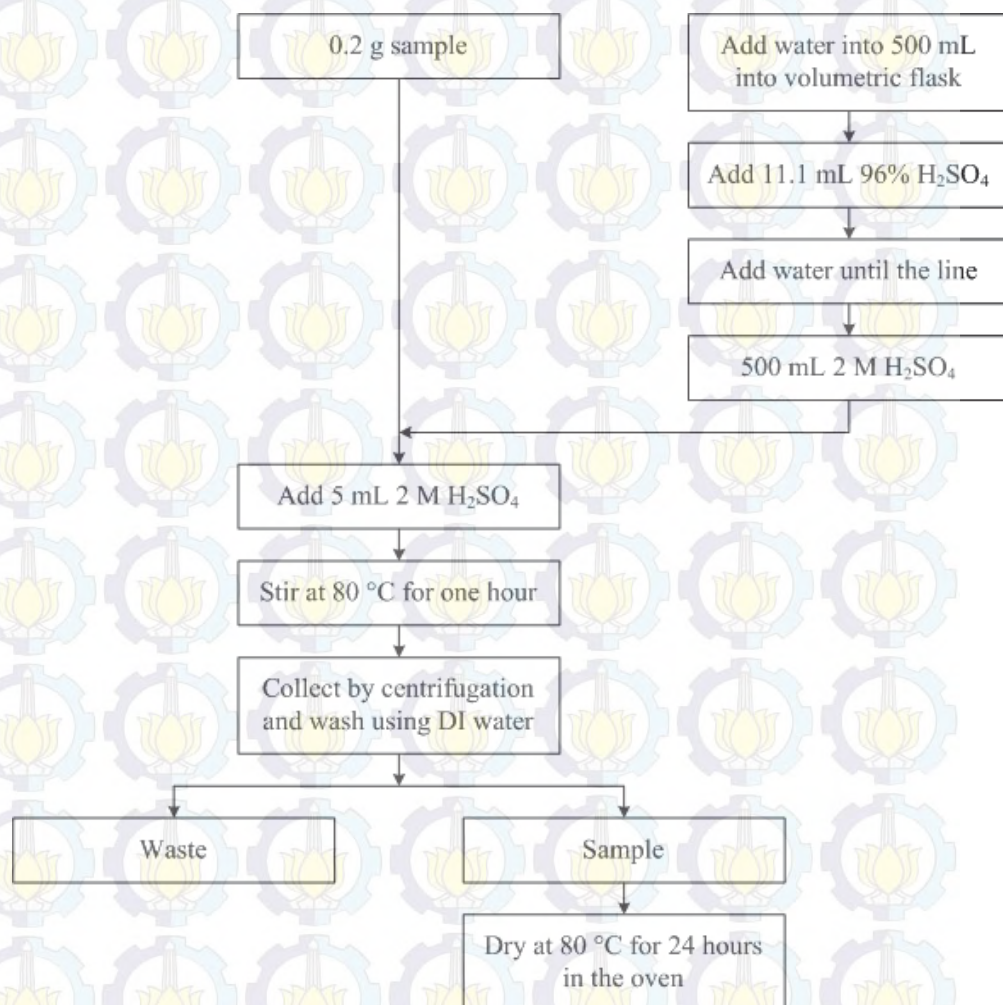




#### A.4 Flowchart of Carbon Removal by Solvent Treatment

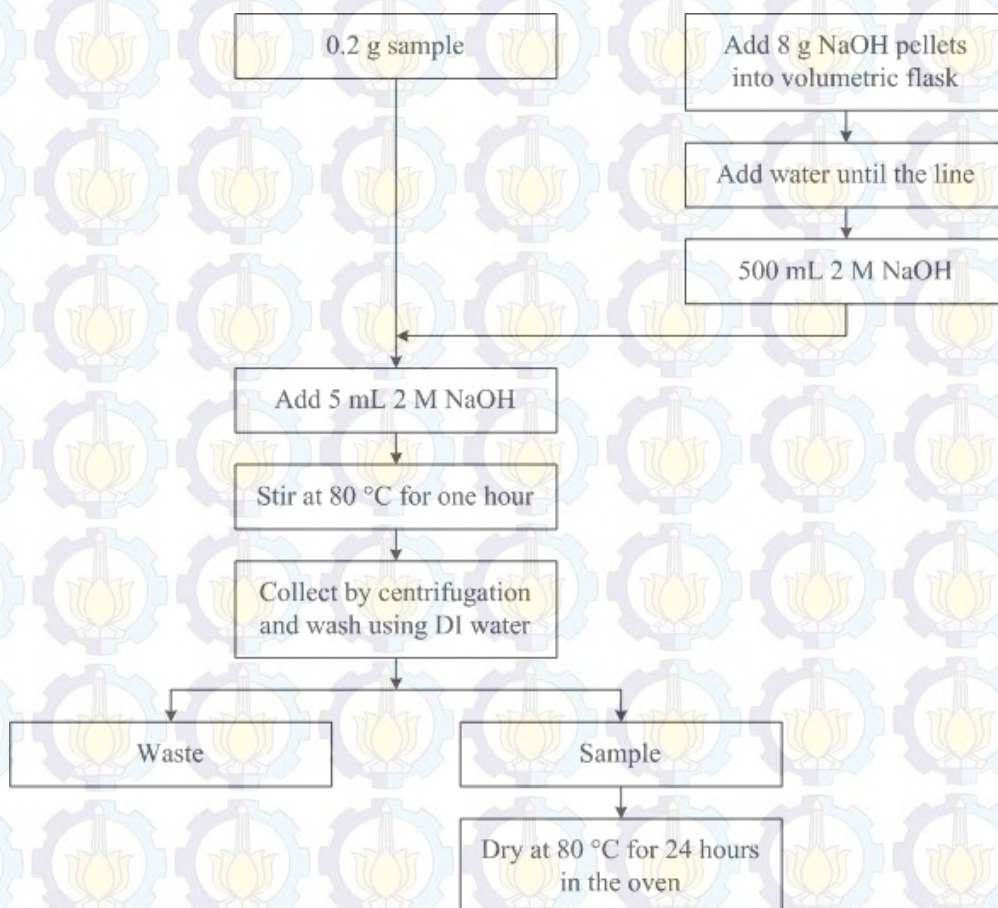


### A.5 Flowchart of Carbon Removal by Acid Treatment

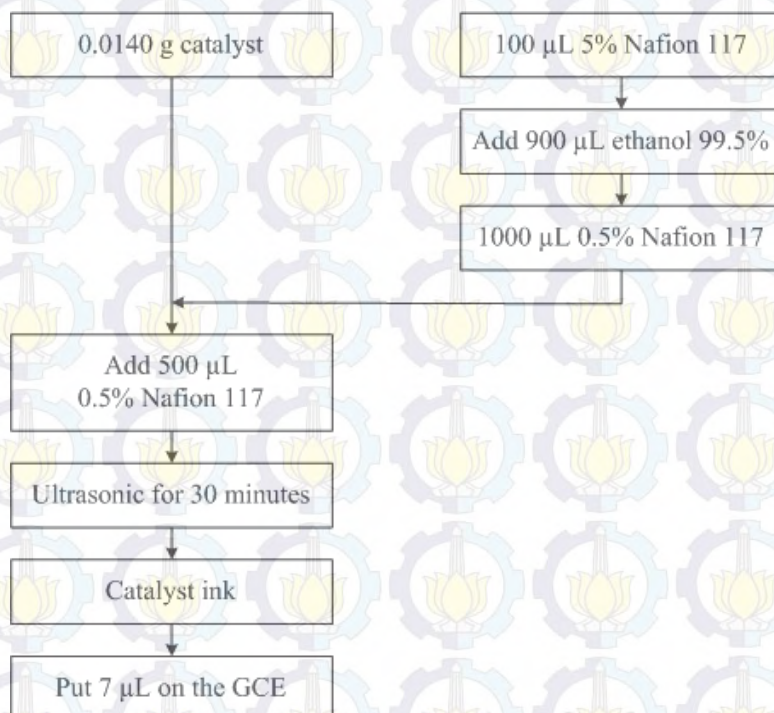




## A.6 Flowchart of Carbon Removal by Base Treatment

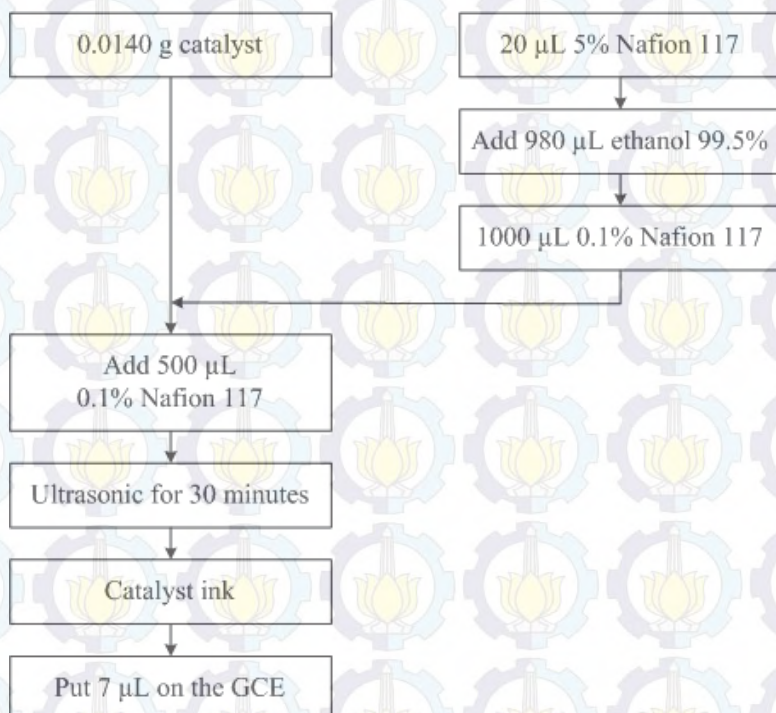


### A.7 Flowchart of Catalyst Ink 1 Preparation

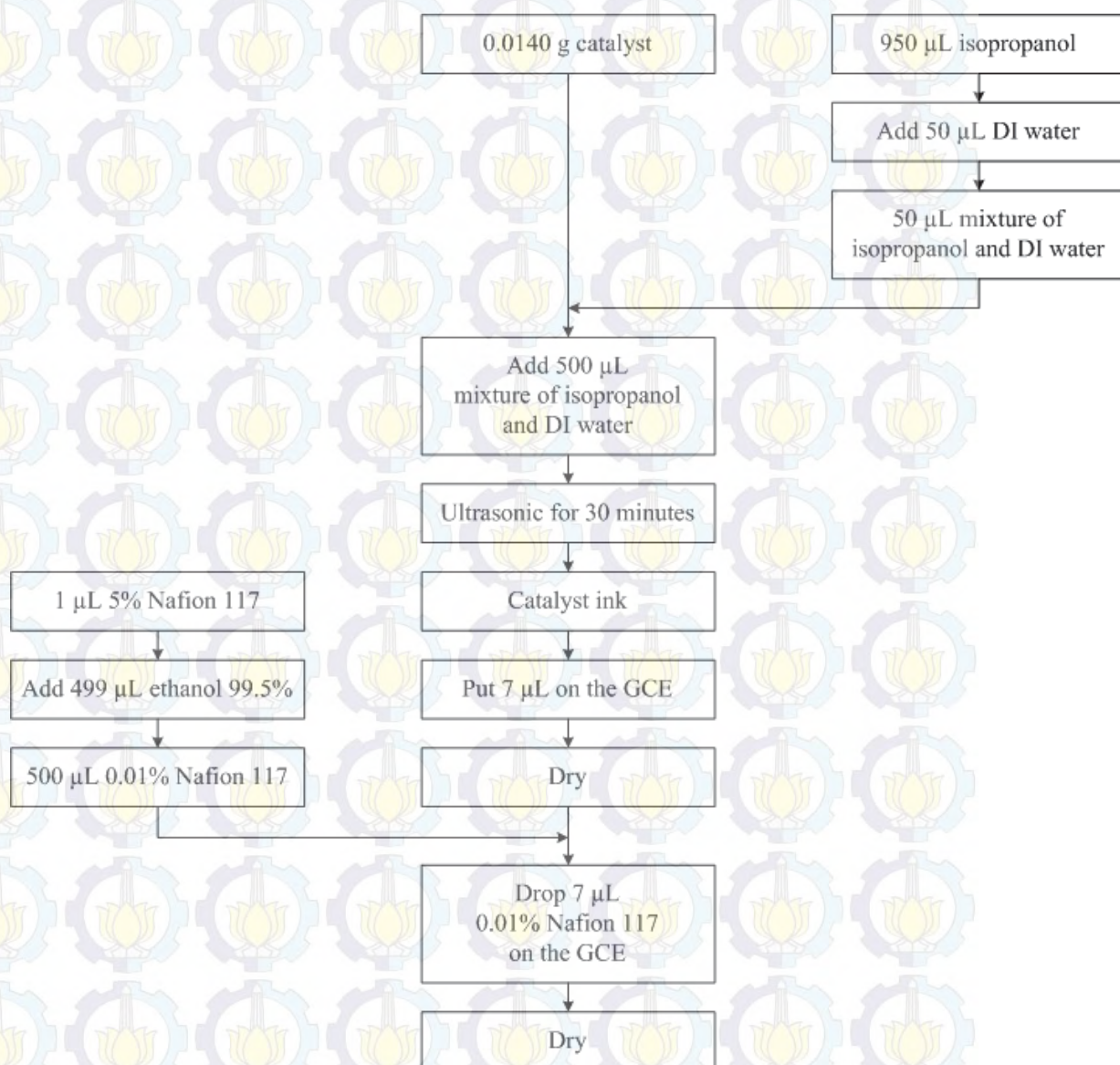




## A.8 Flowchart of Catalyst Ink 2 Preparation

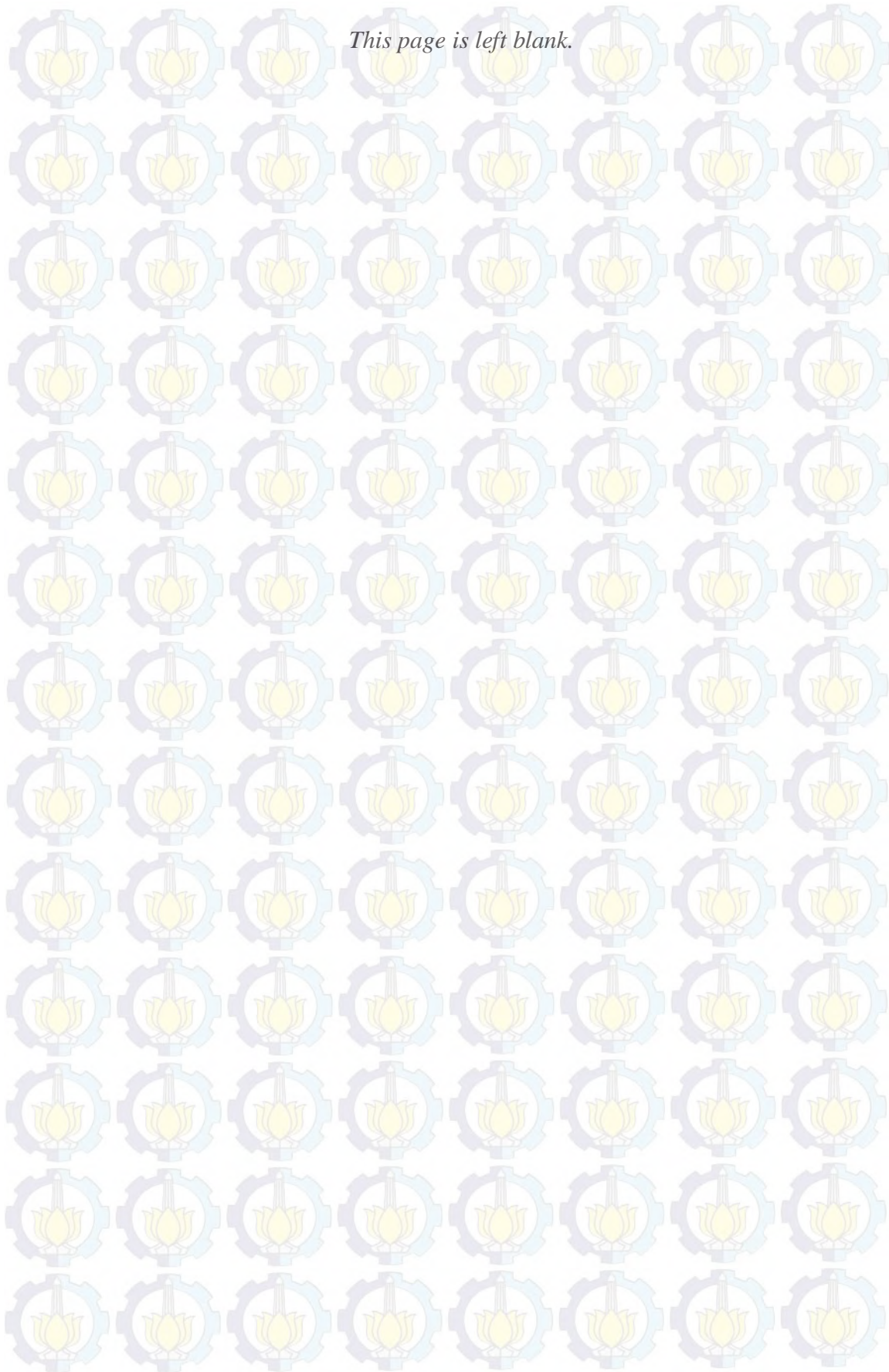


### A.9 Flowchart of Catalyst Ink 3 Preparation





*This page is left blank.*



## BIBLIOGRAPHY

1. Dresselhaus, M. S. & Thomas, I. L. Alternative energy technologies. *Nature* **414**, 332–337 (2001).
2. Schiermeier, Q., Tollefson, J., Scully, T., Witze, A. & Morton, O. Energy alternatives: Electricity without carbon. *Nature* **454**, 816–823 (2008).
3. Ogden, J. High hopes for hydrogen. *Sci. Am.* **295**, 94–101 (2006).
4. Tollefson, J. Hydrogen vehicles: Fuel of the future? *Nature* **464**, 1262–1264 (2010).
5. Sharaf, O. Z. & Orhan, M. F. An overview of fuel cell technology: Fundamentals and applications. *Renew. Sustain. Energy Rev.* **32**, 810–853 (2014).
6. Zhang, Z., Liu, J., Gu, J. & Cheng, L. An overview of metal oxide materials as electrocatalysts and supports for polymer electrolyte fuel cells. *Energy Environ. Sci.* **7**, 2535–2558 (2014).
7. Yamamoto, K. *et al.* Size-specific catalytic activity of platinum clusters enhances oxygen reduction reactions. *Nat. Chem.* **1**, 397–402 (2009).
8. Wang, D. *et al.* Structurally ordered intermetallic platinum–cobalt core–shell nanoparticles with enhanced activity and stability as oxygen reduction electrocatalysts. *Nat. Mater.* **12**, 81–87 (2012).
9. Hsieh, Y.-C. *et al.* Ordered bilayer ruthenium–platinum core-shell nanoparticles as carbon monoxide-tolerant fuel cell catalysts. *Nat. Commun.* **4**, 2466 (2013).
10. Jang, J.-H. *et al.* Rational syntheses of core-shell  $\text{Fe}_x\text{@Pt}$  nanoparticles for the study of electrocatalytic oxygen reduction reaction. *Sci. Rep.* **3**, 2872 (2013).
11. Chang, S. H. *et al.* Structural and electronic effects of carbon-Supported  $\text{Pt}_x\text{Pd}_{1-x}$  nanoparticles on the electrocatalytic activity of the oxygen-reduction reaction and on methanol tolerance. *Chem. - A Eur. J.* **16**, 11064–11071 (2010).
12. Chen, Z., Higgins, D., Yu, A., Zhang, L. & Zhang, J. A review on non-precious metal electrocatalysts for PEM fuel cells. *Energy Environ. Sci.* **4**, 3167 (2011).



13. Ioroi, T. *et al.* Platinum-titanium alloy catalysts on a Magnéli-phase titanium oxide support for improved durability in Polymer Electrolyte Fuel Cells. *J. Power Sources* **223**, 183–189 (2013).
14. Kumar, A. & Ramani, V. K. Strong metal-support interactions enhance the activity and durability of platinum supported on tantalum-modified titanium dioxide electrocatalysts. *ACS Catal.* **4**, 1516–1525 (2014).
15. Lavacchi, A., Miller, H. & Vizza, F. in *Nanotechnology in Electrocatalysis for Energy* **170**, 63–89 (Springer New York, 2013).
16. Wang, Y.-J., Wilkinson, D. P. & Zhang, J. Noncarbon support materials for polymer electrolyte membrane fuel cell electrocatalysts. *Chem. Rev.* **111**, 7625–51 (2011).
17. Andersson, S. *et al.* Phase Analysis Studies on the Titanium-Oxygen System. *Acta Chemica Scandinavica* **11**, 1641–1652 (1957).
18. Bartholomew, R. F. & Frankl, D. R. Electrical properties of some titanium oxides. *Phys. Rev.* **187**, 828–833 (1969).
19. Graves, J. E., Pletcher, D., Clarke, R. L. & Walsh, F. C. The electrochemistry of Magnéli phase titanium oxide ceramic electrodes Part I. The deposition and properties of metal coatings. *J. Appl. Electrochem.* **21**, 848–857 (1991).
20. Ioroi, T. *et al.* Stability of Corrosion-Resistant Magnéli-Phase Ti<sub>4</sub>O<sub>7</sub>-Supported PEMFC Catalysts at High Potentials. *J. Electrochem. Soc.* **155**, B321 (2008).
21. Ioroi, T., Siroma, Z., Fujiwara, N., Yamazaki, S. I. & Yasuda, K. Sub-stoichiometric titanium oxide-supported platinum electrocatalyst for polymer electrolyte fuel cells. *Electrochem. commun.* **7**, 183–188 (2005).
22. Zhu, R., Liu, Y., Ye, J. & Zhang, X. Magnéli phase Ti<sub>4</sub>O<sub>7</sub> powder from carbothermal reduction method: formation, conductivity and optical properties. *J. Mater. Sci. Mater. Electron.* **24**, 4853–4856 (2013).
23. Senevirathne, K., Hui, R., Campbell, S., Ye, S. & Zhang, J. Electrocatalytic activity and durability of Pt/NbO<sub>2</sub> and Pt/Ti<sub>4</sub>O<sub>7</sub> nanofibers for PEM fuel cell oxygen reduction reaction. *Electrochim. Acta* **59**, 538–547 (2012).
24. Yao, C., Li, F., Li, X. & Xia, D. Fiber-like nanostructured Ti<sub>4</sub>O<sub>7</sub> used as durable fuel cell catalyst support in oxygen reduction catalysis. *J. Mater. Chem.* **22**, 16560 (2012).

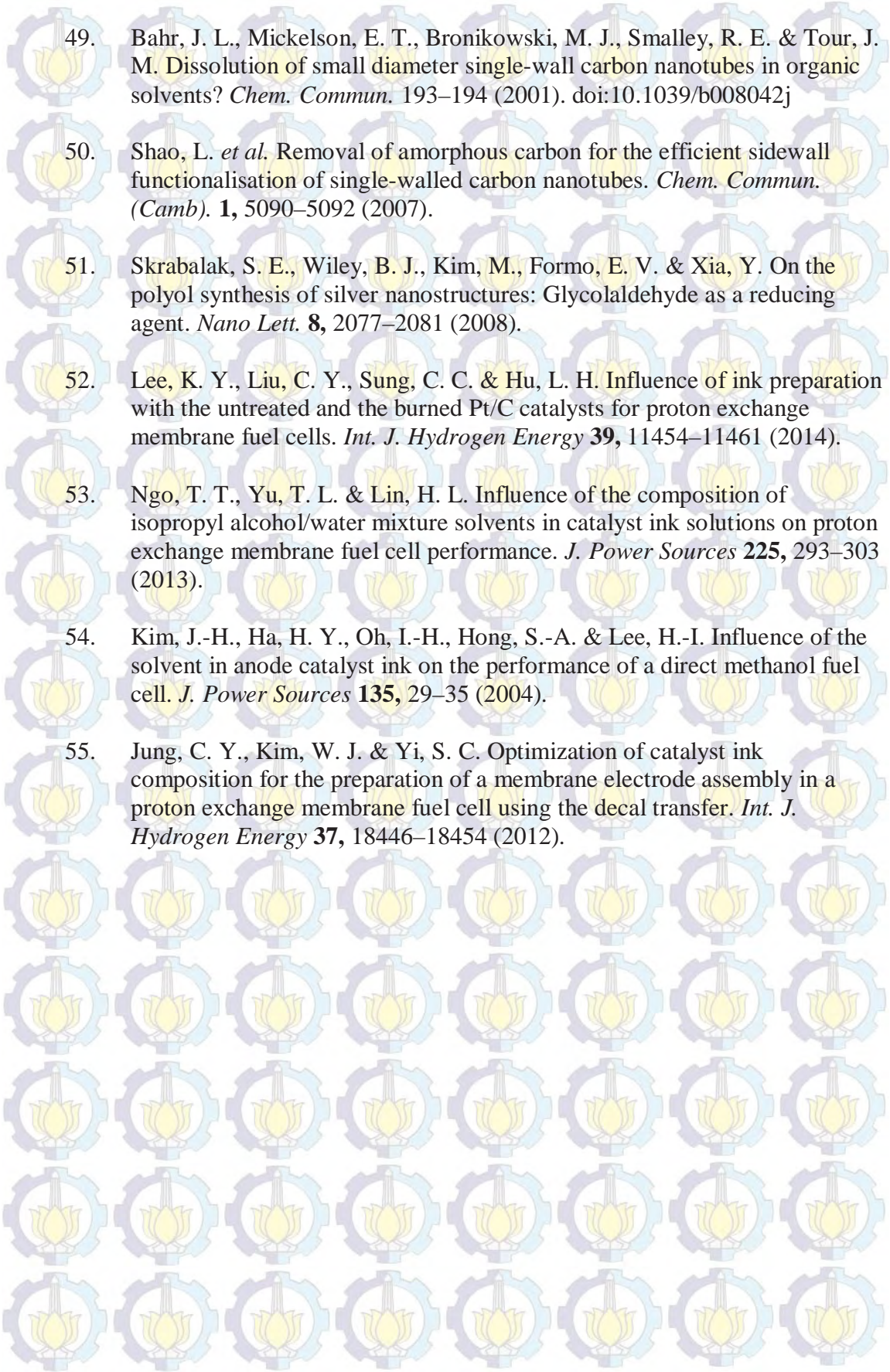


25. Pang, Q., Kundu, D., Cuisinier, M. & Nazar, L. F. Surface-enhanced redox chemistry of polysulphides on a metallic and polar host for lithium-sulphur batteries. *Nat. Commun.* **5**, 1–19 (2014).
26. Ismail, A. F., Naim, R. & Zubir, N. A. in *Polymer Membranes for Fuel Cells* 27–49 (Springer US, 2009). doi:10.1007/978-0-387-73532-0\_3
27. Ho, V. T. T., Pan, C. J., Rick, J., Su, W. N. & Hwang, B. J. Nanostructured Ti<sub>0.7</sub>Mo<sub>0.3</sub>O<sub>2</sub> support enhances electron transfer to Pt: High-performance catalyst for oxygen reduction reaction. *J. Am. Chem. Soc.* **133**, 11716–11724 (2011).
28. Ioroi, T. *et al.* Corrosion-Resistant PEMFC Cathode Catalysts Based on a Magnéli-Phase Titanium Oxide Support Synthesized by Pulsed UV Laser Irradiation. *J. Electrochem. Soc.* **158**, C329 (2011).
29. Lv, H. & Mu, S. Nano-ceramic support materials for low temperature fuel cell catalysts. *Nanoscale* **6**, 5063–74 (2014).
30. Meier, J. C. *et al.* Design criteria for stable Pt/C fuel cell catalysts. *Beilstein J. Nanotechnol.* **5**, 44–67 (2014).
31. Yuan, X. Z. & Wang, H. in *PEM Fuel Cell Electrocatalysts and Catalyst Layers: Fundamentals and Applications* 1–87 (Springer-Verlag, 2008). doi:10.1007/978-1-84800-936-3\_1
32. Lavacchi, A., Miller, H. & Vizza, F. in *Nanotechnology in Electrocatalysis for Energy* **170**, 25–61 (Springer New York, 2013).
33. Song, C. & Zhang, J. in *PEM Fuel Cell Electrocatalysts and Catalyst Layers: Fundamentals and Applications* 89–134 (Springer-Verlag, 2008). doi:10.1007/978-1-84800-936-3\_2
34. Sarma, L. S., Taufany, F. & Hwang, B. J. Electrocatalyst Characterization and Activity Validation - Fundamentals and Methods. *Electrocatal. Direct Methanol Fuel Cells From Fundam. to Appl.* 115–163 (2009). doi:10.1002/9783527627707.ch3
35. Su, L., Jia, W., Li, C.-M. & Lei, Y. Mechanisms for enhanced performance of platinum-based electrocatalysts in proton exchange membrane fuel cells. *ChemSusChem* **7**, 361–78 (2014).
36. Hwang, B. J. *et al.* An Investigation of Structure–Catalytic Activity Relationship for Pt–Co/C Bimetallic Nanoparticles toward the Oxygen Reduction Reaction. *J. Phys. Chem. C* **111**, 15267–15276 (2007).



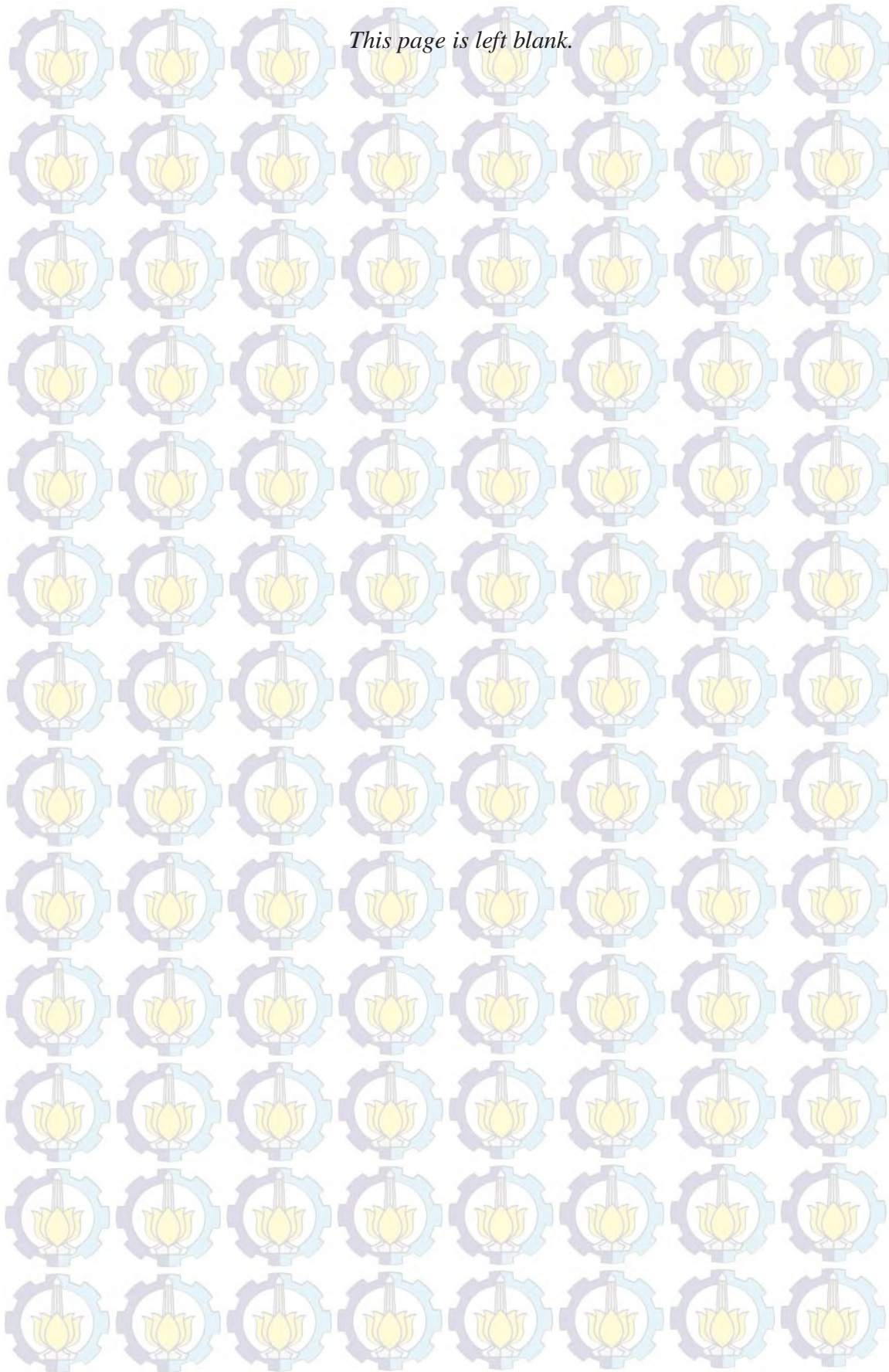
37. Kitada, A. *et al.* Selective preparation of macroporous monoliths of conductive titanium oxides  $\text{Ti}(n)\text{O}(2n-1)$  ( $n = 2, 3, 4, 6$ ). *J. Am. Chem. Soc.* **134**, 10894–8 (2012).
38. Li, X. *et al.* Magneli phase  $\text{Ti}_4\text{O}_7$  electrode for oxygen reduction reaction and its implication for zinc-air rechargeable batteries. *Electrochim. Acta* **55**, 5891–5898 (2010).
39. Krishnan, P., Advani, S. G. & Prasad, A. K. Magneli phase  $\text{Ti}_n\text{O}_{2n-1}$  As corrosion-resistant PEM fuel cell catalyst support. *J. Solid State Electrochem.* **16**, 2515–2521 (2012).
40. Nguyen, S. T., Lee, J. M., Yang, Y. & Wang, X. Excellent durability of substoichiometric titanium oxide as a catalyst support for Pd in alkaline direct ethanol fuel cells. *Ind. Eng. Chem. Res.* **51**, 9966–9972 (2012).
41. Wu, Q., Ruan, J., Zhou, Z. & Sang, S. Magneli phase titanium sub-oxide conductive ceramic  $\text{Ti}_n\text{O}_{2n-1}$  as support for electrocatalyst toward oxygen reduction reaction with high activity and stability. *J. Cent. South Univ.* **22**, 1212–1219 (2015).
42. Zhang, L. *et al.*  $\text{Ti}_4\text{O}_7$  supported Ru@Pt core-shell catalyst for CO-tolerance in PEM fuel cell hydrogen oxidation reaction. *Appl. Energy* **103**, 507–513 (2013).
43. Zhao, H. *et al.* Pt catalyst supported on titanium suboxide for formic acid electrooxidation reaction. *Int. J. Hydrogen Energy* **39**, 9621–9627 (2014).
44. Tominaka, S., Tsujimoto, Y., Matsushita, Y. & Yamaura, K. Synthesis of nanostructured reduced titanium Oxide: Crystal structure transformation maintaining nanomorphology. *Angew. Chemie - Int. Ed.* **50**, 7418–7421 (2011).
45. Kundu, D., Black, R., Berg, E. J. & Nazar, L. F. A highly active nanostructured metallic oxide cathode for aprotic Li–O<sub>2</sub> batteries. *Energy Environ. Sci.* (2015). doi:10.1039/C4EE02587C
46. Ma, W. *et al.* Investigating electron-transfer processes using a biomimetic hybrid bilayer membrane system. *Nat. Protoc.* **8**, 439–50 (2013).
47. Zdravkov, B. D., Čermák, J. J., Šefara, M. & Janků, J. Pore classification in the characterization of porous materials: A perspective. *Cent. Eur. J. Chem.* **5**, 1158–1158 (2007).
48. Carmo, M., dos Santos, A. R., Poco, J. G. R. & Linardi, M. Physical and electrochemical evaluation of commercial carbon black as electrocatalysts supports for DMFC applications. *J. Power Sources* **173**, 860–866 (2007).



- 
49. Bahr, J. L., Mickelson, E. T., Bronikowski, M. J., Smalley, R. E. & Tour, J. M. Dissolution of small diameter single-wall carbon nanotubes in organic solvents? *Chem. Commun.* 193–194 (2001). doi:10.1039/b008042j
50. Shao, L. *et al.* Removal of amorphous carbon for the efficient sidewall functionalisation of single-walled carbon nanotubes. *Chem. Commun. (Camb)*. **1**, 5090–5092 (2007).
51. Skrabalak, S. E., Wiley, B. J., Kim, M., Formo, E. V. & Xia, Y. On the polyol synthesis of silver nanostructures: Glycolaldehyde as a reducing agent. *Nano Lett.* **8**, 2077–2081 (2008).
52. Lee, K. Y., Liu, C. Y., Sung, C. C. & Hu, L. H. Influence of ink preparation with the untreated and the burned Pt/C catalysts for proton exchange membrane fuel cells. *Int. J. Hydrogen Energy* **39**, 11454–11461 (2014).
53. Ngo, T. T., Yu, T. L. & Lin, H. L. Influence of the composition of isopropyl alcohol/water mixture solvents in catalyst ink solutions on proton exchange membrane fuel cell performance. *J. Power Sources* **225**, 293–303 (2013).
54. Kim, J.-H., Ha, H. Y., Oh, I.-H., Hong, S.-A. & Lee, H.-I. Influence of the solvent in anode catalyst ink on the performance of a direct methanol fuel cell. *J. Power Sources* **135**, 29–35 (2004).
55. Jung, C. Y., Kim, W. J. & Yi, S. C. Optimization of catalyst ink composition for the preparation of a membrane electrode assembly in a proton exchange membrane fuel cell using the decal transfer. *Int. J. Hydrogen Energy* **37**, 18446–18454 (2012).



*This page is left blank.*



## BIOGRAPHY



Idris Ibnu Malik is a Muslim and was born in Surabaya, December 3rd 1990. The author studied chemistry at Department of Chemistry, Faculty of Mathematics and Natural Sciences, Institut Teknologi Sepuluh Nopember Surabaya on 2009 and he got Bachelor of Science on 2013 under supervision of Eko Santoso, M.Si. Later, he directly continued the study by joining master program in at the same department on 2013, and he joined the double degree program between Institut Teknologi Sepuluh Nopember and National Taiwan University of Science and Technology on 2014 under supervision of Hamzah Fansuri, Ph.D. and Prof. Bing-Joe Hwang. He interested in the material development for energy storage and conversion.

The author can be contacted by phone at +6287852662463 or email at [malik.ibnu@gmail.com](mailto:malik.ibnu@gmail.com).



*This page is left blank.*

